AD NUMBER

AD852999

NEW LIMITATION CHANGE

TO

Approved for public release, distribution unlimited

FROM

Distribution authorized to U.S. Gov't. agencies and their contractors; Administrative/Operational Use; FEB 1969. Other requests shall be referred to Air Force Matwerials lab., Wright-Patterson AFB, OH 45433.

AUTHORITY

AFML ltr, 21 Mar 1972

AFML-TR-69-27

NICKEL-BASE SUPERALLOY OXIDATION

G. E. Wasielewski and C. S. Wukusick

General Electric Co.

TECHNICAL REPORT AFML-TR-69-27

February 1969

Air Force Materials Laboratory
Air Force Systems Command
Wright-Patterson Air Force Base, Ohio

NOTICE

When Government drawings, specifications, or other data are used for any purpose other than in connection with a definitely related Government procurement operation, the United States Government thereby incurs no responsibility nor any obligation whatsoever; and the fact that the Government may have formulated, furnished, or in any way supplied the said drawings, specifications, or other data, is not to be regarded by implication or otherwise as in any manner licensing the holder or any other person or corporation, or conveying any rights or permission to manufacture, use, or sell any patented invention that may in any way be related thereto.

This document is subject to special export controls and each transmittal to foreign governments or foreign nationals may be made only with prior approval of the Metals and Ceramics Division (MAAM) Air Force Materials Laboratory, Wright-Patterson Air Force Base, Ohio 45433.

The distribution of this report is limited because the report contains technology identifiable with items on the strategic embargo lists excluded from export under the U. S. Export Control Act, as implemented by AFR 310-2 and AFSC 80-20.

Copies of this report should not be returned unless return is required by security considerations, contractual obligations, or notice on a specific document.

NICKEL-BASE SUPERALLOY OXIDATION

G. E. Wasielewski and C. S. Wukusick

FOREWORD

This report was prepared by the Materials and Processes Technology Laboratories of the General Electric Company under USAF Contract No. AF33(615)-2861. The program was administered under the direction of the Air Force Materials Laboratory, Metals and Ceramics Division, Wright-Patterson Air Force Base, Ohio, with Mr. C. A. Lombard and Mr. J. J. Crosby as Project Engineers. This report describes the results of research conducted during the period May 1, 1967 through December 31, 1968. This report was submitted by the authors for publication April 1969.

Mr. G. E. Wasielewski was Project Manager for General Electric. Other General Electric personnel who contributed to this work are:

F. B. Brate, V. M. Poynter - Electron Microscopy and Microprobe

C. R. Lehmann, F. Davidson and S. Hischemiller - Metallography

O. L. Isaacs - X-ray Diffraction

R. Raper, W. Underwood, C. Koehler - General Assistance in Experimental Work

This technical report has been reviewed and is approved.

I. Perlmutter

I. Perlmutter, Chief
Metals Branch
Metals and Ceramics Division
Air Force Materials Laboratory

ABSTRACT

A program to improve the surface stability of nickel-base turbine blade alloys is described. In Phase I, additions of rare-earth type elements and Mn were made singularly and in combination to cast Rene' 100 and wrought Unitemp AF-2-IDA alloys. The results indicated that certain reactive metal additions are markedly effective in improving surface stability but tend to degrade mechanical properties. The loss in mechanical properties was attributed to segregation of reactive metal containing phases at the grain boundaries. In the wrought AF-2-IDA alloy the reactive metal additions seriously impared hot workability so that mechanical property test specimens could not be obtained.

In Phase II of the program, 15 pound heats of Rene' 100 which contained only moderate (< 0.1 a/o) amounts of doping additions were studied. The objective was to obtain an improved balance of surface stability and mechanical properties. With levels of ~ 0.05 a/o dopants, mechanical properties were equivalent to the base Rene' 100 alloy, with marginal improvements in surface stability. The surface stability of cast Rene' 100 alloys was found to be dependent on structural effects as well as chemical composition. Drop cast alloys, having a refined microstructure generally exhibited much better surface stability than investment cast material. The most promising directions for future studies are suggested.

TABLE OF CONTENTS

TABLE OF CONTENTS (Cont'd)

LIST OF ILLUSTRATIONS

LIST OF TABLES

1.0 INTRODUCTION

Advancements in aircraft gas turbine technology continue to call for increased turbine inlet temperatures and consequently more arduous demands on materials for components such as vanes, combustion liners, afterburner flameholders and particularly turbine blades. The resultant high temperature turbine environment, which can include sulphur from the fuel and various halides from sea water, drastically reduces superalloy component life and reliability by increasing the extent of oxidation and/or hot corrosion. Thus, although we have developed superalloys whose mechanical properties may be adequate at the higher temperatures, their superior properties cannot be fully utilized due to inherent limitations in surface stability.

It may be possible to minimize these deficiencies by major alloy modifications i.e. Cr, Al, Ti. However, applying this approach to the complex high strength alloys would undoubtedly alter structural stability and might detrimentally affect mechanical properties. Hence, this approach would most likely require a major alloy development effort to improve surface stability without adverse structural effects. During previous studies promising techniques for improving surface stability without major changes in alloy composition were identified. This was accomplished by the addition of small quantities of the "rare earth" type elements and manganese which increase the effectiveness of major alloy elements already present in the alloy by producing protective oxide scales. This latter method of improving surface stability is particularly attractive since the amount of addition required may be small enough to have an insignificant effect on other properties.

In brief, this investigation was conducted as a continuation of previous work under contract AF 33(615)-2861 to identify an approach for improving the surface stability of turbine blade materials through minor additions of Group III B Metals, the rare earth metals, thorium, and manganese. The

approach consisted of the following two steps:

1. Develop an understanding of the effects of minor addition elements toward improved environmental resistance of Rene' 100, one of the strongest commercially available cast alloys, and Unitemp AF 2-1DA, a high strength developmental wrought alloy.

2. Apply this knowledge to scaled-up heats of the most promising alloys from above, more fully characterize the oxidation and hot corrosion behavior and the effect of the minor addition elements on the mechanical properties.

2.0 BACKGROUND

2.1 General

This laboratory, which has long been aware of the needs for improved materials, has emphasized studies of the high temperature oxidation behavior of superalloys. In particular, earlier programs have considered the oxidation mechanisms of a number of commercial superalloys such as Hastelloy X[1], Rene' 41, Udimet 700[2], TD-Nickel[3], L-605, and X-40[4]. These studies formed a pioneering effort toward improvement of oxidation resistance of commercial superalloys by establishing an understanding of the oxidation mechanisms involved through characterizing the oxidation behavior as a function of time, temperature, and alloy composition. The application of this understanding toward the design and selection of alloys with improved surface stability has been successful, leading to development alloys such as Rene' X[5], RE-12[6], and Rene' Y.

Interest in minor element additions stems from two recent Air Force sponsored studies (7-9) in which the oxidation behavior of five commercial nickel-base alloys (Rene' 100, SM-200, Inco 713C, Rene' 41, and U-700) and one experimental alloy (Rene' Y*) were fully characterized. All alloys, with the exception of Rene' Y, displayed a similar mode of oxidation and the same undesirable features. This was particularly true for the cast alloys (Rene' 100, SM-200, and Inco 713C)

whose usefulness at temperatures above 1700°F is limited by: 1) excessive oxide spalling in a thermal cycling environment; 2) oxide vaporization in a high velocity atmosphere; and 3) a general lack of resistance to hot corrosion environments. These deficiencies were attributed to the formation of heterogeneous oxide scales which contained non-protective and volatile oxide phases. Rene' Y on the other hand, was notably immune to these deficiencies at temperatures up to 2000°F due to the La-induced formation of a tenacious $MnCr_2O_4$ spinel oxide. This La + Mn doped alloy displayed far superior oxidation behavior than its counterpart, Hastelloy X[10].

As evidenced by the Rene Y findings, the most obvious and ideal solution to the adverse oxidation and hot corrosion resistance of Rene' 100, Sm-200, and Inco 713C involves the promotion of a stable, single phase oxide which possesses compatibility with the substrate metal. Theoretically, this can be obtained through control of the scale and subscale reactions by addition of elements which increase the effective activity of critical constituents, such as aluminum or chromium, thereby increasing the propensity for their incorporation into the surface oxide. The "rare-earth" elements, which are less noble than any other normal superalloy solute could be used for sacrificial oxidation and in the process, increase the concentration of otherwise subscale components in the surface scale.

2.2 The Effect of "Rare Earth" Type Elements* On Alloy Behavior

2.2.1 General

The use of rare earth elements to improve the characteristics of metals and alloys is no new innovation: a study of the effects of rare earth elements on the properties of cast iron were first made more than forty-five years ago by Moldenke[11]. Approximately twenty years later in Germany, Hessenbruch[12], investigating alloys for electrical heaters, discovered that reactive metal additions greatly improved the service life of Ni-Cr and Fe-Cr-Al alloys. The stainless steel industry, seeking better workability of austenitic Cr-Ni steels, investigated the effect of additions of rare earths in the form of mischmetal Such additions were found to be effective for Ni-Cr-Mo base alloys which formerly were not even hot workable[13].

*For the purpose of this discussion these elements refer to the strong oxide formers such as the lanthanons, calcium, cerium, beryllium, scandium, thorium and yttrium.

The metallurgical applicability of the rare earths increased markedly during the next few years. A comprehensive bibliography by Prochornich[14] contains sixty-nine references from foreign and domestic investigators, and demonstrates the active interest in rare earth research. A more recent review of the subject has been presented by Collins and co-workers[15]. A number of texts on the subject have also been published recently[16-20].

2.2.2 The Influence of the Rare Earth Elements on Oxidation Resistance

The improvements resulting from small additons of reactive elements to heat resisting Ni-Cr alloys have been fully verified[21-25]. However, with the exception of some stainless steels,[26-28] Fe-Cr-Al-Y[29] and T. D. Nickel[30] only a few commercial alloys have been developed utilizing this knowledge to improve oxidation resistance. The absence of more profound oxidation resistant nickel-base superalloy developments using this technology is obvious, and appears to stem from a lack of understanding as to the manner in which these doping additions afford improvement. Very few systematic studies have been conducted to establish if this group of some fifteen elements all act similarly or if some produce greater beneficial effects than others. Only the most common of this group of elements (i.e.m calcium, cerium, yttrium, and lanthanum) have received evaluation regarding their ability to enhance surface stability.

Collins[31] evaluated the effect of various concentrations of thirteen of the rare earths in an effort to improve the oxidation/nitridation behavior of chromium. The scaling behavior was found to vary considerably with both the specific rare earth element and concentration. All, however, offered an improvement relative to chromium, by reducing the spalling tendencies of the oxide and the amount of nitrogen absorbed. With praseodymium, neodymium, gadolinium, erbium, lutetium, and yttrium additions, the improved scaling resistance continued for exposure temperatures in excess of 2500°F. Of these elements, however, it was concluded that additions of yttrium yielded the most marked improvement in oxidation behavior. More recent studies by Clark and Wukusick[32,33] to develop high-temperature chromium alloys have included the effects of reactive metal additions such as Y, Ce, La, Th, Pr, Be and mischmetal on the nitrification inhibiting properties and general oxidation behavior. Additions of La and La plus Y were found to be most effective.

Felton[34,35], in studying more oxidation resistant Fe-Cr alloys, investigated the effects of additions of equal amounts of yttrium, lanthanum, gadolinium, dysprosium, and erbium. His results indicated that all the rare earth elements evaluated improved the oxidation behavior of Fe-Cr alloys by enhancing scale adherence through filamentary internal oxide growth. Similar results were reported by Wlodek[5] in his initial studies to modify Hastelloy X with cerium, lanthanum, yttrium, magnesium,and beryllium additions.

Recent unpublished work by Lombard[36] indicates that Y, La, Pr, Nd, Sm, Dy, Ho, Er, Yb and Th additions to IN-100 can produce variable results. The results of these cursory studies illustrate a variation in the static oxidation behavior with both concentration and type of rare earth addition. These results further demonstrate Y to be the most effective addition and that rare earth additions to IN-100 must be kept below 0.4% if a maximum beneficial effect is to be derived.

Since the development of Rene' X[5], this laboratory has conducted various exploratory studies to determine the influence of rare earth additions on nickel-base superalloys. Oxidation studies have been conducted on TD Ni-Cr, Rene'-100* and INCO 713C doped with lanthanum plus manganese, and Rene' Y with variable lanthanum content. These studies have, in general, indicated that the beneficial effect derived from rare earth element additions is dependent upon their concentration in the alloy, the alloy base used, and the type of atmosphere the alloy is exposed to.

It is interesting to note that with the exception of INCO 713C, and in some instances Rene' Y, little significant difference was observed between the thermogravimetrically determined oxidation rates of these alloys at 1900°F in the doped and undoped condition, indicating that rare earth additions primarily promote the formation of more adherent oxide scales. The actual mechanism by which rare earths increase scale adhesion and general oxidation resistance has not been fully defined. Wenderott[37] presented a good summary of the various theories which have been put forth and the conflicts that exist. The various mechanisms proposed can be generalized as follows:

*Modified IN-100 for internal phase stability

(1) "Blocking" of diffusion within the oxide scale due to the high ionic volume of the rare earths[12].

(2) Formation of a "barrier" oxide at the oxide metal interface[22,38]

(3) Enhanced diffusion of desirable elements by altering base metal properties[25,37].

(4) Mechanical "keying" via grain boundary oxidation[24,29,35]

Without expounding upon the various theories suffice it to say that no single proposed mechanism appears to fully account for the oxidation behavior of Rene' Y[9]. The oxidation behavior of Rene' Y has tenatively explained[39] utilizing a number of mechanisms which interact as follows: The lanthanum originally presented as a complex carbide is liberated by reaction with oxygen ($LaC + O^{2} \rightarrow CO_2 + La$) and concentrates in the surface oxide near the grain boundary "cusps" at the oxide metal interface. Here it accomplishes the following:

(1) Reduces internal oxidation of SiO_2 by forming a more stable grain boundary interface oxide (lower dissociation pressure)

(2) Reduces scaling rate (high temp/long time) by interacting with tramp elements (S, P, Pb, Sn, etc) which normally diffuse via grain boundaries and would increase the vacancy concentration within the oxide.

(3) Increases oxide plasticity at grain boundary/interface regions reducing interfacial shear stresses during thermal cycling thus enhancing scale adherence.

(4) Alters the activity/diffusivity of Cr, and Mn to produce a more stable $MnCr_2O_4$ spinel.

However, the <u>exact</u> mechanisms responsible for these effects remain somewhat elusive.

2.2.3 The Effect of Minor Element Additions on the Resistance to High Velocity and Hot Corrosion Atmospheres

In the presentation of this background of published information and our own experience, we have, so far, restricted the discussion to date in static or slow flowing air. However, a high temperature component in a jet engine may be exposed to a more complex environment. The combustion products of jet engine fuel produce a high velocity environment containing O_2, N_2, CO_2 and H_2O, which might also be contaminated with SO_2 and alkali metal halide and sulfate salts.

With the exception of studies by Preece and Lucas[40], relatively little data exist regarding the behavior of superalloys in high velocity combustion products. Our previous studies[9] have demonstrated that significant metal loss can result from the volatilization of Cr_2O_3 from oxide scales produced on nickel-base superalloys. During development studies of Rene' Y the effectiveness of lanthanum and manganese in reducing such metal losses during exposure to high velocity combustion products was demonstrated. The first modification of Hastelloy X, called Rene' X, was essentially Hastelloy X with lanthanum added but no manganese. In static air exposure, Rene' X showed a marked improvement over Hastelloy X in terms of scale adherence and internal oxidation. However, when exposed to high velocity atmospheres the extent of metal loss for Rene' X was greater than for Hastelloy X. An examination of reaction products formed during static oxidation indicated that the addition of lanthanum to Hastelloy X promoted an oxide scale consisting solely of Cr_2O_3, whereas the normal Hastelloy X contained a more stable $NiCr_2O_4$ + Cr_2O_3 scale. Although the Cr_2O_3 oxide was extremely protective in static air environments, the vapor pressure of CrO_3 over Cr_2O_3 was sufficient to produce a loss of chromium in high velocity atmospheres. Therefore, as an additional modification 1.0 w/o manganese was added to Rene' X yielding the far superior Rene' Y. The decrease in CrO_3 volatilization for this alloy is due to the formation of a highly protective $MnCr_2O_4$ spinel overgrowth on the original Cr_2O_3. The formation of this protective scale is attributed to the combined action of lanthanum and manganese, since Hastelloy

---

* The term "dope" as used in this text refers to "a preparation for giving a desired quality to a substance or surface" --- ref. Webster's Seventh New Collegrate Dictionary

X contains nearly the same manganese level (0.8 w/o) but does not exhibit as stable an $MnCr_2O_4$ spinel[9]. The effect of manganese in promoting spinel formation has been observed by other investigators[12,22,41] but its beneficial effect has never truly been demonstrated before.

It is well known that nickel-base alloys are not inherently resistant to sulfur-containing hot corrosion atmospheres[42-45]. However, recent studies[46,47] performed by the Flight Propulsion Division, General Electric Company, Lynn, Massachusetts and the Materials and Process Laboratory of the Large Steam Turbine Department, General Electric Company, Schenectady, New York, have demonstrated that minor additions of lanthanum and yttrium to both nickel and cobalt alloys reduce the extent of attack.

To more fully explore the potential of minor element additions toward improving the surface stability of nickel-base alloys a series of cursory hot corrosion tests were conducted[48]. These tests were conducted on laboratory size chill-castings of commercial and experimental nickel-base superalloys whose properties are attractive for future gas turbine applications. As shown in Figures 1 and 2 and summarized in Figure 3 all alloys tested were benefitted by the "rare-earth" additions and the extent of improvement appeared to increase as the Al/Cr ratio within the alloy increased. The effect of doping element additions on the hot corrosion resistance of Rene' 100 is vividly illustrated by the general appearance and microstructures shown in Figure 4. The reaction products formed on those specimens with 0.31 w/o La or greater were extremely dense and tenacious even at the edges of the specimens whereas the alloys with lesser amounts of La suffered severe sulfidation attack. On the basis of metal loss, Rene' 100 with $\geq$ 0.31 w/o La was a factor of 300 better than the undoped material and far superior to any uncoated nickel-base alloy developed to date. However, recent attempts at this laboratory to produce investment castings with similar resistance have not been as successful.

In summary, the additions of doping elements have been demonstrated to grossly improve both the oxidation behavior and sulfidation resistance of alloys with otherwise poor resistance. As such this approach offers considerable merit as an extension of current superalloy development technology and a fruitful means of improving future generation alloys.

2.2.4 Effect of Minor Element Additions on Mechanical Properties and Internal Stability

There is little information available regarding the effect of these minor element additions on the mechanical properties and internal phase stability of these already complex γ' strengthened nickel-base alloys. The literature contains many references regarding the beneficial effect of rare earths for improving the properties of the cast irons and stainless steels. The rare earths generally act as scavengers in these alloys usually yielding a finer grain size, finer carbide dispersion, and an accompanying increase in ductility and workability.

Current chromium alloy development studies[49] being conducted at this laboratory have shown a marked increase in workability, ductility and grain refinement with the addition of rare earth elements. Similarly, small additions of the rare earths to pure nickel completely eliminate the "hot brittleness" zone* and greatly increase plasticity through an interaction with low melting sulfides and phosphides[50]. However, excessive amounts of rare earth additions produced brittle phases and a reversed effect.

Lanthanum and yttrium additions now being evaluated for the development of hot corrosion resistance nickel and cobalt base alloys[47] did not produce any detrimental effects on microstructure or mechanical properties of the alloys studied. In fact, yttrium additions of 0.15 w/o to cobalt base alloys appear to promote precipitation of carbides in a finer, more evenly distributed form, yielding an increased rupture life.

Studies at the Naval Research Laboratory on doped cobalt alloys[51] indicated significant improvements in high temperature tensile strength, stress rupture life and ductility as a result of mischmetal additions. The more current Haynes Stellite alloy HS-188[52] shows no degradation in properties as a result of the La and Mn additions.

A mechanical property evaluation of Rene' X[5] indicated that 0.15 w/o lanthanum additions to Hastelloy X significantly increased the tensile ductility without altering the 100 hour stress rupture life. However,

*The sharp reduction in plasticity observed for nickel between 550° and 950°C.

work with Rene' Y indicated that a lanthanum content greater than 0.2 w/o and manganese higher than 1.5 w/o contributed to hot working and welding problems due to apparent incipient melting.

On the pessimistic side, studies have been conducted[53,54] which indicate that rare earth additions to stainless steels drastically impair hot workability and high temperature strength due to grain boundary and interdendretic segregation of low melting rare earth phases. Recent work at this laboratory[48] on commercial size castings of doped Rene' 100 also exhibit a degradation of high temperature properties. However, the actual severity of this problem is difficult to assess due to complicating factors such as zirconium pickup during melting.

3.0 TECHNICAL WORK PLAN

The investigation summarized in this report was conducted in two phases. Phase I was concerned primarily with screening the effects of various doping additions with respect to oxidation/hot corrosion resistance and mechanical properties. Phase II applied the knowledge gained from Phase I to further optimize the doping additions and produce scale-up heats for a more thorough evaluation of surface stability, mechanical properties, and phase stability. Details of the Phase I work plan have been reported previously[55] but Phase II studies have been modified slightly to better utilize knowledge gained from Phase I.

3.1 Phase I Screening Tests

Phase I involved a study of the effects of small additions of Group III B elements, the rare earths, thorium, and manganese, both separately and in combination, on the surface stability of Rene' 100 and AF 2-1D. Rene' 100* was selected since it is one of the strongest available cast turbine blade alloys with demonstrated metallurgical stability. Universal Cyclops developmental[57] alloy Unitemp AF2-1DA was selected since it represents a high strength forgeable nickel-base alloy showing potential for forged turbine wheels and blades. It was desirable to include a wrought alloy in this program since the optimum effect of minor element additions may be dependent on mechanical working to

*IN-100 with composition modified for maximum internal stability.[56]

refine grain size and provide a uniform distribution of secondary phases containing the minor addition elements.

A total of six doping elements, each at two concentration levels were added to Rene' 100. Two concentration levels of five rare earth elements were added to AF 2-IDA. In addition, to study interaction effects between the rare earths and Mn, alloys incorporating two or more doping elements were considered. Selection of rare earth elements was based on the physical/chemical property data tabulated in Table I. Additional considerations involved the solubility of these elements in nickel and their cost or availability. Assuming physical/chemical properties govern behavior, the elements can be divided into at least four distinct groups as shown in Table I. This breakdown along with economic factors reduces the number of rare earth elements to be evaluated. Since the addition elements vary considerably in atomic weight, their concentrations were selected on the basis of atomic weight to more equally assess their effect.

All of the alloys produced for Phase I studies were screened through a similar evaluation procedure to determine:

(1) cyclic oxidation at 2000°F and 1800°F
(2) oxidation kinetics
(3) hot corrosion at 1725 ± 25°F/50 hr with 100 ppm salt
(4) metallographic evaluation of extent of attack
(5) X-ray and microprobe identification of reaction products
(6) 1500°F stress rupture and room temperature tensile properties

In those instances where gross differences in the oxidation behavior of the various alloys was observed additional evaluation was conducted to identify the cause(s) of such behavior. This was accomplished by using the various evaluation techniques employed by M&PTL in the past[9].

3.2 Phase II Studies

After completion of Phase I, the two compositions demonstrating the greatest improvement in oxidation resistance and hot corrosion behavior were to be selected for scale up to larger size ingots for a more complete oxidation study and mechanical property evaluation. The compositions were to be selected after a review of the data and consultation with the Air Force Materials Laboratory Project Engineer. However, Phase II was subsequently redirected based on Phase I results. Phase I successfully demonstrated that certain rare earth additions at specific levels improve the surface stability of Rene' 100, however, mechanical property degradation also resulted. Therefore, no single alloy composition which contained both oxidation/hot corrosion resistance and mechanical retention was identified. Phase II effort redirection, therefore, emphasized meeting this objective by melting and testing at least six large heats (15 lbs) of selected Rene' 100 compositions designed to:

(1) further evaluate the surface stability and mechanical properties of some of the better alloys from Phase I.

(2) optimize the type and concentration of rare earths to obtain a good combination of oxidation/hot corrosion resistance and mechanical properties

(3) study the influence of vanadium on the surface stability of doped Rene' 100

(4) obtain some understanding of the factors responsible for the differences in surface stability observed between doped "chill-castings" and doped investment castings

The experimental techniques for evaluating these alloys were similar to those employed in Phase I. However, more extensive mechanical property evaluations were included.

4.0 EXPERIMENTAL PROCEDURES AND APPARATUS

The testing procedures, apparatus and evaluation techniques utilized in these studies have all been thoroughly described in other reports[7,9]. In some instances deviations from these standardized techniques were required. These deviations are described in the text to insure proper interpretation of data.

5.0 ALLOY PROCESSING AND CHARACTERIZATION

5.1 General

It is important in any alloy development program to document the processing of material and to characterize the resulting material. An understanding of material processing variables permits a better interpretation of subsequent material behavior. This was particularly true in this program where material processing proved more of a problem than originally anticipated. The following sections present a description of the processing used for the two base alloys, the difficulties encountered, and characterization (i.e., chemical analysis and structure) of the resultant material.

5.2 Preparation of Rare Earth Master Alloy

To facilitate the additions of the reactive metals to the nickel-base alloys without excessive reaction and "sputtering" losses, they were added as Ni_5 (R.E.) master alloys. Over fifty such inert arc melted alloy buttons were prepared from the elemental additions. Care was taken to insure homogeneity in each button by remelting at least four times. The elements were charged as Ni_5(R.E.) and it was originally intended to employ melting loss measurements to determine the R.E. retention of each button assuming only R.E. was lost. However, the master alloys were so brittle that they usually crumbled during removal from the furnace and determination of melting losses was impossible. A metallographic examination of the Ni_5(R.E.) alloys, typified by interdendritic phase was present. The amount of this phase was minor and seldom more than 30 volume percent. Examination under polarized light

Figure 5A(b) indicated an optically active matrix but only a portion of

the second phase polarized. Since the eutectic for the Ni-R.E. systems are near the Ni_5(R.E.) compound, the structure observed was considered hypereutectic. As a check, at least one button of each rare earth element was chemically analyzed. The results shown in Table II indicate the alloys were essentially Ni_5R.E. and the low melting phase probably a R.E. rich eutectic.

To minimize the volatility of Mn it was also added to the melts as a 50-50 Ni-Mn master alloy.

5.3 Preparation of Doped Unitemp AF-21DA

5.3.1 Melting and Extrusion of Initial Unitemp AF2-1DA Alloys

The Unitemp AF 2-1DA master alloy[57] was induction melted (~300 lb) under an argon blanket. Thirty (30) pound charges of this heat were vacuum remelted and cast into individual 15 lb ceramic hot top molds at two dopant concentration levels. This was accomplished by first adding the Ni_5R.E. master alloy to the 30 lb charge at the 0.1 a/o level, pouring one half the charge then increasing the R.E. addition to 0.2 a/o and pouring the remaining 15 lbs into another mold. The general procedures employed during the melting were as follows:

(1) Charge and vacuum remelt material from the master heat
(2) Make required additions to meet base chemistry
(3) Fully deoxidize
(4) Add rare earths and wait for the reaction to cease
(5) Tap first ingot
(6) Add more rare earths and wait for reaction to stop
(7) Tap second heat
(8) Tap chemistry heat

All of the heats acted similarly. When the deoxidizers were added the pressure in the melting chamber increased significantly. As the deoxidation reaction quieted, the pressure dropped to the level attained during melting of the bulk charge. The vacuum employed during melting was relatively high and the pressure

at tapping varied from 80 to 300 microns. A chemical analysis of the alloys determined by Spectrochemical Laboratories and GE-M&PTL, are reported in Table III. Although the metallic and non-metallic elements are within specification, the gas content is considerably higher than desired.

An evaluation of these results indicate that insufficient degassing during remelting of the master heat and furnace leakage during melting are responsible for the high gas content obtained. The increase in pressure noted upon the addition of the rare earths may be the result of reaction with the MgO crucible. Making the additions while under vacuum may also account for the reaction noted. Previous doped nickel alloy melting experience (Rene' Y) gave no such reactions when a ZrO_2 crucible was used and melting performed under a partial pressure of argon.

One half the ingot from each of two similar rare earth containing alloys were machined and canned together for "piggy-back" type extrusions. The conditions for extrusion entailed consideration of (1) rare earth phase distribution; (2) incipient melting; and (3) alloy formability. The alloys were extruded at 2025°F and an 8.5:1 ratio. An X-ray and metallographic evaluation indicated poor quality material. Figure 6 shows microstructures typifying the problems encountered with some of the extrusions, i.e. massive inclusions and stringering; extensive surface cracking; and, internal grain boundary tearing. Figure 7 illustrates the variation in stringering among the alloys. The extent of stringering was directly related to the gas content. The general structure of the alloys after electroetching is shown in Figure 8. The grain size was uniformily fine between alloys but different degrees of primary γ' formation, stringering, and carbonitride formation were noted. The rare earth rich phase could not be truly identified. Considering the gas content of the alloys and the fact that approximately 6 ppm of R.E. will react with 1 ppm O to form RE_2O_3, most of the rare earths would have reacted to form stable oxides or carbonitrides. This was borne out by an x-ray analysis of extracted residues in which considerable RE_2O_3, was detected in the alloys.

5.3.2 Remelting and Processing of Unitemp AF2-1DA Alloys

As indicated above the initial AF2-1DA alloys were unsuitable due to excessive gas contamination. All of the doped AF 2-1DA alloys were remelted utilizing the following modifications in casting technique as a means of minimizing gas contamination and poor quality castings:

(1) The use of vacuum melted base alloy melting stock
(2) The use of stabilized ZrO_2 crucibles as opposed to the less stable MgO crucibles
(3) Discard any heats where vacuum was worse than 7_u during melting
(4) Use 1/3 atm argon prior to the R.E. and Mn additions
(5) Cast directly into thick walled mild steel molds

As for the initial heats approximately thirty (30) pound charges of the vacuum melted master heat were vacuum remelted and cast into individual 15 lb. ceramic hot topped mild steel molds at the two dopant concentrations. The general procedures employed during melting are outlined below:

(1) Charge and vacuum remelt master heat
(2) Make required additions to satisfy AF 2-1DA chemistry
(3) Fully deoxidize with Al and Ti
(4) Back fill with 1/3 atm argon
(5) Add initial charge of rare earth and manganese as Ni master alloys
(6) Increase superheat, hold for approx. 3 minutes, and tap first ingot
(7) Add remainder of rare earth and manganese
(8) Repeat step #6
(9) Tap chemistry heat

Contrary to the behavior of the first series of these alloys, no excessive reaction was observed upon adding the reactive metal additions indicating deoxidation was complete. The resultant ingots were very clean with little or no surface slag formation, had good surfaces, and contained no blow holes. The chemical analyses of these alloys (Table IV) verify high quality ingots. With the exception of higher than normal Zr these chemistries are within specification. The high Zr content is the result of reaction between the reactive metal additions and the ZrO_2 crucible. The retention of the reactive metal additions was well within the 80 $\pm$ 5% initially predicted.

Since all of the ingots were cast into 2" dia. steel pipe with 1/2" wall, the mold was utilized as part of the extrusion billet. The ingots and molds were cut in two, a nose and tail plate welded to the mild steel mold, and machined into extrusion billets. The actual extrusion parameters used and the general condition of each alloy after extrusion are summarized in Table V. As indicated the extrusions of La and Ce containing alloys "rattle-snaked" badly. This was considered to be the result of extruding the ingots with "as-cast" surfaces. Thus, all ingots were de-canned, the surfaces of the ingots machined and reinserted into thicker walled extrusion cans. Upon re-extrusion, the condition of the La and Ce containing alloys, was not much improved but the other alloys all appeared to extrude well. However, subsequent metallographic examination revealed all alloys, including those which extruded well, contained microfissures. The extent of this hot tearing appeared to vary inversely as the melting point of the R.E. -Ni eutectic as shown below.

System	Ni-Rich Eutectic	R.E.-Rich Eutectic
Ni-Th	2372°F	1832°F
Ni-Gd	2354°F	1425°F
Ni-Y	2336°F	1535°F
Ni-La	2270°F	923°F
Ni-Ce	2210°F	878°F
Ni-Er	N.D.	N.D
Ni-Sm	N.D.	N.D.

N.D. - no data available

The extent of hot tearing thus increased in the following order: Th, Gd, U, La and Ce, and also increased with the concentration of the additive. As a result of excessive hot tearing no useable material was obtained from the La and Ce containing alloys (alloy #5, 6, 7 and 8), and no reliable mechanical property test specimens could be machined from any of the alloys.

Certain of the doped alloys, namely 4,8 & 10, were further processed $\approx$ 10% reduction by rod rolling at 2000°F. During this processing all the alloys fractured severely.

5.3.3 Microstructure of AF 2-IDA Alloys

The extrusion of the doped AF 2-1DA was successful in breaking down the as-cast structure thereby yielding a finer dispersion of "rare-earth" containing phases. Figure 9 shows the variation in the as-extruded microstructure of various doped alloys and Figure 10 illustrates the effect of primary working on the phase distribution. Referring to Figure 9, the following microstructural effects can be attributed to reactive element additions:

(1) The carbides of the doped alloys are more massive implying the reactive metal additions alter the carbide/matrix interaction.

(2) The reactive metal additions induce primary γ' prime eutectic formation by altering the phase relations.

Referring to Figure 10(a) and (c), the segregation of rare earth containing phases together with primary γ' eutectic modules form a continuous grain boundary network in the as-cast condition. However, as shown in Figures 10(b) and (d) primary working by extrusion breaks down the original grain boundary network and greatly refines the grains. Additional evidence for "rare-earth" phase segregation and refinement by extrusion is presented by the electron photomicrographs shown in Figures 11 and 12. These clearly depict the morphology of the "rare-earth" phase and the effect of processing on further refinement. The morphology of "rare-earth" shown in Figure 11 is typical of that expected by the last liquid to solidify indicating this phase is relatively low melting. Hence, the hot tearing produced during extrusion may be the result of phase liquation.

Attempts were made to further refine the "rare-earth" phase distribution by rod rolling the extruded material. It was also hoped that the rod rolling might "heal" the micro cracks produced during extrusion. Figure 13 illustrates that considerable refinement could be produced by rod rolling $\approx$ 10% but the material failed during this additional working.

5.4 Preparation of Doped Rene' 100 Phase I Alloys

5.4.1 Melting

The Rene' 100 base alloys for Phase I studies were vacuum melted and investment cast at the General Electric Research & Development Center. Special molds were made at the General Electric Foundry, Evendale, and were designed to provide a variety of cast specimen sizes and shapes for the screening evaluation. The mold which had a 2-1/2 lb capacity yielded the following cast shapes:

2 - 3/8" dia X 2" long bars
4 - 1/4" dia X 2" long pins
6 - 3/16" dia X 2" long pins
4 - 2" X 1/2" X 0.10" slabs
5/8" dia. down pole
1/2" square stringers

Past work on the doping of this alloy[48] has indicated a definite influence of R.E. phase size and distribution on the environmental properties of the alloy with fine intragranular precipitates being preferred. Casting parameters were thus optimized to yield a fine grained material. The initial parameters and procedure selected are outlined below:

(1) Charge and melt master alloy under vacuum ($< 5_u$)
(2) Cool to melt plus 100°F and pressurize chamber with argon to 5/6 atm
(3) Add rare earths
(4) Preheat mold to 1700°F
(5) Increase superheat to 200°F and pour

Although the casting variables selected proved satisfactory for casting La and La $\pm$ Mn containing alloys, when casting cerium containing alloys (lower Ni-R.E. eutectic temperature) hot tearing occurred during freezing. Other difficulties such as gas entrapment and nonuniform grain size were encountered. The general cluster configuration and severity of the casting problems are illustrated in Figures 14 and 15. Figure 14 (a) illustrates the hot tearing previously discussed while Figure 14 (b) illustrates the effect of high inert gas pressure

during pouring. Since the mold is both top and bottom fed, gas becomes entrapped by the molten metal and the metal freezes before the gas can escape. A mold design which feeds from the bottom only should alleviate this and the hot tearing problem. Figure 15 (a) illustrates a sound casting with a fine uniform grain size. However, in a few castings, as shown in Figure 15 (b), the grain size was rather large and varied considerably within the same casting. This effect is difficult to account for in view of the close control of casting variables and may be considered an anomaly.

These casting problems, i.e. hot cracking, and gas entrapment, were eliminated in later castings by increasing the pouring temperature to 230°F superheat and reducing the argon pressure during pouring to 1/3 atm. As a result of these changes the last series of castings produced were very sound. Therefore, although an attempt was made to hold casting variables constant to determine the effect of various rare earths on castability some factors had to be varied slightly to obtain useable material for this investigation. The following variations in casting parameters were used:

Alloys	Mold Temp.(°F)	Argon Pressure	Superheat At Pour (°F)
15-23	1700	5/6 ATM	200
24	1700	1/3 ATM	200
14, 25-35	1700	1/3 ATM	230

The concentration of the reactive metal additions to Rene' 100 is given in Table VI as both atomic and weight percent. A complete chemical analysis of one of the doped Rene' 100 alloys is given in Table VII. All elements except Zr are within the GE specification for Rene' 100. As in the case of the AF 2-1DA alloys, the high Zr content is the result of crucible attack. The alloys were melted in stabilized ZrO_2 crucibles where reduction by the rare earth elements is possible as per the following reaction:

$$4(R.E.) + 3\ ZrO_2 \rightarrow 2(R.E.)_2O_3 + 3Zr$$

According to this reaction each 1 w/o R.E. will yield only 0.5 w/o Zr. The fact that only 25% or ~.08 w/o of the rare earth added was lost during melting indicates that only 0.04 w/o Zr was introduced into the melt by this reaction. It is more likely that the rare earths produced erosion of the ZrO_2 crucible and that the excess Zr in this alloy is present as dispersed ZrO_2. The effect that this relatively high Zr content has on the oxidation or corrosion behavior of these alloys is not known. However, it is expected that the excess Zr would be more detrimental toward mechanical properties than oxidation/hot corrosion resistance.

The rare earth and Mn retention was 80-90%, with few exceptions. There were three instances (alloy #22, 24 and 28) in which the analyses indicated less rare earth than intended. Apparently, the additions in these instances were not added properly (alloy #22) or were completely slagged off during melting (alloy #24 and 28). Despite these chemistry deviations these alloys proved to be of value in determining the effect of very small dopant additions and the independent role of Mn on oxidation behavior.

5.4.2 Microstructure

The morphology of the rare earth rich phase observed in the Rene' 100 alloys was considerably different than that observed in Rene' Y[9]. It was more massive and less nearly associated with carbides. One of the best ways of observing the morphology of this, phase was in the as-polished condition, as shown in Figure 16. Frequently, however, oblique or polarized light could be used to further elucidate this phase.

Figure 17 depicts the differences in the general as-cast structure of the various doped alloys. Although these areas are representative of equivalent positions within the ingots and are taken from specimens of identical section size, marked differences are observed in the general features of the microstructures. The carbides vary from massive script type [17(a)] to a fine spheroidal type [17(e)], the interdendritic spacing varies considerably [see 17(a) and 17(e)], and the rare earth phase morphology differs. Considering the emphasis placed upon control of casting parameters and since no systematic variation in the type or concentration of addition is observed,

these structural variations are unexplainable. Evidently the structure is extremely sensitive to casting technique, or other variables are present such as tramp element contamination, which could have a major influence on morphology. In any event, the result of the oxidation studies indicated no correlation between oxidation resistance and alloy morphology. This is somewhat contrary to an earlier hypothesis based on hot corrosion results of drop castings which indicated a fine rare earth phase distribution to be most desirable. After initial examination, the specimens were etched to better define the "rare-earth" phase and its relation to other microstructure features (i.e. grain boundaries, γ-γ' eutectic nodules, and γ'). Attempts to etch the rare earth containing phase resulted in excessive reaction and eventual pitting. A microstructure sequence illustrating this is shown in Figure 18. Figure 18(a) shows the rare earth phase as a massive intragranular precipitate with some indications of intergranular formation. The hardness, as indicated by the Knoop indentions, is also noted to be greater than the matrix. A very light etch [Figure 18 (b)] more clearly defines the R.E. phase. Heavier etch [Figure 18 (c)] drastically attacks the R.E. phase but defines the microstructural relation between the γ-γ' nodules, the carbides, and the rare-earth phase. After considerable effort a metallographic technique was developed to distinguish the R.E. containing phase while simultaneously defining the other structural features. The technique consisted of electropolishing in a mixed acid solution of 47 v/o H_3PO_4 + 41 v/o H_2SO_4 + 12 v/o HNO_3 or electroetching in an 8:1 H_3PO_4 solution. However, after this treatment it was still difficult to clearly distinguish between the R.E. phase and carbides. Heat tinting at 250-300°F for 2-10 hours sufficiently darkened the rare earth phase for identification. It was then possible to compare doped and undoped Rene' 100 to determine the influence of the additions on the microstructure. The light microscopy shown in Figures 19 and 20 and the electron microscopy shown in Figures 21 and 22 clearly depict the changes in microstructure that occurred as a result of the additions. In general, the rare earth additions affect the γ-γ' eutectic and carbide formation but have little effect on the size and distribution of γ'. The rare earth elements can be classified as those

forming two phases, those concentrating near primary γ' eutectic nodules and grain boundaries, and those concentrating principally near carbides. The yttrium doped alloys are characterized by massive yttrium rich phases concentrating in grain boundaries and near carbides. The morphology of the carbide is affected by the yttrium addition yielding a very irregular shaped rather than blocky MC type carbide. Alloys containing gadolinium also form massive rare earth phases. However, these appear to be more closely associated with the γ- γ' eutectic. The alloys containing La are no different than those with La + Mn and both display rare earth rich phaes principally at carbides. The morphology of these La containing phases would appear to have less detrimental effect on properties than the Y and Gd containing phases.

Some variation is also apparent in the appearance of the rare earth containing phase among the various alloys. This variation is the result of differences in etching characteristics and may reflect differences in compound chemistries. Hence, although the phase is referred to as Ni_5(R.E.) it may actually represent a different stoichiometry or have other constituents in solution. It is worthwhile to note that the alloys displaying the most massive grain boundary rare earth phase are those which are relatively oxidation resistant. This is quite contrary to earlier studies[48].

The results of studies quantitizing the type of "rare-earth" phase formed are presented later in the section regarding structural stability.

6.0 OXIDATION/HOT CORROSION RESULTS (Phase I)

6.1 Oxidation of Unitemp AF 2-1DA Base

6.1.1 Continuous Weight Gain Tests

The kinetics of oxidation of Unitemp AF 2-1DA* have been determined, using techniques previously reported[7-9], for the temperature interval of 1400-2100°F. The continuous weight-gain data for duplicate specimens, as obtained from the actual chart recordings for specific times and temperatures

are summarized in Table VIII. The oxidation behavior of this alloy is illustrated by the log-log plots in Figure 23. These results typify the general behavior previously observed for Ni-base alloys[9] and denote the following features:

(a) Near linear oxidation at low temperature (short times) where lateral oxide growth predominates

(b) Mixed oxidation rates which are linear to quartic between 1600 and 2100°F, indicating complex oxide interactions.

(c) At 2000°F and above a decreasing oxidation rate with increasing time. This behavior implies oxide volatilization since spalling was not observed while at temperature.

The rate constants computed from the best fit curves of weight gain-vs-time or $(time)^{\frac{1}{2}}$ are summarized in Table IX along with the time intervals for which they apply. An Arrhenius type plot yields a straight line function with 1/T ($^{\circ}K^{-1}$) as shown in Figure 24. As in previous oxidation studies, this alloy displays both a linear and a dual parabolic oxidation rate. However, in comparing the oxidation rate of Unitemp AF 2-1DA with other commercial alloys (see Figure 25) certain differences are also evident:

(1) At temperatures greater than 1700°F the oxidation rate is greater than all alloys except possibly IN-100.

(2) At 2000°F the oxidation rate is a factor of 10 greater than Rene' Y.

(3) The parabolic activation energy of 107,600 cal/mole is greater than any alloy studied but similar to SM-200 (92,000 cal/mole) which also contains a high tungsten content.

(4) The initial linear oxidation rate persists at high temperatures and also displays a higher activation energy than any other alloy.

The secondary parabolic rate appears to represent some mechanical rather than thermal processes since it does not vary significantly with temperature. As verified by cyclic oxidation tests, this relatively constant rate may reflect the spalling tendencies of the alloy.

In summary, the complex oxidation behavior of this alloy precludes a meaningful kinetic analysis. However, such an evaluation is useful for comparison with other superalloys or, as will be used in this work, to determine the effect of doping element additions.

6.1.2 Isothermal and Cyclic Oxidation Tests on AF 2 1DA

Weight change results from both cyclic and isothermal static oxidation tests at 1800 and 2000°F for up to 1000 hours are presented in Table X. Both the extent of oxygen (and nitrogen) reaction and spalling tendencies are listed. The total weight change produced during isothermal testing agrees reasonably well with the continuous weight gain data. This alloy displays a marked tendency toward oxide spalling after 700 hours at 1800 and at 2000°F. The fact that the total weight change after 400 hours at 2000°F is less than that measured after 400 hours at 1800°F is further evidence for oxide volatilization at the higher temperature. However, at 1800°F, a comparison of the cyclic data with an extrapolation of the continuous weight gain curve indicates that little volatilization has occurred after 700 hours of cyclic exposure. The total weight change, which actually represents the weight of oxygen which reacts with the metal does not change appreciably with cyclic exposure at 2000°F. This indicates that the rate of volatilization in this relatively slow flowing environment is approximately 1/3 the rate of oxidation (1 unit wt. of oxygen reacts with approximately 3 unit weights of metal). This also correlates with the apparent cessation of oxidation observed during continuous exposure at 2000°F (Figure 23).

6.1.3 Metallographic Evaluation of Oxide Attack

The general appearance of the oxides produced during 100 hours of continuous oxidation at 1800, 1900, and 2000°F is illustrated in Figure 26. As previously reported for nickel-base alloys[9], this alloy demonstrates the competition between scaling and subscale reactions and the temperature dependence of this competition. During oxidation at 1800°F the relatively high activity of Cr and the low combined activities of Al and Ti promote internal

oxide formation. As γ' dissociates and the Al + Ti activity increases, sub-scale formation is favored((see Figure 26 (b) (c))and little or no interna- oxidation is formed.

Metallographic evaluation of specimens after the cyclic exposure at 2000°F denoted an irregular oxide scale with deep intergranular oxide spikes similar to those previously observed for IN-100[9]. The oxide appeared heterogeneous, both parallel and perpendicular to the substrate surface with at least three oxide phases obvious, plus TiN. After 400 hours of cyclic exposure at 2000°F the average and maximum degradation in load bearing capacity was measured to be 1.0 and 2.4 mils/side, respectively. This was considerably less than that observed for IN-100 and INCO 713C[9] after a comparable exposure.

6.1.4 Reaction Product Identification

The reaction products formed during continuous weight-gain testing were analyzed by X-ray diffraction. Both Debye film patterns of the scraped oxides and diffractometer traces of the oxide scale in situ were obtained. The general oxide appears to exist as follows:

Temp. °F	Oxide Products*
1400	$(Cr,Al)_2O_3$
1600	$(Cr,Al)_2O_3+TiO_2(w)$
1800	$Cr_2O_3+TiO_2$
2000	$TiO_2+Al_2O_3+Spinel+Cr_2O_3$
2100	$Spinel(a_o=8.08A)+Al_2O_3+TiO_2$

*Listed in order of predominance

These preliminary results indicate a Cr_2O_3/Al_2O_3 oxide at low temperatures with increasing spinel formation and Cr_2O_3 losses through volatilization at higher temperatures.

6.2 Oxidation of Doped Unitemp AF 2-1DA Alloys

6.2.1 Oxidation Behavior

The relative oxidation resistance of various doped AF 2-1DA alloys after 1000 hours continuous exposure at both 1800 and 2000°F is shown in Table XI which lists total weight change, spalling resistance and metal loss.

The cyclic oxidation behavior after 3-100 hr. cycles at 1800°F and 7-24 hr. cycles at 2000°F is summarized in Table XII. The reliability of weight change results for these specimens is questionable in view of the occurence of hot tears. The depth of penetration was difficult to evaluate for the same reason. Photomicrographs typifying the morphology of the oxidation products formed as a function of additions and exposure are shown in Figures 27 and 28. The results of these tests indicate:

(1) Very little, if any, improvement in the total weight change and only a slight improvement in spalling resistance (a factor of two maximum) with the rare earth additions.

(2) Yttrium, Gd and Mn additions appear to be most effective, but the effectiveness of the R.E. additions decreases with increasing R.E. content (above 0.1 a/o).

(3) Contrary to the results obtained for Rene' 100 alloys, (reported later) no catastrophic oxidation was observed for any alloy.

(4) Any improved behavior observed can be attributed to a combined Mn + R.E. effect although in some instances Mn additions alone are most favorable.

The results of the cyclic tests, although not included here, indicate the same trends observed for the continuously exposed specimens. Two conclusions from these results are of importance. First, catastrophic attack is not observed in any of these alloys at the high temperature indicating the rare earths, Mn or high Zr content are not responsible for this behavior. Secondly, the concentration and type of rare earth element is more significant than its distribution within the alloy.

6.2.2 Reaction Product Identification

The results of X-ray diffraction of the reaction products formed on doped AF2-1DA alloys after various time/temperature exposures are presented in Table XIII. The alloys selected for this evaluation displayed good (#3) medium (#13) and poor (#11) resistance, hence, the reaction products characterize the varying

degrees of attack. The following observations can be made from these data:

(1) Oxide formation on less resistant alloys (#1 and #11) are complex and highly heterogeneous; whereas, those formed on resistant alloys (#2 and #13) are more homogeneous and consist of only one or two oxide phases.

(2) Mn and R.E. additions promote spinel formation.

(3) Spelling occurs at the scale/subscale interfaces such as Spinel/$NiTiO_3$ and/or Spinel/Al_2O_3 + TiO_2.

(4) The activity of Al increases considerably at 2000°F and yields $(Cr,Al)_2O_3$ and spinel phases rich in Al.

6.3 Hot Corrosion of Doped Unitemp AF 2-1DA

The hot corrosion resistance of the first series of doped AF 2-1DA alloys (those that were contaminated with gas) was poor. All alloys completely oxidized/corroded during the 50 hr/1725±25°F rig test. This result, thought not conclusive, may indicate that rare-earth additions in the form of oxides are not particularly effective. However, other complicating fractors such as carbide morphology and the stringering present in these alloys may be the true causes of failure.

Two hot corrosion tests were conducted on the acceptable AF 2-1DA material. The first test displayed excellent resistance in the test environment* during the initial 17 hrs. of test but a temperature excursion ultimately produced failure. During the second hot corrosion test massive attack was observed on the base and base + Mn alloys but those containing Gd+Mn, La+Ma and Th+Mn exhibited at least a factor of 20 improvement in resistance as shown visually in Figure 29 and quantitized by the metal loss data given below:

* natural gas with 100 ppm ingested sea salt of 1.6% solution of 90% Na_2SO_4+10% NaCl

Alloy	Affected Metal (mils/side)* Gross Attack	Max Attack
Base (AF2-1DA)	-18	-20
Base + 0.8 w/o Mn	-28	-29
Base + 0.1 a/o Gd + 0.8 w/o Mn	-0.5	-1.5
Base + 0.2 a/o Gd + 0.8 w/o Mn	-0.2	-0.7
Base + 0.1 a/o La + 0.8 w/o Mn	+0.1	-0.6
Base + 0.1 a/o Th + 0.8 w/o Mn	-	-0.9
Base + 0.2 a/o Th + 0.8 w/o Mn	-0.6	-1.3

*Accuracy $\pm$ 0.5 Mil

The morphology of the reaction products formed in these alloys is shown in Figure 30 and further verifies the beneficial effects of the doping additions. The base AF 2-1DA displays gross subsurface sulfide formation; whereas, the doped alloys are relatively free of sulfide formation or those sulfides that do form are finely distributed.

Contrary to doped Rene' 100 hot corrosion and doped AF 2-1DA oxidation results all rare earth additions appear to have the same beneficial effect. This would imply that the mechanisms controlling hot corrosion and oxidation behavior are unrelated. These results indicate that the distribution of the rare earth phase and not the type of rare earth is the controlling factor. This suggests that prealloyed powder, which ought to have a finer rare-earth distribution may further enhance hot corrosion resistance.

Although AF 2-1DA displayed a favorable response toward the doping additions (particularly Y and Gd) the difficulties encountered in processing the material precluded any additional studies in Phase II. The processing problems are no doubt primarily associated with the rare earth additions but elimination of the Zr contamination by melting in Al_2O_3 crucibles may lessen the problems.

6.4 Oxidation of Doped Rene' 100 Alloys

6.4.1 Continuous Weight Gain Results

The effect of the various reactive metal additions on the oxidation kinetics of Rene' 100 have been determined using techniques previously reported[9]. The continuous weight gain data obtained from actual chart recordings for the majority of the doped alloys exposed 100 hours at 1800°F and for some alloys exposed at 100 hours at 2000°F are illustrated by the

log-log plots shown in Figures 31 through 38. The data are plotted along with undoped base alloy data for direct comparison. The oxidation rate constants computed from the slopes of the best fit straight lines formed by plotting (weight gain)^2 vs time are summarized in Table XIV along with the time interval over which the rate constants apply. Figure 39 illustrates the effect of 0.1 at.% of the various "rare-earths" on the oxidation kinetics of Rene' 100 as a function of temperature.

Most of the alloys displayed the typical dual parabolic oxidation rate at 1800°F, implying complex oxide interactions. A comparison of the oxidation rate constants indicates the initial parabolic rate constant (K_{p_I}) for most of the doped alloys tested is similar to undoped Rene' 100. Only a few of the alloys (#17 and #33) show distinctly superior initial oxidation kinetics while none of the alloys display a marked improvement in the secondary oxidation rate ($K_{p_{II}}$). Similarly, only a few alloys (#19, 25, 27, 28 and 30) show distinctly inferior oxidation kinetics at 1800°F.

All the doped alloys displayed increased oxidation rates at 2000°F when compared to Rene' 100. The behavior of the doped alloys at 2000°F was characterized by a high parabolic oxidation rate and extensive scale exfoliation both during testing and while cooling from the test temperature. The inferior behavior of the doped alloys at 2000°F was observed in all the oxidation tests conducted in Phase I and is discussed more fully later in the text.

Photomicrographs typifying the nature of the scale/subscale reactions produced during the continuous weight gain tests are shown in Figure 40. Oxidation at 1800°F((Figure 40 (a) & (c))) was typified by a semicontinuous, relatively dense, multicomponent oxide scale with little or no internal oxidation, and only minor γ' dissolution. The pitting in the grain boundaries was attributed to preferential leaching of the rare earth containing phase during etching. Figures 40b and 40d illustrate that the oxide scale completely spalled at 2000°F leaving a zone of γ' dissolution and extensive γ' degeneration. This type of reaction is apparently aggravated by the reactive metal additions since this type structure was not observed in the undoped base alloy.

Similar reactions have been observed in alloys whose surfaces have been severely cold worked thereby increasing cation diffusion rates. One might suspect therefore, that reactive element additions promote the outward diffusion of those constituents which stabilize γ' (i.e. Cr and Ti).

In summary, additions of Y, Gd and : + Th + Mn are most effective in decreasing oxidation rates but even these additives afford only a marginal improvement at 1800°F and in fact decrease oxidation resistance at 2000°F. Additions of Ce, Mischmetal, La and La + Mn have the greatest adverse effect. In general, the lower concentration level of the additive provides the greatest improvement, or is the least degrading.

6.4.2 Static Oxidation Results

Static oxidation tests were conducted on the majority of doped Rene' 100 alloys at 1000 hour/1600°F, 1000 hr/1800°F and 400 hour/2000°F. Although not part of the original program plan, these tests were included to complement the cyclic oxidation tests to provide baseline data for determining the influence of temperature cycling on scale adherence.

The static oxidation behavior of the majority of the doped Rene' 100 alloys is illustrated by the weight change, spalling and metal loss data shown in Table XV. The following observations regarding the oxidation behavior of these alloys are noteworthy:

(1) Only alloys 15, 18, 27, 28, 29 and 32 have equivalent or better oxidation resitance than Rene' 100 at 1600°F and 1800°F while all doped alloys are inferior at 2000°F.

(2) Some alloys appear more resistant at 1800°F than 1600°F (see alloy #15 and 27).

(3) In some instances, the total weight change is relatively independent of rare earth concentration (see alloys 19 & 20, 21 & 22) implying that the alloys are saturated at the lower concentration level. In other instances, increasing rare earth concentration decreases oxidation resistance (see alloy #25 and 26).

(4) The influence of Mn additions is evident from these data. A comparison of alloys 21 and 27, 28 and 29, 30 and 31, 32 and 33, and 34 and 35, indicates low levels of Mn are beneficial while increasing Mn above .2 and .25 w/o increases the extent of oxidation and oxide spalling. This is contrary to previous chill-casting results in which 0.50 w/o Mn was found to be optimum.[48]

(5) The behavior of the doped alloys at 2000°F is considered anomalous and erratic. Three different types of behavior observed: 1) The alloy may act normal (Base & #15); 2) exaggerated scale exfoliation may occur (alloys 20, 21, 23, 25, 27, 28 & 32); or 3) catastrophic oxidation may occur with no spalling (alloys 29, 30 & 31).

Attempts to link catastrophic oxidation at 2000°F with alloy composition were unsuccessful. Complete spectrographic and x-ray emission analysis were conducted to determine trump elements were present. The results showed no differenece between "normal" material and that which failed catastrophically. Therefore, the large differences in behavior cannct be explained on the basis of additive compositions. Perhaps the catastrophic attack and exaggerated exfoliation are the result of oxide melting. Examples have been cited in the literature[58] where V_2O_5 + R.E.$_2O_3$ compound oxides can melt at low temperatures. Such interactions have also been observed by NASA and TRW when making V additions to TRW-VI-A type alloys[59]. The oxidation resistance of alloys which failed catastrophically during static air exposure appeared slightly better in a flowing environment. The fact that thirty or more test specimens are usually exposed in a muffle furnace at one time may be sufficient to produce an atmosphere containing volatile and corrosive oxides. The type of attack observed might therefore be considered to be the result of volatile oxide interactions between V_2O_5, ZrO_2, O and MnO or $(R.E.)_2O_3$ oxides. This postulation is also supported by the fact that catastrophic attack was not observed in the doped AF 2-1DA alloys.

6.4.3 Cyclic Oxidation Results

During these tests the specimens were contained in zirconium silicate crucibles and upon withdrawal from the furnace were covered to prevent any loss of spalled oxide products. Hence, after the test, the total weight change of the system represented that of the crucible (less moisture or reaction products), specimen, oxidation products, and any interaction between specimen and crucible.

Initially, the weight-change analysis was conducted by weighing the specimen only (minus spalled products if spalling occurred), and computing the net weight change using the specimen weight prior to oxidation. It was subsequently discovered that this value differed from the post-test crucible plus specimen weight, minus the post-test crucible weight only. This discrepancy was eventually associated with changes in crucible weight during exposure. To correct for this weight change, blank crucibles were tested along with the specimens. In subsequent Phase II cyclic tests the crucibles were prefired at 2100°F for a minimum of 100 hours to minimize crucible weight change during cyclic exposure.

The general appearance of the majority of doped Rene' 100 alloys after ten 100 hour cycles at 1800°F is illustrated in Figures 41 and 42. The crucibles which contained the specimens are included to illustrate the relative amount of spalling which occurred during test. Although the base Rene' 100 alloy is not included in these photos its oxidation behavior is typified by the appearance of alloy #30. The total weight change and the extent of spalling for these alloys during each cycle of exposure at 1800°F are given in Tables XVI and XVII respectively. The data of Table XVI are presented graphically in Figures 43 and 44 for those alloys whose behavior is worse than Rene' 100 (Figure 43) and those alloys which are superior (Figure 44). The depth of affected metal was metallographically measured. These results, which denote both the gross and maximum oxide penetration after a cyclic exposure of 1000 hours at 1800°F, are tabulated in Table XVIII

On the basis of total weight change, spalling resistance and depth of affected metal during 1000 hours cyclic exposure at 1800°F the alloys displaying superiority to undoped Rene' 100 rank as follows:

Ranking[(a)]	Alloy #		
	Weight Gain	Adherence	Affected Metal
1	33*	18*	27
2	18*	16	28
3	28	28	30
4	16	17	32
5	17	33*	17
6	32	32	16
7	15	27	
8	27	15	

(a) order of decreasing resistance

* based on results of 500 hour cyclic exposure

Additions of Y, Gd, Mn, Y + Th + Mn and La + Mn (at certain concentrations) impart significant oxidation resistance to Rene' 100. Specifically, alloys 39, 28, 16, 17, 33 and 32 show the greatest improvement under these corditions. Contrary to those additions which decrease the oxidation resistance of Rene' 100 (i.e. La, Ce & MM), increasing additions of the beneficial elements beyond 0.1% further improves oxidation resistance. The effect of Mn additions is of particular interest. Referring to the alloy series 21, 27, 28 and 29 the influence of Mn additions is evident. Alloy 21 (0.12 a/o La) contains no Mn and displays nearly the poorest oxidation resistance. However, adding 0.12 w/o Mn to this alloy (alloy 27) improves its resistance by a factor of 10 but further additions to 0.67 w/o Mn (alloy 29) produced dation resistance. In other words although alloy #27 has 1/3 the Mn it has three times the resistance of alloy #29. Alloy #28, which contains neglibible La but 0.38 w/o Mn, has the best resistance of this series. This series of alloys illustrates that a complex relation exists between the rare-earths and Mn and that some of the other additions such as Y and Gd may be further improved by Mn additions.

The oxidation resistance of the doped alloys during cyclic exposure at 2000°F is given in Table XIX. Y and Gd additions are still most favorable but Mn additions appear to promote catastrophic oxidation. Of the nine alloys containing Mn, six of them failed catastrophically before 100 hours total exposure whsreas only the Mischmetal containing alloys of the "non-Mn" containing alloys failed catastrophically. This strongly suggests that Mn additions play a role in promoting catastrophic oxidation. The types of failures observed in the doped alloys during the 2000°F cyclic exposure are illustrated in Figure 45. As indicated many of the test coupons were completely converted to oxide within 25 hours exposure. The glassy-type appearance of some specimens implies molten oxide formation. Other specimens such as #34, #26, and #27 simply failed by massive scale exfoliation. Table XX was compiled to facilitate a comparison between the static and cyclic oxidation behavior of these alloys at 1800 and 2000°F. As indicated, those alloys which performed well in a static environment were also resistant to cyclic testing.

The metallographic appearance of the scale/subscale reaction zones produced on various doped Rene' 100 alloys after 1000 hours cyclic exposure at 1800°F are shown in Figures 46-50. In general, those alloys which exhibited good

oxidation resistance had relatively dense oxide scales with little or no internal oxidation. Alloys with poorer resistance (i.e. those containing high Mn content) were typified by considerable internal oxidation. Figure 49 illustrates the multiphase oxide scales which formed on many of the alloys. Figure 50 illustrates the nature of the internal oxidation reaction observed for those alloys subject to this form of attack. The alloy selected to illustrate this effect (alloy #29) displayed discontinuous intergranular oxidation through the entire thickness of the specimen. Initially, it was thought that the deep I.G.A. was brought about by internal oxidation of the Ni_5La phase. However, closer inspection revealed that a precipitate resembling a carbide rather than the Ni_5La phase was oxidized. It is suspected that the Ni_5La phase reacts with carbides (MC) during exposure to form La containing carbides around the Ni_5La. It is this fine La containing carbide which then oxidized internally. The exact role of Mn additions in promoting this type of attack is not precisely known but obviously it alters the competition between scale/subscale reactions.

6.5 Hot Corrosion of Doped Rene' 100 Alloys

The results of hot corrosion rig tests of doped Rene' 100 alloys at test conditions of 1700 ± 25°F/50 hours, 100 ppm Na_2SO_4 + NaCl and a gas velocity of 75 ft./sec. are tabulated in Table XXI. The general appearance of these specimens is illustrated in Figure 51. The results indicate a significant dependence upon both the type and concentration of the additions. As indicated La, Ce and Gd additions can reduce the extent of attack of Rene' 100 by a factor of 10 to 30 when added at concentrations of 0.1 a/o or more. Additions of Y and Th on the other hand were essentially ineffective. Hot corrosion tests were also conducted on the Mn containing alloys but the results were inconclusive.

The morphology of the reaction products formed (oxides and sulfides) on various alloys are shown in Figures 52 and 53. Prior to sectioning for metallorgraphic mounting, the specimens were dipped into epoxy and allowed to dry. This eliminated corrosion product losses during cutting. As a result of this process the finished metallographic section illustrates a definate layering of the surface products and clearly denotes the mode of scale failure. Figure 52 illustrates typical types of sulfidation attack in this series of alloys. The reaction typically consists of an oxide scale with underlying I.O. and sulfides (gray globular phase) within the γ' dissolution zone. The extent of each of these

reaction layers was found to differ from alloy to alloy. The attack in alloy 15 (.09 a/o Y) was characterized by a massive oxide scale and a eutectic type sulfidation zone which may represent a Ni-"NiS" eutectic. On the other hand, alloy #21 (0.12 a/o La) displays a thin relatively dense oxide with a fine uniform dispersion of subscale sulfides (presumably "CrS" type). Alloy 18 (0.23 a/o Gd) has a similar oxide scale to #21 but contained a large amount of continuous intergranular sulfides below the scale which were responsible for ~90% of the reduction in load bearing cross section. Figure 53 illustrates the morphology of the reaction zone formed in the most resistant alloy (#22-0.12 a/o La).

7.0 MECHANICAL PROPERTIES OF PHASE I ALLOYS

7.1 Rene' 100

The 1300°F tensile properties of the alloys tested are shown in Table XXII. As indicated, the strength properties of some of the alloys are within the specification for Rene' 100 but some reduction in ductility, particularly elongation, was noted. The variation in properties observed may not be the result of different reactive metal additions per se, but rather related to the casting history of the alloys or the quality of the tensile bars used. All of these alloys which display good properties, namely, alloys 15, 19, 21, 23 and 24, were cast using a lower superheat (200°F). The remaining alloys with the exception of alloy #17 were cast utilizing a 230°F superheat to improve the macroscopic quality of the casting. This observation may be fortuitous but could be related to the morphology of the rare-earth phases. However, as discussed earlier little correlation appeared to exist between rare-earth additions, casting parameters, and phase morphology.

The creep rupture properties of the same alloys at 1500°F/68 Ksi are tabulated in Table XXIII. These results indicate that the reactive metal additions (at least at the concentrations investigated here) markedly decrease the stress rupture properties of as-cast Rene' 100. However, as for the tensile properties, these results may also be influenced by casting variables.

7.2 AF 2-IDA

Difficulties were encountered in machining doped AF 2-IDA mechanical property specimens which were free from hot tears. Due to the poor quality of the materi[illegible] no useable tensile specimens could be machined.

8.0 PHASE I CONCLUSIONS

Based on the results obtained in Phase I it was concluded that the proper combination of doping elements can markedly improve the surface stability but at a sacrifice in mechanical properties. The primary goal of Phase I - that of providing a means of improving the inherent surface stability of nickel-base alloys was fulfilled. Other conclusions are summarized below:

(1) Reactive metal additions of 0.1 to 0.2 a/o produce low melting phases (presumably Ni_5'R.E.') in the grain boundaries. Modification in the carbide morphology and increasing primary γ' formation result from these additions.

(2) Workability is decreased by these additions in the following order of decreasing fabricability: Mn, Th, Gd, Y and Ce.

(3) The 1800°F oxidation kinetics of Rene' 100 were only slightly affected by the reactive metal additions. Only alloys containing Y and Gd showed improved kinetics.

(4) During static and cyclic oxidation of Rene' 100 alloys at 1600 and 1800°F only certain additions at specific concentration levels improved resistance. Additions of Y, Gd, Mn, Y + Th + Mn, and La + Mn displayed a factor of 2-20 times improvement in oxidation behavior.

(5) Additions of La and Ce, which were least effective in oxidation, improved the hot corrosion of Rene' 100 by a factor of 10 to 30. Gadolinium additions provided the best combination of oxidation/hot corrosion.

9.0 PHASE II ALLOY PROCESSING AND CHARACTERIZATION

9.1 General

Phase II alloys were designed to obtain a better balance between mechanical properties and surface stability than those studied in Phase I. Since Gd provided the best balance in properties in Phase I it was emphasized in Phase II alloys. Y and Th were also selected for study based on the results

from Phase I and from melting point considerations. (Ni-Y, Ni-Gd and Ni-Th binary systems exhibit higher eutectic temperatures than the other systems studied in Phase I). Combinations of doping elements were also selected for study in Phase II. The aim compositions of Phase II alloys are given in Table XXIV. A vanadium - free alloy was studied in Phase II since the results of Phase I prompted the postulation that V, in combination with rare-earth elements caused catastrophic oxidation at 2000°F.

9.2 Preparation of Phase II Alloys

The preparation of the Phase II alloys was similar to Phase I except that the alloys were prepared as 15 lb. heats. The V-free Rene' 100 alloy was prepared at G.E.-MAPTL by induction melting of high purity virgin materials. The Rene' 100 base alloy was purchased in accordance to G.E. spedifications.

Chemical analysis for some of the Phase II base alloys are shown in Table XXV. The alloys were within specification except for the Zr content of the V-free alloys. Apparently the high Zr resulted from reaction of the melt with the ZrO_2 crucible used in preparation of the master alloy. Alumina crucibles were used in melting the individual alloys to prevent further Zr contamination.

The dopant concentrations were determined in each alloy, the results shown in Table XXVI. Doping element retention was excellent, except in alloy #39 where the Gd content was low. There is no obvious explanation for the low Gd level.

Each alloy was cast into standard CTS test bars, flat plates and pins as indicated in Figure 54. The quality of the castings was excellent - only 2 of 108 test bars were rejected by zyglo inspection. None were rejected by x-ray. Typical variations in macrostructure of the various test specimens are shown in Figure 55. The variations in grain size were considered typical of investment cast material.

9.3 Microstructures

Optical photomicrographs of the as-cast Phase II alloys are shown in Figures 56 and 57. A typical microstructure of cast Rene' 100 alloy is shown in Figure 56a. It contains MC carbides and a small amount of $\gamma - \gamma'$ eutectic.

The vanadium-free alloy contains a larger amount of $\gamma - \gamma'$ eutectic[56b]. This is probably due to the higher Al + Ti content in the alloy rather than the absence of V. The doped alloys (56b, c and 57) contain increased amounts of $\gamma - \gamma'$ eutectic and a rare-earth containing phase. Since the rare-earth phase is most probably rich in Ni (e.g. $Ni_5R.E.$), a greater amount of $\gamma - \gamma'$ eutectic is to be expected.

Electron micrographs of selected alloys are shown in Figures 58 - 60. Typical γ', carbide and eutectic structures in base Rene' 100 are shown in Figure 58. Typical rare-earth phase distributions are indicated in Figures 59 and 60. The phase is concentrated in grain and dendrite boundaries and in regions near $\gamma - \gamma'$ eutectic colonies. The location near the coarse part of the eutectic indicates that the phase has a melting point below the $\gamma - \gamma'$ eutectic.

10.0 OXIDATION/HOT CORROSION RESULTS, PHASE II

10.1 Oxidation Tests

Phase II alloys were evaluated similarly to the Phase I alloys, utilizing continuous weight gain tests to establish kinetics and isothermal and cyclic oxidation tests.

10.1.1 Continuous Weight Gain Tests

Continuous weight gain tests were carried out at 2000°F on all the alloys and at 1800°F for alloys 36 (base) and 40 (0.1Gd). A summary of the oxidation rate constants are determined from the data are listed in Table XXVII. At 2000°F all of the alloys exhibited weight gain curves very nearly identical to the base alloy. Alloy 40 (0.1 Gd) was the best of the alloys and its behavior was compared to the base at 1800°F. The results are plotted in Figure 61. At 1800°F the doped alloy was somewhat more oxidation resistant than the base, with its rate constant going to zero after 1200 minutes. At 1800°F the rate constants for both alloys are very nearly the same as for the base and for 0.09 Gd alloy studied in Phase I (Table XIV). The oxidation rate of the base alloy at 2000°F was higher than the average value reported for Rene' 100 in Table XIV. Since only average Rene' 100 data was used for comparison in Phase I it is possible that at 2000°F the difference between

the base and the doped alloys reported in Table XIV may not be real. The rate constants for the doped alloys studied in Phase I were a factor of 10 higher than doped alloys of Phase II. The reasons for the difference are not clear, but it is possible that the base alloy used in Phase I was basically inferior in oxidation resistance at 2000°F. A comparison of the chemistries of the base alloys of Phase I and II indicates that only Zr and possibly Zr/V variations could account for the different behavior.

10.1.2 Isothermal and Cyclic Oxidation Tests

Phase II alloys were oxidized statically for 100 hours at 1600, 1800 and 2000°F. The data are presented in Table XXVIII. All the alloys behaved similarly at 1600°F. At 1800°F the base alloy exhibited the smallest weight gain but the spalling was generally less for the doped alloys indicating improved oxide adherence. At 2000°F there was no indication of catastrophic oxidation which occurred on some of the Phase I alloys in less than 25 hours.

The Phase II base alloy again exhibited much better oxidation resistance than the Phase I base.

The results of the cyclic oxidation tests are presented in Table XXIX. After 5-100 hour cycles at 1800°F the weight changes of all the alloys are probably within the accuracy of the measurements. Again the oxidation resistance of the Phase II base alloy was better than Phase I by a factor of about 3 in terms of weight gain and spalling loss. At 2000°F for 150 hours there was no indication of catastrophic oxidation as occurred on Phase I alloys. Practically all of the metal loss data reported in Table XXX is due to intergranular oxidation rather than surface scale.

10.1.3 Metallographic Observations

Typical microstructures of the alloys after oxidation are shown in Figures 62 and 63. All are characterized by intergranular oxidation, alloy depletion and multicomponent oxides.

10.2 Hot Corrosion of Phase II Alloys

Hot corrosion tests were performed for 50 hours at 1725°F following procedures outlined in Phase I. During the first test all of the alloys were severly corroded.

A second test was run for confirmation. In the second test, the test temperature was about 100°F low for a portion of the test and most of the alloys exhibited only minor corrosion. Only the base without V was moderately corroded. Microstructures of the tested specimens are shown in Figures 64 and 65. The base and the doped alloys all appeared to be about equal in terms of intergranular penetration. Alloy depletion was generally less in the doped alloys than in the base probably caused by more adherent oxide formation on the doped alloys.

Concurrent with the testing of Phase II alloys a series of Phase I alloys were tested in both the "drop cast" and investment cast conditions. "Drop" or chill casting of Rene' 100 type alloys results in a highly refined microstructure and much better distribution of the rare-earth containing phases. A comparison of typical structures is made in Figure 66. It is expected that more efficient utilization of the doping elements can be obtained in a more refined structure. Also, the minimum dopant level required for surface stability will be lower the better is the distribution. The objective of these tests were to better determine the minimum required dopant level with a near-ideal dopant distribution.

A further objective was to provide comparisons with earlier tests[5] where Mn additions were found to be required for hot corrosion resistance. The results of these tests are presented in Table XXX. In cases where a comparison can be made, Mn appears to be beneficial, however, the effects of structure, as controlled by casting technique, overshadow compositional effects. Rene' 100 base alloy exhibits poor corrosion resistance regardless of the microstructure. Most of the alloys exhibited very significantly better corrosion resistance in the "drop cast" condition. This is attributed to the improved distribution of the rare-earth containing phases in the "drop cast" alloys. Typical microstructures of the tested alloys are shown in Figures 67 and 68. Figure 67 compares the drop-cast with investment cast 0.13 w/o Y alloy. The drop-cast material exhibits a much finer microstructure and much better corrosion resistance. Additional alloys are shown in Figure 68. In 68a, the base alloy, drop-cast, exhibits no significant improvement even though the structure is refined. In 68b is shown the 0.24 w/o Y alloy which exhibited improved corrosion resistance in spite of the coarse grain structure present in the investment cast material.

The above tests demonstrate that both compositional and structural variables play a significant role in the hot corrosion behavior. Also, the results provide a plausible explanation for the wide variation in hot corrosion behavior of investment cast material even from the same alloy and same casting. A wide variety of structures can, and are found in a single casting and thus result in a variable response to a corrosive environment. It is apparent that rare-earth elements in concentrations greater than about 0.1 a/o are required for hot corrosion resistance even when the structures are near ideal (drop cast). In investment cast material the amount required must depend to a larger degree on the structure but amounts of the order of 0.2 a/o appear to be minimal.

10.3 Identification of Reaction Products

The reaction products formed on Rene' 100 alloys in both Phase I and II were examined in attempting to explain the oxidation/hot corrosion behavior of the alloys. The reaction products formed during static and cyclic oxidation testing at 1600 and 1800°F as determined by x-ray diffraction analysis are summarized in Tables XXXI through XXXIII.

Referring to Table XXXI little difference is observed in the reaction products formed on various doped Rene' 100 specimens after 1000 hours exposure at 1600°F. The principal reaction products formed ar NiO, cubic spinel, and a perovskite phase $NiTiO_3$. The lattice parameter ($a = 4.19 \text{Å}$) of the NiO phase observed on these alloys is intermediate between pure NiO ($a = 4.178 \text{Å}$) and CoO ($a = 4.26 \text{Å}$) indicating the oxide may actually be (Ni, Co) O. The lattice parameter of the spinel phase ($a = 8.32 \text{Å}$) most likely represents a (Ni, Co) Cr_2O_4 oxide phase. The parameter of the spinel of the Mn containing alloys is no different indicating little Mn present in the spinel. Contrary to earlier work the Mn additions do not appear to promote spinel formation.

The reaction products formed during the 1800°F exposure (Table XXXII and XXXIII) indicate the following:

(1) The relative resistance of the alloy is related to the intensity of the matrix lines and for static oxidation specimens the amount of spinel formed. The greater the matrix intensity - the greater the amount of spalling, and the more predominant the spinel phase-the most oxidation resistant the alloy.

(2) Oxide exfoliation initially occurs at the NiO/spinel interface and subsequently at the spinel/$NiTiO_3$ interface.

(3) The lattice parameter of the cubic spinel was found to vary from a = 8.2 Å to a = 8.35 Å implying a mixture of Ni, Co, Cr and Al. Mn additions do not promote spinel formation.

(4) The lattice parameter of the matrix decreased with decreasing oxidation resistance. This no doubt reflects a decrease of solute elements within the alloy depletion zone to yield nearly pure Ni.

(5) Those alloys exhibiting poor resistance indicated the presence of TiO_2 and Al_2O_3, indicating these compounds formed as internal oxides which were exposed due to excessive spalling.

(6) Although there were isolated diffraction patterns with one or two unidentified lines, no connection between these "unknowns" and rare-earth containing oxides could be established. Hence, rare-earth containing oxides could not be detected using this technique.

The oxidation products formed during catastrophic oxidation at 2000°F indicate principally NiO (a = 4.18 Å) and Spinel (a = 8.30 Å). The postulated low melting compound oxides of V_2O_5 + $(R.E.)_2O_3$ were not detected by x-ray.

In the absence of catastrophic oxidation at 2000°F, the spalled oxidation products are also NiO and spinel as indicated in Table XXXIII. At 2000°F the alloys which exhibit the best oxidation resistance form Al_2O_3 - rich oxides. It appears that as the temperature is increased, selective oxidation of Al occurs and results in layer formation rather than internal particle formation such as occurs at 1800°F. The beneficial effect of the doping elements at the higher temperature would appear to be in promoting the formation of a protective Al_2O_3 film. However this effect is not clearly indicated by the present data.

11.0 MECHANICAL PROPERTIES OF PHASE II ALLOYS

Phase II alloys were evaluated for tensile and stress rupture properties. The results of 1300°F tensile tests are shown in Table XXXIV. The tensile strength and the ductility of the alloys are comparable to the base Rene' 100 alloy.

Stress rupture data are presented in Tables XXXV through XXXVIII. In general the strengths of the doped alloys are equal to or higher than the base at 1500°F in high stress, short time tests. In long time tests (100-200 hrs.) at 1500°F the alloys are about equivalent although considerable scatter is evident. At 1800°F/27.5 Ksi some of the doped alloys are equivalent to the base in both rupture life and ductility. At 1800°F 20 Ksi the base alloy exhibits better life and ductility than the doped alloys. Rupture ductility, particularly the R.A., is low in the doped alloys in the long time 1800°F tests and in some cases probably limits the strength. Alloy #40 exhibits the best strength properties of the Phase II alloys both at low and high temperatures. The rupture strengths of the better alloys lie within the expected scatterband for Rene' 100 alloy as indicated in Figure 69.

12.0 DISCUSSION

The results of this investigation have demonstrated that the addition of small amounts of reactive "doping" elements can significantly improve the surface stability of Ni-base superalloys. However the attainment of significant improvements in surface stability is not without some sacrifice in other properties such as workability (in the case of wrought alloys) or strength and ductility (in the case of cast alloys).

Considering first the wrought alloys, the principal problem with high strength Ni-base superalloys is the hot working characteristics. In order to provide alloys with increased high temperature strength total alloying contents must necessarily be increased. Therefore solution temperatures for phases such as γ' are increased and the minimum hot working temperature is increased. At the same time, however, the solidus temperature is decreased because of the increased alloying. The hot working temperature range becomes almost impossibly narrow. For an alloy of the Astroloy type the range is 50 to 100°F. For AF 2-IDA the range is somewhat greater on the high temperature end due to the high carbon level which inhibits grain growth. However, the addition of rare-earth type elements result in formation of low melting compounds which narrows the hot working range. Most of the successful applications of "doping" principles have been in wrought alloys because working of the structure results in more uniform distribution of the low melting phases. More efficient use of the dopant is obtained with less detrimental effect on mechanical properties. Also, a larger amount of dopant can be added without reducing mechanical properties.

In considering future direction it would seem necessary to broaden the hot working range by adding dopant compounds having higher melting points or by starting with a more homogeneous material, such as for example might be produced through powder metallurgy techniques.

Turning to the cast alloys such as Rene' 100, additions of even small amounts of "foreign" elements cannot be considered as "minor"additions . The chemical compositions of high strength turbine blade alloys are highly balanced. This is necessary to obtain nearly equal matrix and grain boundary strengths. Addition of very small amounts of Zr and B have profound effects on the properties of Ni-base superalloys. It is generally agreed that these elements operate on grain boundary regions in an as yet incompletely explained manner. It is not too surprising then that rather large amounts of "dopants" (large compared to Zr and B contents) adversely affect the mechanical properties. As indicated in Figure 59, the rare-earth compounds in the grain boundaries can occupy a large fraction of the boundaries. Extensive microprobe studies have shown that the compounds lie in dendrite and grain boundaries - not in the matrix.

The results of Phase II demonstrate that near-parent-metal properties can be retained in an alloy which contains ~ 0.03 a/o Gd. Further, some improvement in surface stability was noted although the degree of improvement appears minor. It is possible that under actual service conditions, where the hot corrosion environment is much less severe than in the lab tests, the degree of improvement could be significant.

13.0 CONCLUSIONS

From the results of this investigation the following conclusions are offerred:

(1) Reactive metal additions can significantly improve the surface stability of Ni-base superalloys.

(2) In cast alloys the amount of doping elements required for significant surface stability improvement seriously degrade the mechanical properties.

(3) In wrought alloys, dopants seriously impair hot workability through a lowering of the solidus temperature.

14.0 RECOMMENDATIONS

Future effort on improvement of the surface stability of complex alloys through addition of reactive element additions should be concentrated on 2 fronts: First, consolidation of the alloys should include techniques which will result in a greatly improved distribution of the reactive element phase. In this way, improvements in surface stability without loss of mechanical properties may be obtained. At the present time powder metallurgical techniques would appear to offer the most promise for a successful demonstration. Secondly, considerable effort should be expended in determining the basic mechanisms through which reactive metal additions improve surface stability - particularly with respect to effects on "hot corrosion" resistance. This is particularly challenging because the hot corrosion behavior of conventional alloys is relatively imperfectly understood. Better understanding of the reactions which occur in service environments could eventually result in the development of alloys which exhibit significantly superior combinations of strength and surface stability.

15.0 REFERENCES

1. Wlodek, S.T., "The Oxidation of Hastelloy Alloy X", Trans AIME, 230, p177 (1964).

2. Wlodek, S.T., "The Oxidation of Rene' 41 and Udimet 700", Trans AIME, 230, p1078 (1964).

3. Wlodek, S.T., "The Oxidation of Ni-2% ThO_2", R62FPD140, General Electric Company, Evendale, Ohio, 4 May 1962.

4. Wlodek, S.T., "The Oxidation of L-605 and X-40", R64FPD12, General Electric Company, Evendale, Ohio, 24 January 1962.

5. Wlodek, S.T., "The Oxidation of Rene' X", DM64-438, General Electric Company, Evendale, Ohio, 9 November 1964.

6. Wlodek, S.T., "An Oxidation Study of Twelve Experimental Modifications of Rene' 41", DM64-271, General Electric Company, Evendale, Ohio, 9 July 1964.

7. Wasielewski, G.E., "Nickel-Base Superalloy Oxidation", General Electric Company Interim Progress Report No. 1, for the Period 1 July 1965 through 31 December 1965, Contract AF 33(615)-2861, DM66-23, 15 January 1966.

8. Wasielewski, G.E., "Nickel-Base Superalloy Oxidation", General Electric Company, Interim Progress Report No. 2, for the Period 1 January 1966 through 30 June 1966, Contract AF 33(615)-2861, DM66-304, 15 July 1966.

9. Wasielewski, G.E., "Nickel-Base Superalloy Oxidation", Summary Report AFML-TR-67-30, Contract AF 33(615)-2861, January 1967.

10. Wasielewski, G.E., "Effect of Minor Additions on the Hot Corrosion/Oxidation Resistance of Nickel-Base Superalloys", presented at the AIME annual meeting, 28 February 1968.

11. Moldenke, M., "Cerium in Cast Iron", Trans Am. Foundrymens Soc, 28, 368 (1919).

12. Hessenbruck, W., "Metals and Alloys for High Temperatures", Julius Springer, Berlin (1940).

13. Post, C.B. and Schoffstall, D.G., assignors to Carpenter Steel Company, "Hot Workable Alloy", U.S. Patent 2,553,330 (1951).

14. Prochovnick, A., "Metallurgical Applications of the Rare Earths", Davidson Chemical Company, Pompton Plains, New Jersey (1958).

15. Collins, J.F., Calkins, V.P., and McGurty, J.A., AECU-4424, December 1959.

16. Kleber, E V., "Rare Earth Research", The Macmillan Company, New York, 1961.

17. Eyring, Leroy, "Progress in the Science and Technology of the Rare Earths", The Macmillan Company, New York, 1964.

18. Gschnider, K.A., Jr., "Rare Earth Alloys", D. Van Nostrand Company, Inc., New York, 1961.

19. Samsonov, G.V., "High Temperature Compounds of Rare Earth Metals with Nonmetals", Consultants Bureau, New York, 1965.

20. Spedding, F.S. and Daane, A.H., "The Rare Earths", John Wiley and Sons, Incorporated, New York, 1961.

21. Hickman, J.W. and Gulbransen, E.A., Trans AIME (1949), 180, p519.

22. Gulbransen, E.A. and McMillan, W.R., "Oxide Films on Nickel-Chromium Alloys", Industrial and Engineering Chem (1953), 45, p1734.

23. Gulbransen, E.A. and Andrew, K.F., "Oxidation Studies on the Nickel-Chromium and Nickel-Chromium-Aluminum Heater Alloys", J. Electrochem Soc (1959), 106, p941.

24. Lustman, B "The Intermittent Oxidation of Some Nickel-Chromium-Base Alloys", J. of Metals, (1950), 188, p995.

25. Horn, L., Z. Metallkde. (1949), 40, p73.

26. Post, C.B., Schoffstall, D.C., and Beaver, H.O., "Hot Workability of Stainless Steel Improved by Adding Cerium and Lanthanum", J. of Metals, (1951), 3, p973.

27. Beaver, H.O., "Rare Earths in Stainless Steels", Metal Progress, (1954), 66, p115.

28. Perkins, R.A. and Binder, W.O., "Improving Hot Ductility of 310 Stainless", J. of Metals, (1957), 9, p239.

29. Wukusick, C.S. and Collins, J.E., "An Iron-Chromium-Aluminum Alloy Containing Yttrium", Materials Research, (1964), 4, p637.

30. Pettit, F.S. and Felton, E.J., J. Electrochem Soc, (1964), 111, p135.

31. Collins, J.F., Calkins, V.P. and McCurty, J.A., "Application of Rare Earths to Ferrous and Non-Ferrous Alloys", presented at ASM-AEC Symposium on the Rare Earths and Related Metals, Chicago (1959).

32. Clark, J.W. and Wukusick, C.S., "Development of High-Temperature Chromium Alloys", Semi-Annual Report No. 1, NASA CR-54486, October 1965.

33. Ibid, Semi-Annual Report No. 2, NASA CR-54486, April 1966.

34. Felton, E.J., "High Temperature Oxidation of Fe Cr Base Alloys with Particular Reference to Fe-Cr-Y Alloys", J. Electrochem Soc 108, No. 6, p490 (1961).

35. Felton, E.J., "Internal Oxidation in Iron-Chromium-Yttrium Alloys", Trans AIME, (1962), 224, p202.

36. Lombard, C.A., AFML, WPAFB, Ohio private communication.

37. Wenderott, B., "The Effect of Trace Elements in Nickel-Chromium Heat-Resisting Alloys", Z. Metallkunde, 56, No. 2, p63 (1965).

38. Seybolt, A.U., "High-Temperature Oxidation of Chromium Containing Y_2O_3", Corrosion Science, (1966), 6, p263.

39. Wasielewski, G.E., "The Oxidation Behavior of Rene' Y", submitted for publication.

40. Preece, A. and Lucas, G., "The High Temperature Oxidation of Some Cobalt-Base and Nickel-Base Alloys", J. Inst. Metals, 81, p219 (1952-53).

41. Yearian, H.J., et al, "Structure of Oxide Scales on Nickel Chromium Steels", Corrosion, 12, No. 11, p561 (1956).

42. Hancock, P., "The Corrosion of Nickel-Chromium Alloys in Sulfur-Containing Atmospheres at High Temperatures", First International Congress on Metallic Corrosion, Butterworths Press, London (1961) p193.

43. Lewis, H. and Smith, R.A., "Corrosion of High-Temperature Nickel-Base Alloys by Sulfate-Chloride Mixtures", First International Congress on Metallic Corrosion, Butterworths Press, London (1961) p202.

44. Danek, G.J., "State-of-the-Art Survey on Hot Corrosion in Marine Gas-Turbine Engines", AD-461181, March 1965.

45. Seybolt, A.U., "Observations on the High-Temperature Sulfur-Oxygen Corrosion of Nickel", General Electric Company, Research and Development Center, No. 65-C-060, October 1965.

46. Bergman, P.A., "Hot Corrosion Behavior of Nickel and Cobalt Binary and Ternary Alloys", R66SE20, SAED, General Electric Company, Lynn, Massachusetts, April 1966.

47. "Development of Hot-Corrosion Resistant Alloys for Marine Gas Turbine Service", Final Report to U.S. Navy Marine Engineering Laboratory, Contract No. 600 (61533)-63218, 1 January 1966.

48. Wasielewski, G.E., "The Effect of Rare-Earth and Manganese Additions on the Surface Stability of Nickel-Base Superalloys", R68AEG430, G.E. Co., 12/4/68

49. Clark, J.W., GE-[redacted]PTL, private communication.

50. Volkogon, G.M. and Rogelbery, I.L., "Effect of Certain Elements on the Plasticity of Nickel at Higher Temperatures", AD-618012, 7 July 1965.

51. Breen, JE. and Lane, J.R., "Effect of Rare-Earth Additions on the High-Temperature Properties of a Cobalt-Base Alloy", NRL Report No. 4523, 12 April 1955.

52. Herchenroeder, R.B., "Haynes Alloy No. 188 Aging Characteristics", Presented at International Symposium on Structural Stability, September 4-6, 1968. Seven Springs, Pa.

53. Pinnow, K.E., "The Influence of Cerium on the Hot Workability of an Austenitic Iron-Chromium-Nickel Alloy in the Cast Condition", Ph.D. Thesis, Pennsylvania State University, August 1961.

54. Pridantsev, M.V., "Influence of Impurities and Rare-Earth Elements on the Properties of Alloys", AD 634687, 18 February 1966.

55. Wasielewski, G.E., "Nickel-Base Superalloy Oxidation", General Electric Company, Interim Progress Report No. 3, for the period 15 March 1967 through 15 September 1967, TM 67-560, 15 September 1967.

56. Ross, E.W., "Rene' 100, A Sigma Free Turbine Blade Alloys", J. of Metals, December 1967, p12-14.

57. Rizzo, F.J. and Lherbier, L.W., "Development of a Wrought Nickel-Base Superalloy for Turbine Wheel/Bucket Applications", Universal Cyclops, Third Quarterly Technical Engineering Report, AF Contract 33 615-67-C1056, 1 May to 1 August 1967.

58. Kofstad, P., High Temperature Oxidation of Metals, John Wile & Sons, Inc., New York (1966).

59. Collins, H.E., "Development of High Temperature Nickel-Base Alloys for Jet Engine Turbine Bucket Applications", NASA CR-54507/TRW ER-7162, 20 June 1967.

TABLE I

SOME PROPERTIES OF THE RARE EARTHS Y, Sc AND Th

Element	At No	MP (°F)	BP (°F)	ΔH_{vap} (Kcal/mole	Oxidation States	Ionic Radii (Å)	Metal Crystal Structure [a]	Transition Temp (°F)	Atomic Radii (Å) [b]	R_2O_3 Oxide Crystal Structure [a]	R_2O_3 Oxide Transition Temp (°F)	$\Delta H_{298} R_2O_3$ (Kcal/mole)
Y	39	2748	[illegible]	95	3	0.88	hcp/bcc	2714	1.801/1.83	bcc	-	-455.45
Gd	64	2394	[illegible]	73	3	0.94	hcp/bcc	2307	1.802/1.81	bcc/mono	~ 2460	-433.94
Dy	66	2565	4226	67	3	0.91	hcp	-	1.773	bcc	-	-445.84
Ho	67	2662	4226	67	3	0.89	hcp	-	1.766	bcc	-	-449.55
Er	68	2727	4760	67	3	0.88	hcp	-	1.757	bcc	-	-453.59
Tm	69	2813	3130	56	3	0.87	hcp	-	1.746	bcc	-	-451.4
Lu	71	3006	3506	59	3	0.85	hcp	-	1.734	bcc	-	-452.8
Sc	21	2802	4946	75	3	0.68	hcp/fcc	2633	1.641/1.605	bcc	-	-410.0
Ce	58	1479	6278	93	3,4	1.02/0.92	fcc/bcc	1346	1.825/1.84	hcp/bcc	-	-435.0
Pr	59	1686	5468	79	3,4	1.00/0.90	hcp/bcc	1458	1.828/1.84	hcp/bcc	-	-435.8
La	57	1656	6278	90	?	1.05	hcp/fcc/bcc	590/1587	1.88/1.90	bcc/hcp	~ 890	-428.57
Nd	60	1866	5746	70	3	1.00	hcp/bcc	1584	1.82/1.84	bcc/hcp	~ 1075	-432.15
Sm	62	1962	2966	46	2,3	1.11/0.97	rhom/bcc	1683	1.80/1.81	bcc/mono	~ 2015	-433.39
Eu	63	1519	2712	41	2,3	1.09/0.96	bcc	-	2.042	bcc/mono	~ 2015	-
Yb	70	1515	2786	39	2,3	0.93/0.86	fcc/bcc	1468	1.94/1.98	bcc	-	-433.68
Tb	65	2472	4586	70	3,4	0.92/0.84	hcp/	2403	1.782/	fcc	-	-436.8
Th	90	3182	7592	130	4	-	fcc/bcc	2552	1.80/1.82	-	-	-293.2

[a] Above room temperature

[b] Calculated from Lattic Constants Assuming CN = 12

TABLE II

CHEMICAL ANALYSIS OF NICKEL MASTER ALLOYS

Master Alloy	Nominal[(a)] w/o R.E.	Actual * w/o R.E.	Actual * w/o Ni
Ni_5La	32.1	34.2	68.4
Ni_5Ce	32.3	33.9	67.3
Ni_5Gd	34.8	36.5	65.3
Ni_5Y	23.0	22.8	78.2
Ni_5Th	44.2	46.0	55.8
Ni_5(MM)**	-	33.4	67.7
NiMn	50.0	50.7	48.9

R.E. reactive element

(a) Assuming Stoichiometry

* Total More Than 100%

**Y Rich Mischmetal

TABLE III

CHEMICAL ANALYSIS OF CONTAMINATED AF 2-1DA ALLOYS

Wt %	MASTER	KB 2120-1	KB 2120-2	KB 2120-3	KB 2121-1	KB 2121-2	KB 2122-1	KB 2122-2	KB 2123-1	KB 2123-2	KB 2124-1	KB 2124-2	KB 2125-1	KB 2125-2
B	0.015	-	-	0.012	-	0.015	-	0.012	-	0.012	-	0.012	-	0.012
C	0.34	-	-	0.36	-	0.35	-	0.34	-	0.34	-	0.35	-	0.34
Mo	2.93	-	-	3.00	-	2.95	-	2.98	-	2.98	-	2.90	-	2.99
W	5.85	-	-	5.90	-	5.89	-	5.93	-	6.04	-	5.94	-	5.94
Zr	0.07	-	-	0.16	-	0.16	-	0.15	-	0.18	-	0.18	-	0.17
Co	9.95	-	-	9.87	-	9.85	-	9.95	-	9.98	-	9.80	-	9.90
Ti	2.93	-	-	2.95	-	2.89	-	2.93	-	3.04	-	2.98	-	3.05
Ta	1.45	-	-	1.45	-	1.42	-	1.44	-	1.50	-	1.49	-	1.46
Al	4.54	-	-	4.58	-	4.66	-	4.60	-	4.70	-	4.63	-	4.59
Cr	11.90	-	-	11.96	-	12.02	-	11.90	-	11.83	-	11.89	-	12.02
Ni	BAL	-	-	58.48	-	59.07	-	58.85	-	58.56	-	58.77	-	58.71
O_2	.025	-	-	.0022	-	.0013	-	.0084	-	.0212	-	.0249	-	.0143
N_2	.028	-	-	.016	-	.008	-	.007	-	.025	-	.026	-	.046
O_2 *	-	.0606	.0193	.0088	.1040	.0050	.030	.0067	.0236	.0139	.0266	.0145	.0124	.050
N_2 *	-	.0565	.0172	.0092	.0780	.0069	.0344	.0113	.026	.0236	.0414	.031	.018	.065
Total Gas*		.1171	.0365	.0180	.1820	.0119	.0644	.0180	.0496	.0375	.0680	.0176	.0304	.115
R.E.(a)		-	.25La .25Mn	15La .80Mn	.14 Y	.28 Y	.23Gd	.46Gd	.21Ce	.42Ce	.21La	.42La	.32Th	.64Th

(a) Nominal Analysis Assuming 80% Retention

* Analysis Performed at MDAC - All other analysis Conducted by Vendor

TABLE IV

CHEMICAL ANALYSIS OF DOPED AF 2-1DA ALLOYS

Alloy No.	Nominal w/o R.E.	Actual w/o R.E.	Analysis (w/o) C	Cr	Mn	Co	Mo	W	Ta	Al	Ti	B	Zr	ppmO(c)	ppmN(c)	Bal.
1(a)	-	-	0.34	12.01	-	9.00	2.90	6.11	1.53	4.81	3.05	0.015	0.16	87	8	Ni
1(d)	-	-	0.34	12.14	<0.10	9.96	3.23	3.87	1.68	5.01	2.93	0.014	0.28	87	8	Ni
2(d)	0.14Y	0.11(b)	0.34	12.06	0.81(b)	9.68	3.20	3.92	1.67	4.98	2.78	0.012	0.35	21	9	Ni
3(a)	0.28Y	-	0.34	11.85	0.75	10.02	2.90	5.96	1.53	4.64	2.95	0.015	0.19	35	13	Ni
4(d)	0.23Gd	0.22(b)	0.34	12.19	0.80(b)	9.85	3.26	4.07	1.67	4.97	2.88	0.012	0.26	75	2	Ni
5(a)	0.46Gd	-	0.34	11.83	0.76	9.99	2.90	5.93	1.53	4.90	3.03	0.015	0.21	35	1	Ni
6	0.21Ce	0.34(b)	-	-	-	-	-	-	-	-	-	-	-	97*	28*	Ni
7(a)	0.42Ce	-	0.34	11.86	0.75	10.21	2.90	5.96	1.49	4.87	2.98	0.015	0.19	436*	81*	Ni
8(d)	0.21La	0.20(b)	0.34	12.28	0.79(b)	9.86	3.18	4.02	1.67	5.07	2.86	0.016	0.29	18	10	Ni
9(a)	0.42La	-	0.34	11.85	0.75	9.89	2.90	5.91	1.50	4.72	3.05	0.015	0.31	28	10	Ni
10(d)	0.32Th	0.38(b)	0.34	12.01	0.84(b)	9.57	3.17	3.91	1.65	5.05	2.76	0.013	0.24	5	1	Ni
11(a)	0.64Th	-	0.34	11.85	0.75	9.89	2.90	5.91	1.50	4.72	3.05	0.015	0.31	47	1	Ni
12	0.31La	-	0.34	-	-	-	-	-	-	-	-	-	-	21	12	Ni
13(d)	-	-	0.34	12.07	0.84(b)	9.81	3.24	4.00	1.64	4.95	2.81	0.014	0.26	21	12	Ni

(a) Chemical analysis by vendor except as indicated

(b) Analysis conducted by Bowser-Morner Testing Laboratories, Inc.

(c) Analysis conducted by GE-MDL (ppm)

(d) Analysis conducted by National Spectrographic Laboratories, Inc.

* Probably pickup during extrusion

TABLE V

DATA FOR THE RE-EXTRUSION OF DOPED UNITEMP AF 2-1DA ALLOYS

Alloy No.	Heat	Minor Element Addition(w/o)	Extrusion Temp (°F)	Extrusion Ratio	Max Load (Ksi)	Max Ram Speed (IPS)	Extrusion Condition(a)
1	KB2178-1	Base	2025	8.9:1	124	2.75	Fair*
12	KB2178-2	0.31La	2025	9.1:1	128	4.5	Poor*
8	KB2179-1	0.21La+0.8Mn	1975	8.8:1	108	3.0	Poor*
9	KB2179-2	0.42La+0.8Mn	1975	9.0:1	117	5.0	Poor*
6	KB2180-1	0.21Ce+0.8Mn	1975	8.9:1	128	6.0	Poor*
7	KB2180-2	0.42Ce+0.8Mn	1975	8.8:1	130	6.0	Very Poor*
4	KB2181-1	0.23Gd+0.8Mn	2025	9.1:1	84	2.75	Good
5	KB2181-2	0.46Gd+0.8Mn	2025	9.1:1	89	3.0	Good
10	KB2182-1	0.32Th+0.8Mn	2025	8.9:1	101	2.75	Good
11	KB2182-2	0.64Th+0.8Mn	2025	9.0:1	100	3.0	Good
13	KB2183-1	0.8Mn	2025	9.0:1	101	3.0	Good
2	KB2183-2	0.14Y+0.8Mn	2025	9.1:1	99	3.0	Good
3	KB2183-3	0.28Y+0.8Mn	2025	8.4:1	100	3.0	Good
8	KB2179-1N	0.21La+0.8Mn	2025	6.9:1	136	3.0	Fair
9	KB2179-2T	0.42La+0.8Mn	2025	6.9:1	136	3.0	Poor
6	KB2180-1N	0.21Ce+0.8Mn	2025	7.1:1	116	3.25	Fair
7	KB2180-2T	0.42Ce+0.8Mn	2025	7.1:1	116	3.25	Poor
1	KB2178-1N	Base	2025	7.4:1	126	3.0	Good
12	KB2178-2T	0.31La	2025	7.4:1	126	3.0	Fair

* Were extruded again (last 6 extrusions).

(a) based upon visual, radiographs and load cells on extrusion ram.

TABLE VI

CONCENTRATION OF DOPANTS IN PHASE I RENE' 100 ALLOYS

Alloy No.	Nominal		Actual		Actual
	w/o R.E.	w/o Mn	w/o R.E.	w/o Mn	a/o R.E.
14	-	-	-	-	-
15	0.14Y	-	0.13Y	-	0.09Y
16	0.28Y	-	0.24Y	-	0.17Y
17	0.23Gd	-	0.20Gd	-	0.09Gd
18	0.46Gd	-	0.53Gd	-	0.23Gd
19	0.21Ce	-	0.18Ce	-	0.09Ce
20	0.42Ce	-	0.42Ce	-	0.21Ce
21	0.21La	-	0.24La	-	0.12La
22	0.42La	-	0.24La	-	0.12La
23	0.32Th	-	0.20Th	-	0.06Th
24	0.64Th	-	N.D.	-	N.D.
25	0.25MM	-	~0.2MM	-	~0.1MM
26	0.50MM	-	~0.4MM	-	~0.2MM
27	0.31La	0.2	0.25La	0.2/0.19	0.12La
28	0.31La	0.5	0.015La	0.38	Nil
29	0.31La	0.8	0.31La	0.72/0.62	0.15La
30	0.15La+0.2Th	0.25	0.12La+0.18Th	0.22/0.25	.06La+.06Th
31	0.15La+0.2Th	0.8	0.11La+0.17Th	0.72	.06La+.06Th
32	0.1Y+0.2Th	0.25	0.07Y+0.16Th	0.24	.05Y+.05Th
33	0.1Y+0.2Th	0.8	0.08Y+0.18Th	0.69	.06Y+.06Th
34	0.2Ce+0.31Th	0.25	-	-	-
35	0.2Ce+0.31Th	0.8	-	-	-

N.D. Below Detectable Limits

TABLE VII

CHEMICAL ANALYSIS OF SOME PHASE I DOPED RENE' 100 ALLOYS

	ANALYSIS (w/o)[a]									
Alloy No.	-	15	17	19	20	21	22	23	25	28	31
Nominal Dopant (w/o)	Base	0.14Y	0.23Gd	0.21Ce	0.42 Ce	0.21 La	0.42 La	0.32 Th	0.25 MM	0.31La 0.5 Mn	0.15 La 0.2 Th 0.8 Mn
Heat No.	C.E. Spec.	3255	3264	3253	3254	3249	3250	3266	3282	3273	3279
C	0.15-0.20	-	-	-	-	-	-	-	-	-	-
Mn	0.50 Max	<.05	<.05	<.05	<.05	<.05	<.05	<.05	<.05	0.25	0.56
Si	0.50 Max	<.05	-	<.05	<.05	<.05	<.05	<.05	<.05	<.05	<.05
S	0.015 Max	-	-	-	-	-	-	-	-	-	-
Cr	9.0-10.0	9.53	9.46	9.51	9.45	9.45	9.39	9.49	9.48	9.46	9.21
Ti	4.0-4.4	4.35	4.06	4.32	4.30	4.18	4.02	4.00	4.14	4.00	4.00
Al	5.3-5.7	5.70	5.38	5.60	5.70	5.69	5.61	5.30	5.36	5.30	5.30
Zr	0.03-0.09	0.21	-	0.27	0.36	0.19	0.13	-	-	-	-
Co	14.0-16.0	15.17	14.99	15.23	15.12	15.10	15.52	14.96	14.82	14.95	14.83
Mo	2.7-3.3	2.76	2.84	3.02	2.94	2.94	2.96	2.82	2.79	2.88	2.87
Fe	1.0 Max	0.21	0.15	0.23	0.13	0.13	0.17	0.15	0.15	0.15	0.15
V	0.9-1.1	0.95	0.93	0.97	0.97	0.96	0.97	0.93	0.92	0.94	0.92
B	0.01-0.02	0.0122	-	0.0113	0.0125	0.014	0.010	-	-	-	-
Cu	-	<.02		<.02	<.02	<.02	<.02	-	-	-	-

(a) All Analyses are Spectrographic.

TABLE VIII

SUMMARY OF CONTINUOUS WEIGHT GAIN OXIDATION TESTS OF UNITEMP AF 2-1DA AT VARIOUS TEMPERATURES

WEIGHT GAIN/AREA (mg/cm^2)

Time Mins.	1600°F (#C-3)	1600°F	1800°F (#C-9)	1800°F (#C-5)	1900°F (#C-11)	1900°F (#C-13)	1900°F (#C-4)	2000°F (#C-10)*	2000°F (#C-2)	2100°F (#C-12)*
1	-		-	-	-	-	0.042	0.041	0.140	0.122
3	-		-	-	-	-	0.097	0.081	0.280	0.351
5	-		-	-	-	0.002	0.180	0.150	0.410	0.519
10	0.014		0.015	0.014	0.015	0.014	0.332	0.310	0.560	0.748
20	0.025		0.030	0.028	0.030	0.041	0.540	0.560	0.640	1.007
30	-		0.059	0.042	0.046	0.057	0.679	0.770	0.720	1.221
40	0.039		0.074	0.042	0.046	0.072	0.962	0.950	0.950	1.404
60	0.049		0.077	0.056	0.061	0.089	0.928	1.210	1.140	1.724
80	0.052		0.082	0.077	0.076	0.108	1.050	1.360	1.290	2.045
100	0.056		0.096	0.084	0.084	0.151	1.150	1.480	1.430	2.304
120	-		0.104	0.098	0.091	0.176	1.220	1.590	1.570	2.503
150	-		0.114	0.112	0.122	0.214	1.300	1.750	1.760	2.793
180	-		0.129	0.127	0.145	0.248	1.390	1.930	1.890	3.052
240	-		0.141	0.134	0.183	0.306	1.540	2.170	2.250	3.464
300	0.070		0.148	0.141	0.213	0.394	1.650	2.370	2.410	3.799
360	-		0.159	0.155	0.244	0.473	1.750	2.530	2.590	4.074
420	-		0.178	0.183	0.274	0.560	1.810	2.670	2.760	4.303
480	-		0.178	0.197	0.305	0.676	1.870	2.780	2.900	4.517
540	-		0.178	0.225	0.335	0.778	1.910	2.870	3.050	4.609
600	0.077		0.193	0.239	0.366	0.859	1.950	2.970	3.170	4.731
720	-		0.208	0.281	0.441	0.945	2.020	3.120	3.300	5.021
840	-		0.223	0.309	0.457	1.065	2.080	3.240	3.420	5.280
960	-		0.230	0.337	0.503	1.158	2.160	3.360	3.540	5.494
1200	0.112		0.252	0.408	0.533	1.615	2.230	3.510	3.830	5.829
1500	-		0.275	0.661	0.625	2.277	2.300	3.640	4.050	6.104
1800	0.119		0.289	0.717	0.671	2.955	2.410	3.720	4.330	6.211
2400	0.126		0.312	0.745	0.808	4.044	2.550	3.880	4.730	6.302
3000	0.140		0.260	0.956	0.960	4.897	2.670	3.920	4.920	6.317
3600	0.168		0.252	1.055	1.082	6.086	2.780	3.990	5.030	6.440
4200	0.182		0.267	1.153	1.188	6.844	2.830	4.090	5.070	6.455
4800	0.189		0.326	1.237	1.265	7.568	2.910	4.140	5.130	6.516
5400	0.224		0.282	1.322	1.356	8.237	3.130	4.170	5.110	6.531

* Specimens had fabrication cracks.

TABLE IX

SUMMARY OF RATE CONSTANTS FOR THE

OXIDATION OF AF 2-IDA (HT# KC 1564)

TEST NO.	TEMP (°F)	RATE CONSTANTS
C-1	1400	K_L=3.85 X 10^{-7} (300 - 4800 MIN)
C-3	1600	K_L=9.36 X 10^{-6} (10 - 40 MIN) TRANSITION (100 - 3000 MIN) K_{P_I}=2.0 X 10^{-7} (3000 - 6000 MIN)
C-9	1600	K_L=3.34 X 10^{-6} (10 - 40 MIN) K_P=7.64 X 10^{-7} (200 - 1500 MIN)
C-5	1800	K_L=5.0 X 10^{-5} (10 - 20 MIN) K_{P_I}=4.87 X 10^{-6} (360 - 6000 MIN)
C-11	1800	K_L=4.20 X 10^{-5} (10 - 30 MIN) K_{P_I}=6.11 X 10^{-6} (1000 - 6000 MIN)
C-13	1900	K_L=2.09 X 10^{-4} (1 - 20 MIN) K_{P_I}=2.76 X 10^{-5} (100 - 3600 MIN) $K_{P_{II}}$=1.67 X 10^{-6} (3600 - 6000 MIN)
C-4	2000	K_L=5.75 X 10^{-4} (1 -10 MIN) K_{P_I}=2.17 X 10^{-4} (20 - 120 MIN) $K_{P_{II}}$=1.91 X 10^{-5} (1000 - 6000 MIN)
C-10	2000	K_L=5.50 X 10^{-4} (1 - 15 MIN) K_{P_I}=1.40 X 10^{-4} (500 - 1000 MIN) $K_{P_{II}}$=1.72 X 10^{-5} (1800 - 6000 MIN)
C-2	2100	K_{P_I}=1.21 X 10^{-4} (500 - 2200 MIN) $K_{P_{II}}$=4.50 X 10^{-5} (2200 - 4800 MIN)
C-12	2100	K_{P_I}=4.5 X 10^{-4} (100 - 1000 MIN) $K_{P_{II}}$=1.23 X 10^{-5} (1800 - 4000 MIN)

K_L=mg/cm^2/sec, K_P=mg^2/cm^4/sec

Values in parenthesis indicate time during which each rate constant applies.

TABLE X

STATIC OXIDATION OF UNITEMP AF 2-IDA*

Temp °F	Time Hrs.	Spec. Wt. Gain[a] (mg/cm²)	Spalling Loss[b] (mg/cm²)	Total Wt. Change[c] (mg/cm²)
		Isothermal		
1800	100	+1.314	0.128	+1.442
1800	400	+0.368	2.979	+3.347
2000	25	+0.815	0.663	+1.478
2000	100	-0.358	3.753	+3.328
2000	400	-4.014	9.233	+5.219
		Cyclic[d]		
1800	100	+1.314	-	+1.242
1800	200	+1.714	0.157	+1.871
1800	300	+2.100	0.199	+2.299
1800	400	+2.428	0.199	+2.627
1800	500	+2.693	0.428	+3.127
1800	600	+2.613	0.957	+3.570
1800	700	+1.785	1.927	+3.712
1800	800	-2.256	6.425	+4.169
1800	900	-3.318	7.416	+4.098
1800	1000	-6.526	10.595	+4.069
2000	25	+0.815	0.663	+1.477
2000	50	+0.195	1.712	+1.947
2000	75	-2.361	4.556	+2.430
2000	100	-2.872	5.289	+2.568
2000	125	-3.286	5.938	+2.872
2000	150	-3.452	4.791	+1.533
2000	175	-3.659	4.971	+1.491
2000	200	-3.742	5.413	+1.726
2000	225	-4.101	5.828	+1.727
2000	250	-4.529	6.477	+1.948
2000	275	-5.772	8.106	+2.334
2000	300	-5.979	8.244	+2.265
2000	325	-6.407	8.892	+2.485
2000	350	-8.740	11.007	+2.267
2000	375	-9.666	11.934	+2.268
2000	400	-10.812	13.146	+2.334

* Ht KC 1564

(a) Weight change of specimen only.

(b) Algebraic sum of (a) - (b) represents oxide lost through spalling.

(c) Total weight change of crucible containing specimen and spalled products (corrected for crucible wt. change).

(d) Cycled to room temperature at each time interval.

TABLE XI

STATIC OXIDATION BEHAVIOR OF SOME DOPED AF2-1DA ALLOYS

Alloy No.	w/o R.E.	w/o Mn	1000 Hr/1800°F Specimen (mg/cm²)	Total (mg/cm²)	Spalling(a) (mg/cm²)	Metal Loss(b) Gross	Max	1000 Hr/2000°F Specimen (mg/cm²)	Total (mg/cm²)	Spalling(a) (mg/cm²)	Metal Loss(b) Gross	Max
1	-	<0.1	-1.99	5.57	7.56	1.7	2.2	-8.74	8.06	16.79	2.0	4.2
2	0.11Y	0.81	1.80	5.40	3.60	0.7	1.3	-6.42	8.28	14.70	1.9	3.5
3	0.28Y*	0.75	7.55	11.21	3.66	0.9	2.7	-4.68	7.40	12.09		
4	0.22Gd	0.80	-0.81	6.29	7.10	0.5	1.1	-11.95	7.37	19.32		
5	0.46Gd*	0.76	-6.96	7.18	14.14	0.2	1.3	-19.70	12.93	32.63		
10	0.38Th	0.84	-0.06	5.04	5.10	0.4	1.2	-7.09	12.17	19.26		
11	0.64Th	0.75	-14.28	13.91	28.19	2.1	3.7	-32.12	19.71	51.83	3.5	6.0
12	-	0.84	1.67	4.49	2.82	1.6	2.8	-9.21	7.20	16.40	2.3	4.9

* Nominal analysis

(a) Spalling occurs predominantly on cooling

(b) Mils/Side

TABLE XII

CYCLIC OXIDATION BEHAVIOR OF SOME DOPED AF2-1DA ALLOYS

Alloy No	Nominal w/o Dopant	w/o Mn	1800°F/300 hrs (100 hr cycles) Specimen (mg/cm²)	Spalling (mg/cm²)	Metal Loss Gross	Max	2000°F/175 hrs (25 hr cycles) Specimen (mg/cm²)	Spalling (mg/cm²)	Metal Loss Gross	Max
1	Base	-	2.18	N.D.	0.4	1.2	-4.13*	N.D.	0.75*	2.50*
2	0.08Y	0.8	0.40		0.8	1.2	-3.07		0.25	0.95
3	0.20Y	0.8	4.37		0.1	1.1	2.11		0.25	1.5
4	0.10Ce	0.8	-1.46		0.15	1.0	-7.94		0.05	1.2
5	0.20Gd	0.8	2.05		0.75	2.0	-13.44		1.20	2.9
8	0.10La	0.8	1.96		-	1.1	-12.11		1.70	2.9
9	0.20La	0.8	4.08		0.05	0.7	-22.50		3.80	5.3
10	0.14Th	0.8	0.53		0.5	1.2	-7.27		0.70	1.6
11	0.20Th	0.8	2.75		1.3	2.6	-18.77		1.4	2.8
13	-	0.8	1.64		0.8	1.3	-		2.0	3.0

N.D. No date due to erratic crucibles

* After 125 hrs exposure with 25 hr cycles

TABLE XIII

REACTION PRODUCTS FORMED DURING OXIDATION OF VARIOUS DOPED AF2-1DA ALLOYS

Alloy #	w/o Additions	Wt. Gain(3) (mg/cm^2)	Type Spec.	Reaction Products
1800°F/1000 Hr.				
1-8A	Base	5.57	(1)	NiO(vs)+Spinel(a_o=8.35Å)(m)+TiO_2(m) +Matrix+Spinel(a_o=8.13Å)(mw)$NiTiO_3$(w)
1-8A	Base	5.57	(2)	Spinel(a_o=8.31Å)(vs)+NiO(m)
2-9	0.11Y+0.8Mn	5.40	(1)	Spinel(a_o=8.35Å)(vs)+$NiTiO_3$(mw)
2-9	0.11Y+0.8Mn	5.40	(2)	Spinel(a_o=8.35Å)(vs)
11-9	0.64Th+0.8Mn	13.91	(1)	NiO(a_o=4.17Å(s)+Spinel(a_o=8.36Å(ms) +TiO(m)Cr_2O_3(m)
11-9	0.64Th+0.8Mn	13.91	(2)	NiO(a_o=4.19Å)(s)+Spinel(a_o=8.34Å)(s) + Cr_2O_3(w)+TiO_2(vvw)
13-8A	0.8Mn	4.49	(1)	Spinel(a_o=8.35Å)(vs)+$NiTiO_3$(vvw)
13-8Z	0.8Mn	4.49	(2)	Spinel (a_o=8.13Å)(vs)
1800°F/3-100 Hr. Cycles				
1-8	Base	2.19	(1)	TiO_2(s)+Cr_2O_3(m)+Matrix(m)
2-8	0.11Y+0.8Mn	0.39	(1)	Spinel(a_o=8.32Å)(s)+NiO(s)+$NiTiO_3$(m) +Matrix(w)
11-8	0.64Th+0.8Mn	2.76	(1)	NiO(vs)+Spinel(a_o=8.40Å)(s)+TiO_2(vw)
13-8	0.8Mn	1.04	(1)	Spinel(a_o=8.34Å)(vs)+NiO(w)+Matrix(w) +TiO_2(w)+$NiTiO_3$(w)
2000°F/1000 Hr.				
1-11	Base	8.06	(1)	TiO_2(s)+Al_2O_3(ms)+Spinel(a_o=8.10Å)
2-11	0.11Y+0.8Mn	8.28	(1)	Spinel(a_o=8.10Å)(s)+Al_2O_3(ms)+TiO_2(m)
11-11	0.64Th+0.8Mn	19.71	(1)	Spinel(a_o=8.11Å)(vs)+Al_2O_3(m)+TiO_2(m)
13-11	0.8Mn	16.4	(1)	Spinel(a_o=8.12Å)(m)+Al_2O_3(m)+TiO_2(m)

s-strong, m-medium, w-weak, v-very

(1) Oxids in situ.

(2) Spalled oxide products

(3) Total specimen wt. gain plus spalled products

TABLE XIV

SUMMARY OF OXIDATION RATE CONSTANTS FOR SOME DOPED RENE 100 ALLOYS

1800°F

Test No.	Alloy No.	a/o R.E. + w/o Mn	K_{P_I} (a)	$K_{P_{II}}$ (b)
*	-	Base	1.5×10^{-5} (10-400 Min)	3.0×10^{-6} (400-6000 Min)
C-47	14	Base	1.20×10^{-5} (10-900 Min)	2.22×10^{-6} (900-6000 Min)
C-25	15	.09Y	1.30×10^{-6} (20-2300 Min)	5.41×10^{-6} (2300-6000 Min)
C-51	17	.09Gd	6.00×10^{-6} (50-1500 Min)	2.62×10^{-6} (1500-4200 Min)
C-49	18	.23Gd	1.47×10^{-5} (20-500 Min)	3.48×10^{-6} (840-6000 Min)
C-33	19	.09Ce	7.40×10^{-5} (10-400 Min)	1.50×10^{-5} (400-6000 Min)
C-27	20	.21Ce	3.12×10^{-5} (10-6000 Min)	-
C-28	21	.12La	2.04×10^{-5} (10-625 Min)	2.65×10^{-5} (625-6000 Min)
C-48	23	.06Th	1.76×10^{-5} (20-900 Min)	1.36×10^{-6} (900-6000 Min)
C-37	25	~.10MM	4.30×10^{-5} (10-500 Min)	1.16×10^{-5} (1800-6000 Min)
C-39	27	.12La + .2Mn	1.38×10^{-4} (10-600 Min)	1.59×10^{-5} (700-6000 Min)
C-43	28	Nil + .38Mn	4.94×10^{-6} (10-900 Min)	6.29×10^{-6} (900-6000 Min)
C-46	30	.06La+.06Th+.22Mn	4.35×10^{-5} (170-625 Min)	9.55×10^{-6} (625-6000 Min)
C-50	33	.06Y+.06Th+.69Mn	1.14×10^{-5} (50-3000 Min)	-

2000°F

*	-	Base	6.8×10^{-5} (10-150 Min)	3.7×10^{-6} (400-6000 Min)
C-24	15	.09Y	1.80×10^{-4} (10-150 Min)	2.29×10^{-5} (300-6000 Min)
C-32	19	.09Ce	5.26×10^{-2} (10-80 Min)	2.91×10^{-3} (80-500 Min)
C-26	20	.21Ce	2.14×10^{-3} (20-700 Min)	-
C-30	22	.12La	1.42×10^{-3} (10-250 Min)	1.12×10^{-3} (250-1030 Min)
C-36	25	~.10Mn	2.79×10^{-3} (10-350 Min)	-
C-38	27	.12La + .2Mn	1.17×10^{-3} (10-200 Min)	4.32×10^{-4} (200-3000 Min)
C-40	28	Nil + .36Mn	2.01×10^{-3} (10-840 Min)	-
C-41	29	.15La +.67Mn	1.30×10^{-3} (10-50 Min)	4.69×10^{-2} (50-80 Min)

* Avg. rate constants from previous tests on René 100

(a) K_{P_I} = Initial parabolic rate constant ($mg^2/cm^4/sec$)

(b) $K_{P_{II}}$ = Secondary parabolic rate constant ($mg^2/cm^4/sec$)

Values in parenthesis indicate duration which rate constant applies

TABLE XV

STATIC OXIDATION BEHAVIOR OF SOME DOPED RENE' 100 ALLOYS

Alloy No.	Wt% B.S.	Wt% Hf	[illegible] Hr/1800°F Total Wt/A (mg/cm²)	[illegible] Hr/1800°F Spalling[a] (mg/cm²)	1000 Hr/1800°F Total (mg/cm²)	1000 Hr/1800°F Metal Loss (Mils/Side)[b] Gross	1000 Hr/1800°F Metal Loss (Mils/Side)[b] Max.	1000 Hr/1800°F Spalling[a] (mg/cm²)	400 Hr/2000°F Total (mg/cm²)	400 Hr/2000°F Metal Loss (Mils/Side)[b] Gross	400 Hr/2000°F Metal Loss (Mils/Side)[b] Max.	400 Hr/2000°F Spalling[a] (mg/cm²)
14	[illegible]	-	2.48	[illegible]	[illegible]	1.0	2.9	1.25(c)	3.57	-	-	4.06(c)
15	.09Y	-	1.80	-0.13	2.29	0.3	1.3	0.16(c)	3.90	0.35	1.8	7.34(d)
16	.23Gd	-	-	-	3.74	0.1	0.9	0.98(c)	-	-	-	-
19	.09Ce	-	8.54	0.37	19.16	2.1	5.1	69.19(e)	44.32	6.2	11.1	156.22(e)
20	.21Ce	-	6.47	0.63	18.88	2.5	7.3	87.17(e)	48.99	9.5	11.5	174.52(e)
21	.12La	-	3.74	-0.21	16.08	2.8	6.1	53.61(e)	26.89	5.0	9.2	95.08(e)
22	.12La	-	4.53	-0.26	15.80	2.8	4.8	49.43(e)	25.58	4.2	8.0	91.23(e)
23	~.1%Hf	-	4.42	-0.04	9.36	-	4.5	22.79(e)	58.72	-	-	214.02(e)
26	~.2%Hf	-	4.96	-0.15	19.62	-	7.0	62.76(e)	-	-	-	-
27	.12La	.2	2.81	-0.17	2.52	-	1.0	-0.04(c)	44.25	-	-	159.07(e)
28	Bil	.38	1.53	-0.10	2.56	-	0.8	0.45(c)	38.63	-	-	141.47(e)
29	.12La	.67	2.02	-0.16	3.43	-	2.6	1.15(c)	152.05	-	-	1.59(f)
30	.08La+.08Th	.22	2.58	-0.25	4.70	-	2.8	5.82(d)	198.33	-	-	1.84(f)
31	.08La+.08Th	.72	2.76	-0.08	12.27	1.5	7.3	40.12(e)	284.27	-	-	5.11(f)
32	.05Y+.05Y	.34	2.40	-0.13	4.70	-	-	4.59(d)	85.97	-	-	115.13(e)
33	.05Y+.05Y	.89	-	-	11.22	1.7	4.5	11.7%(d)	-	-	-	-
34	.05Ce+.10Th	.35	-	-	5.22	1.8	4.9	7.88(c)	-	-	-	-
35	.05Ce+.10Th	.89	-	-	7.51	1.3	5.3	21.39(e)	-	-	-	-

(a) Spalling which occurs predominantly during cooling

(b) Gross refers to metal loss due to conversion to massive oxide - maximum refers to metal lost due to internal oxide formation

(c) Film spalling

(d) Medium flakes (1/32" - 1/16" dia)

(e) Large flakes (> 1/16" - 1/8" dia)

(f) Oxidation catastrophic (Specimen completely to oxide) - No metal spalling observed, value represents reaction between crucible and specimen.

TABLE XVI

EFFECT OF 1800°F CYCLIC OXIDATION ON THE WEIGHT CHANGE OF VARIOUS DOPED RENÉ 100 ALLOYS

Alloy No.	a/o R.E.	w/o Mn	Total Weight Change (mg/cm^2)(a) No. of 100 Hr. Cycles(b) 1	2	3	4	5	6	7	8	9	10
14		-	-	-	2.15	2.86	3.29	4.02	4.58	5.33	5.72	6.13
15	.09Y	-	2.20	2.67	2.62	3.15	3.36	3.68	3.51	4.28	4.99	5.44
16	.17Y	-	1.64	2.13	2.17	2.14	2.60	2.75	2.61	2.67	2.78	2.87
17	.09Gd	-	1.92	2.43	2.61	2.86	3.11	3.28	3.25	3.42	3.58	3.95
18(c)	.23Gd	-	1.85	2.37	2.24	2.31	2.08	-	-	-	-	-
19	.09Ce	-	2.73	3.83	3.05	2.83	5.15	6.77	8.87	12.92	16.25	18.79
20	.21Ce	-	3.52	7.02	7.47	8.31	13.12	17.73	20.98	27.17	28.18	31.88
21	.12La	-	2.95	6.26	4.67	1.32	1.07	4.64	8.60	13.80	17.65	21.75
22	.12La	-	2.59	4.82	5.16	-0.14	3.53	4.74	8.67	8.77	12.45	13.66
23	.06Th	-	3.01	3.73	4.82	6.41	8.20	9.88	11.87	15.80	19.51	23.03
24	<.001Th	-	2.16	2.54	3.28	4.70	6.00	6.97	8.08	10.04	12.08	14.35
25	~0.1MM	-	2.22	3.37	4.31	5.68	8.51	11.10	12.34	17.25	19.75	23.80
26	~0.2MM	-	3.31	5.28	5.87	8.46	12.00	16.72	21.91	26.84	20.85	35.47
27	.12La	.19	2.43	2.36	2.38	2.82	3.05	3.40	3.68	4.50	5.21	6.20
28	Nil	.38	1.88	2.58	2.45	2.38	2.75	2.62	2.49	2.41	2.60	2.68
29	.15La	.67	2.38	3.70	4.02	4.24	5.31	6.65	7.49	9.09	10.60	14.77
30	.06La+.06Th	.23	1.76	2.56	2.69	3.02	3.04	3.49	3.86	4.70	5.40	6.90
31	.06La+.06Th	.72	2.41	3.20	3.71	4.63	6.36	8.04	10.08	13.05	16.08	19.65
32	.05Y+.05Th	.24	-	-	-	-	-	3.30	3.46	3.68	3.87	4.39
33(c)	.06Y+.06Th	.69	1.74	1.67	1.96	2.18	2.29	3.01	4.15	-	-	-
34(c)	.09Ce+.10Th	.25	3.33	3.57	5.44	6.62	7.94	11.97	15.38	-	-	-
35(c)	.09Ce+.10Th	.80	4.02	4.81	6.99	8.67	12.37	15.73	18.79	-	-	-

(a) Total weight change of specimen assuming all reaction products remained adherent. - Ave. of duplicate specimens.

(b) Cooled to room temperature and weighed after each cycle.

(c) Data questionable due to anomolous crucible behavior.

TABLE XVII

EFFECT OF 1800°F CYCLIC OXIDATION ON THE SCALE ADHERENCE OF VARIOUS DOPED RENÉ 100 ALLOYS

Alloy No.	a/o R.E.	w/o Mn	Amount of Spalling (mg/cm²)(a) No. of 100 Hour Cycles(b) 1	2	3	4	5	6	7	8	9	10
14	-	-	0.21	0.74	1.96	3.67	4.32	7.10	9.11	11.03	13.13	16.68
15	.09Y	-	0.08	0.32	0.28	0.76	1.12	1.38	1.79	3.38	7.99	10.50
16	.17Y	-	0.07	0.31	0.08	0.11	0.49	0.50	0.44	0.43	0.59	0.70
17	.09Gd	-	0.16	0.43	0.61	0.78	1.27	1.63	1.83	2.46	2.87	3.80
18(c)	.23Gd	-	0.41	-0.04	-0.27	0.04	0.21	-	-	-	-	-
19	.09Ce	-	0.06	1.11	3.88	10.65	20.84	30.03	46.85	67.77	84.52	100.46
20	.21Ce	-	-0.02	4.77	8.42	36.83	57.02	80.01	101.72	124.65	142.30	158.84
21	.12La	-	-0.02	6.10	8.11	24.98	28.64	50.79	74.36	97.33	116.25	134.61
22	.12La	-	2.03	3.95	5.37	14.42	32.43	35.82	57.94	68.90	87.92	100.72
23	.06Th	-	0.35	0.64	4.35	11.07	17.21	23.86	32.83	55.43	94.16	91.38
24	<.001Th	-	0.20	2.70	7.24	12.76	18.47	25.07	30.86	41.98	53.25	65.46
25	~0.1MM	-	-0.12	0.51	2.72	10.70	24.38	37.68	45.77	70.20	82.09	99.74
26	~0.2MM	-	0.34	4.55	18.34	27.14	45.02	66.68	89.32	113.03	134.19	157.58
27	.12La	.19	-0.03	2.34	0.13	0.22	0.47	1.29	2.33	3.93	6.56	9.76
28	Nil	.38	0.09	0.51	0.78	1.04	1.59	1.88	1.96	2.06	2.38	2.70
29	.15La	.67	0.08	0.46	0.69	0.95	2.46	6.29	14.14	18.47	35.29	56.84
30	.06La+.06Th	.23	-0.19	0.12	0.23	0.45	0.54	2.12	3.07	6.36	11.49	17.48
31	.06La+.06Th	.72	-0.06	0.25	2.08	5.27	12.18	21.17	28.99	49.20	64.08	74.31
32	.05Y+.05Th	.24	-0.04	0.73	1.12	1.24	1.86	1.90	2.44	3.51	4.15	6.16
33(c)	.06Y+.06Th	.69	0	-0.20	-0.20	0.36	2.14	7.09	11.76	-	-	-
34(c)	.09Ce+.10Th	.25	0.35	0.12	6.77	9.93	20.80	45.23	62.41	-	-	-
35(c)	.09Ce+.10Th	.80	0.36	0.57	18.34	23.80	98.26	74.20	79.23	-	-	-

(a) Weight of spalled products collected in the crucible per unit original spec. surface area - average of duplicate specimens

(b) Cooled to room temperature between cycles

(c) Data questionable due to anomolous crucible behavior.

TABLE XVIII

DEPTH OF METAL ATTACK DURING CYCLIC OXIDATION AT 1800°F

DOPED RENÉ 100 ALLOYS

Alloy No.	a/o R. E.	w/o Mn	Spalling (mg/cm^2)[a]	AFFECTED METAL (MILS/SIDE) Gross Attack[b]	Max. Attack[b]
14	-	-	16.68	0.8	2.8 (c)
15	.09Y	-	10.50	1.8	4.2 (c)
16	.17Y	-	0.70	0.5	2.9 (c)
17	.09Gd	-	3.80	0.3	2.6 (c)
18	.23Gd	-	0.21*	-	-
19	.09Ce	-	100.46	6.3	11.1 (d)
20	.21Ce	-	158.84	8.0	11.4 (d)
21	.12La	-	134.61	7.0	10.2 (d)
22	.12La	-	100.72	6.9	10.5 (d)
23	.06Th	-	91.38	6.3	19.5 (d)
24	<.001Th	-	65.46	4.2	5.6 (d)
25	~.1 MM	-	99.74	5.1	8.5 (d)
26	~.2 MM	-	157.58	8.1	10.8 (d)
27	.12La	.19	9.76	0.1	1.7 (c)
28	Nil	.38	2.70	0.6	1.7 (d)
29	.15La	.37	56.84	4.4	9.4 (c)
30	.06La + .06Th	.28	17.48	0.1	2.5 (c)
31	.06La + .06Th	.72	74.31	3.6	5.7 (d)
32	.05Y + .05Th	.24	6.16	0.4	2.5 (c)
33	.06Y + .06Th	.69	1.47*	-	-
34	.09Ce + .10Th	.25	20.08*	-	-
35	.09Ce + .10Th	.80	47.65*	-	-

* Spalling after five cycles - tests still in progress.

(a) That metal loss due to formation of massive surface oxide (including spalled oxide). Determined by measuring unaffected cross section.

(b) That metal loss due to (a) plus any I.G.A. and I.O. or max. penetration where scale is irregular measured as above.

(c) Erratic scale with little or no I.O.

(d) Uniform scale with I.G.A. or I.O.

TABLE XIX

CYCLIC OXIDATION BEHAVIOR OF DOPED RENE' 100 ALLOYS AT 2000°F

Alloy No.	a/o R.E.	w/o Mn	Total Weight Change and Spalling (mg/cm^2)(a) No. of 5 Hour Cycles(b) 1 Δ W/A	1 Spall	2 Δ W/A	2 Spall	3 Δ W/A	3 Spall	4 Δ W/A	4 Spall	4 Gross(d)	4 Max(d)	16 Δ W/A	16 Spall	16 Gross(d)	16 Max(d)
14	-	-	3.18	7.59	3.89	9.53	3.59	9.74	4.30	11.16	-2.0	-3.8	-	-	-	-
15	.09Y	-	1.83	0.52	2.33	0.95	2.55	1.25	2.71	1.98	-	-	13.41	51.66	- 3.0	- 5.2
16	.17Y	-	1.57	3.20	2.02	4.64	1.54	4.80	1.70	5.28	-0.4	-4.7	-	-	-	-
17	.09Gd	-	1.96	1.93	5.13	15.97	7.55	24.59	10.27	57.44	-0.6	-1.8	40.53**	213.57**	-	-
18(c)	.23Gd	-	2.12	1.44	2.78	5.95	2.10	5.05	2.66	7.49	-0.8	-2.4	-	-	-	-
19	.09Ce	-	9.22	30.11	14.53	54.80	20.57	81.66	27.02	112.62	-	-	211.63	729.93	-	-
20	.21Ce	-	10.44	33.86	17.17	62.74	18.74	87.34	25.74	120.31	-	-	146.87	487.10	-	-
21	.12La	-	3.68	1.99	3.76	2.08	4.45	7.10	7.14	21.67	-	-	184.06	730.29	-18.2	-19.2
22	.12La	-	1.92	0.12	2.48	0.56	2.56	0.88	3.28	6.02	-	-	74.89	361.46	-	-
23(c)	.06Th	-	1.87	1.42	3.12	6.11	5.22	14.81	10.83	38.11	-5.0	-6.4	-	-	-	-
24	N.D.	-	2.14	1.83	3.42	5.31	6.94	21.48	10.51	41.67	-	-	38.51**	203.89**	-	-
25	.10MM	-	11.11	37.93	182.82*	-	-	-	-	-	-	-	-	-	-	-
26	.20MM	-	9.13	31.34	166.22*	-	-	-	-	-	-	-	-	-	-	-
27	.12La	0.19	9.51	29.51	24.18	93.33	225.57*	-	-	-	-	-	-	-	-	-
28	Ni	0.38	4.63	13.35	13.75	54.17	24.89	109.4	41.31	181.0	-7.4	-10.0	90.10**	418.28**	-	-
29	.15La	0.67	166.59*	-	-	-	-	-	-	-	-	-	-	-	-	-
30	.06La+.06Th	0.23	227.49*	-	-	-	-	-	-	-	-	-	-	-	-	-
31	.06La+.06Th	0.72	207.81*	-	-	-	-	-	-	-	-	-	-	-	-	-
32	.05Y+.05Th	0.24	3.76	7.84	5.25	26.38	15.98	59.57	24.76	08.33	-1.5	-3.4	74.78**	331.86**	-	-
33(c)	.06Y+.06Th	0.69	3.87	6.83	5.77	16.89	9.53	33.87	15.21	07.15	-7.1	-9.3	-	-	-	-
34(c)	.09Ce+.10Th	0.25	8.82	35.99	88.96	356.49	210.35*	-	-	-	-	-	-	-	-	-
35(c)	.09Ce+10Th	0.80	252.35*	-	-	-	-	-	-	-	-	-	-	-	-	-

* Failed catastrophically during this cycle

** Test stopped after ten cycles

(a) Total weight change assumes all products remain adherent - all data average of two duplicate specimens

(b) Cooled to room temperature after each cycle

(c) Data questionable due to anomolous crucible behavior

(d) Refers to metal loss in Mils/Side

TABLE XX

COMPARISON OF CYCLIC AND STATIC OXIDATION

OF SOME DOPED RENÉ 100 ALLOYS

	1000 hr/1800°F					
	Cyclic [a]			Continuous		
Alloy No.	Specimen (mg/cm^2)	Total (mg/cm^2)	Spalling (mg/cm^2)	Specimen (mg/cm^2)	Total (mg/cm^2)	Spalling (mg/cm^2)
14	-10.55	6.13	16.68	1.82	3.07	1.25
15	-5.06	5.44	10.50	2.12	2.29	0.16
16	3.57	2.87	0.70	-	-	-
17	0.15	3.95	3.80	-	-	-
18	2.29*	2.08*	0.21*	2.75	3.74	0.98
19	-81.67	18.79	100.46	-42.02	19.16	61.19
20	-126.96	31.88	158.84	-48.28	18.88	67.17
21	-112.86	21.75	134.61	-37.54	16.08	53.61
22	-87.06	13.66	100.72	-33.63	15.80	49.43
23	-68.35	23.03	91.38	-	-	-
24	-51.11	14.35	65.46	-	-	-
25	-75.94	23.80	99.74	-13.43	9.36	22.79
26	-122.11	35.47	157.58	-43.13	19.62	62.76
27	-3.56	6.20	9.76	2.56	2.52	-0.04
28	-0.02	2.68	2.70	2.11	2.56	0.45
29	-42.07	14.77	56.84	2.28	3.43	1.15
30	-10.58	6.90	17.48	-1.12	4.70	5.82
31	-55.66	18.65	74.31	-27.85	12.27	40.12
32	-1.77	4.39	6.16	-0.49	4.10	4.59
33	0.16*	1.63	1.47*	-12.84	-1.22	11.74
34	-12.86	7.22*	20.08*	-4.63	3.22	7.85
35	-35.89*	11.76*	47.65*	-14.08	7.21	21.29

	400 hr/2000°F					
	Cyclic [b]			Continuous		
15	-38.3	13.4	51.7	-3.37	3.96	3.62
19	-517.5	212.0	729.5	-111.89	44.32	156.22
20	-339.5	147.0	486.5	-127.53	46.99	174.52
21	-545.0	184.0	729.0	-68.19	26.89	95.08
22	-286.6	74.9	361.5	-65.67	25.56	91.23

(a) 10-100 hour cycles to room temperature

(b) 16-25 hour cycles to room temperature

* 5-100 hour cycles completed - Data Questionable

TABLE XXI

EFFECT OF RARE EARTH ADDITIONS ON THE

HOT CORROSION RESISTANCE OF DOPED RENE' 100

(1700°F/50 Hr in 100 ppm Na_2SO_4 + NaCl)

Alloy No.	a/o R.E.	Depth of Attack (mils/dia) Gross[a]	Total[b]	Metallographic Description
14	-	-59.0	-68.0	Massive Oxidation and Sulfidation
15	0.09Y	-20.7	-22.3	Massive Oxidation - Sulfidation Looks Like Eutectic
16	0.17Y	-22.3	-27.0	Massive Oxidation - Little Sulfidation
17	0.09Gd	-	-49.1	Massive Oxidation - Medium Sulfidation
18	0.23Gd	- 0.2	- 2.8	Medium Oxidation - Heavy Sulfidation
19	0.09Ce	- 7.4	- 8.5	Massive Oxidation - Few Sulfides
20	0.21Ce	- 1.9	- 3.7	Massive Oxidation - Few Sulfides
21	0.12La	- 1.2	- 2.3	Little Oxidation - Very Fine Sulfides
22	0.12La	- 0.2	- 1.6	Little Oxidation - Very Fine Sulfides
23	0.06Th	- 6.3	-15.5	Massive Oxidation - Heavy Sulfidation
24	<0.02Th	-40.0	-50.6	Massive Oxidation and Sulfidation

(a) Depth of Massive Oxide/Sulfide Attack

(b) Total Attack Including Internal Oxides and Sulfides

TABLE XXII

INFLUENCE OF DOPING ADDITIONS ON THE 1300°F TENSILE PROPERTIES OF RENÉ 100

Alloy No.	a/o R.E.	w/o Mn	UTS (Ksi)	.02% Y.S. (Ksi)	0.2% Y.S. (Ksi)	R.A. (%)	Elong (%)
-	G.E. Spec		120	-	100	8.0	-
14	-	-	140	85	104	15.0	10.0
15	.09Y	-	125	94.5	110	6.5	1.5
16	.17Y	-	58	58	*	Nil	1
17	.09Gd	-	65	61.6	*	Nil	Nil
19	.09Ce	-	117	97	115	5.0	1.5
21	.12La	-	112	90.9	108	4.5	1.5
23	.06Th	-	114	91.5	107	6.5	1.5
24	.02Th	-	117	91.9	106	8.0	2.5
25	.10MM	-	33	31	*	Nil	Nil
27	.12La	.2	29.1	27.4	*	Nil	Nil
28	NiL	.38	111	86.5	105	4.5	1.5
29	.15La	.67	68.5	68.5	*	Nil	Nil
31	.06La+.06Th	.72	106	91	106	Nil	Nil
33	.06Y+.06Th	.69	99.5	83.2	99.3	4.5	1.5
35	.09Ce+.10Th	.8	50.5	50.5	*	0.5	1

* Specimen broke before 0.2% Y.S. was obtained

TABLE XXIII

INFLUENCE OF DOPING ADDITIONS ON THE CREEP RUPTURE PROPERTIES OF RENÉ 100

Alloy No.	a/o R. E.	w/o Mn	1500°F/68 ksi (a) Time (hrs) To % Creep of 0.1	0.2	0.5	1.0	Rupture Life (hrs)	R.A. (%)	Elong (%)
14	-	-	0.1	0.7	6	21	106.2	15.0	10.3
15	.09Y	-	-	0.05	0.3	-	0.6	1.3	2.2
16	.17Y	-	-	-	-	-	FOL	1.3	1.4
17	.09Gd	-	0.1	0.2	2.4	-	4.0	1.3	1.2
19	.09Ce	-	0.3	-	-	-	1.3	0.8	1.4
21	.12La	-	0.4	-	-	-	1.1	1.0	1.8
23	.06Th	-	0.2	0.3	-	-	4.5	0.7	1.7
24	<.02Th	-	0.2	1.1	6	15	20.3	5.2	2.9
25	~.10MM	-	-	-	-	-	FOL*	-	-
27	.12La	.2	-	-	-	-	FOL	0.7	1.5
28	Nil	.38	0.3	-	-	-	0.9	5.3	1.7
29	.15La	.67	-	-	-	-	FOL	Nil	1.7
31	.06La + .06Th	.72	-	-	-	-	0.2	0.7	2.2
33	.06Y + .06Th	.69	-	-	-	-	FOL	2.6	0.8
35	.09Ce + .06Th	.8	0.3	-	-	-	1.3	1.3	1.4

FOL - Failed on loading

(a) Nominal gage section: 0.14" dia. X 0.64" long

* Failed in threads before total load was applied.

TABLE XXIV

PHASE II ALLOYS AIM CHEMISTRY

Alloy #	Composition
36	Rene' 100 Base
37	Rene' 100 (Less V)
38	Rene' 100 + 0.03 a/o Gd + 0.2 w/o Mn
39	Rene' 100 (Less V) + 0.03 a/o Gd + 0.2 w/o Mn
40	Rene' 100 + 0.03 a/o Gd
41	Rene' 100 + 0.10 a/o Gd
42	Rene' 100 + 0.02 a/o Y + 0.03 a/o Th + 0.25 Mn
43	Rene' 100 + 0.02 a/o Y + 0.03 Gd + 0.25 Mn
44	Rene' 100 (Less V) + 0.03 a/o Y + 0.25 w/o Mn

TABLE XXV

CHEMICAL ANALYSIS Of SOME PHASE II DOPED ALLOYS

Alloy No.	36	37	38	43	44
Nominal Dopant (w/o)	Base	Base	Base (Less V)	0.07Gd 0.02Y 0.25Mn	0.07Gd 0.02Y 0.25Mn
Heat No.	G.E. Spec.	S948	S950	S955	S956
C	0.15- 0.20	-	-	-	-
Mn	0.50 Max	< 0.05	< 0.05	0.22	0.22
Si	0.50 Max	-	-	-	-
S	0.015 Max	-	-	-	-
Cr	9.0-10.0	9.27	9.23	9.16	9.23
Ti	4.0- 4.4	4.16	4.30	4.16	4.30
Al	5.3- 5.7	5.54	5.60	5.41	5.53
Zr	0.03-0.09	0.08	0.45	0.12	0.52
Co	14.0-16.0	15.42	14.94	15.08	15.01
Mo	2.7- 3.3	2.96	2.96	2.98	3.04
Fe	1.0 Max	0.18	0.13	0.15	0.13
V	0.9- 1.1	0.94	0.08	0.94	0.09
B	0.01-0.02	-	-	-	-
N_2	-	5 ppm	5 ppm	4 ppm	4 ppm
O_2	-	30 ppm	25 ppm	40 ppm	23 ppm
H_2	-	2 ppm	3 ppm	3 ppm	2 ppm

(a) All analysis except gases were spectrographic

TABLE XXVI

CONCENTRATION OF DOPANTS IN PHASE II RENE' 100 ALLOYS

Alloy No.	Nominal w/o R.E.	Nominal w/o Mn	Actual w/o R.E.	Actual w/o Mn	Actual a/o R.E.
36	-	-	--	< 0.05	-
37	-	-	--	< 0.05	-
38	0.11Gd	0.2	0.10Gd	0.24	0.043Gd
39	0.11Gd	0.2	0.065Gd	0.24	0.028Gd
40	0.10Gd	-	0.09Gd	-	0.040Gd
41	0.23Gd	-	0.24Gd	-	0.106Gd
42	0.02Y + 0.095Th	0.25	0.015Y ' 0.07Th	0.28	0.01Y ' 0.02Th
43	0.07Gd + 0.02Y	0.25	0.055Gd + 0.014Y	0.28	0.02Gd + 0.01Y
44	0.07Gd + 0.02Y	0.25	0.055Gd + 0.011Y	0.29	0.02Gd + 0.005Y

N.D. Below Detectable Limits

TABLE XXVII

SUMMARY OF OXIDATION RATE CONSTANTS FOR PHASE II ALLOYS

Temp.	Alloy No	Test No.	KPI[a]	KPII[b]
2000	36	1-B	2.74×10^{-4} (10-60 min)	1.1×10^{-5} (100-1500 min)
2000	37	2-B	2.90×10^{-4} (1-60 min)	1.03×10^{-4} (400-2400 min)
2000	38	3-B	Linear (1-8 min)	1.49×10^{-5} (100-3000 min)
2000	39	4-B	1.64×10^{-4} (3-30 min)	1.16×10^{-4} (180-3000 min)
2000	40	5-B	4.3×10^{-4} (1-10 min)	1.42×10^{-5} (100-2400 min)
2000	41	6-B	3.08×10^{-4} (1-10 min)	---
2000	42	7-B	---	2.3×10^{-5} (150-3000 min)
2000	43	8-B	Linear (1-7 min)	1.62×10^{-5} (180-3000 min)
2000	44	9-B	Linear (1-10 min)	5.67×10^{-5} (40-360 min)[c]
				1.32×10^{-5} (480-3000 min)[b]
1800	36	1-A	3.85×10^{-5} (3-100 min)	4.79×10^{-6} (420-3000 min)
1800	40	5-A[d]	5.8×10^{-6} (3-420 min)	1.07×10^{-6} (420-1200 min)

(a) KPI = Initial Parabolic Rate Constant ($Mg^2/Cm^4/sec$)

(b) KPII = Secondary Parabolic Rate Constant ($Mg^2/Cm^4/sec$)

(c) KPII = Transition (Not Predictable)

Values in Parenthesis indicate duration which rate constant applies

(d) After 1200 min. K became zero

TABLE XLVIII

STATIC OXIDATION BEHAVIOR OF PHASE II DOPED RENE' 100 ALLOYS

Alloy No.	Nominal Composition w/o	Total Δ wt (mg/cm^2)	Spalling (mg/cm^2)	Max. Metal Loss (mils/side)
			100 Hr/1600°F	
36	Rene' 100 Base	0.26	N.D.	-1.3
37	Rene' 100 (Less V)	0.33	N.D.	-0.7
38	R'100 + 0.11Gd + 0.2Mn	0.25	N.D.	-0.3
39	R'100 (Less V) + 0.11Gd + 0.2Mn	0.38	N.D.	-1.6
40	R'100 + 0.10Gd	0.19	N.D.	-1.5
41	R'100 + 0.23Gd	0.29	N.D.	-1.1
42	R'100 + 0.02Y + 0.095Th + 0.25Mn	0.35	N.D.	-0.1
43	R'100 + 0.07Gd + 0.02Y + 0.25Mn	0.32	N.D.	-1.5
44	R'100 (Less V) + 0.07Gd + 0.02Y + 0.25Mn	0.35	N.D.	-1.2
			100 Hr/1800°F	
36	Rene' 100 Base	0.72	0.21	-1.0
37	Rene' 100 (Less V)	0.98	1.13	-1.6
38	R'100 + 0.11Gd + 0.2Mn	0.75	0.13	-1.4
39	R'100 (Less V) + 0.11Gd + 0.2Mn	1.09	0.14	-2.0
40	R'100 + 0.10Gd	0.83	0.11	-1.5
41	R'100 + 0.23Gd	0.89	0.09	-2.5
42	R'100 + 0.02Y + 0.095Th + 0.25Mn	0.92	0.23	-0.7
43	R'100 + 0.07Gd + 0.02Y + 0.25Mn	0.88	0.07	-2.0
44	R'100 (Less V) + 0.07Gd + 0.02Y + 0.25Mn	1.17	0.29	-2.2
			100 Hr/2000°F	
36	Rene' 100 Base	1.95	3.73	-2.0
37	Rene' 100 (Less V)	4.62	10.86	-4.6
38	R'100 + 0.11Gd + 0.2Mn	2.04	5.25	-3.1
39	R'100 (Less V) + 0.11Gd + 0.2Mn	2.78	4.38	-2.7
40	R'100 + 0.10Gd	2.17	3.05	-1.9
41	R'100 + 0.23Gd	2.02	2.49	-2.9
42	R'100 + 0.02Y + 0.095Th + 0.25Mn	4.74	11.11	-3.6
43	R'100 + 0.07Gd + 0.02Y + 0.25Mn	2.76	5.79	-2.3
44	R'100 (Less V) + 0.07Gd + 0.02Y + 0.25Mn	2.17	2.30	-3.1

N.D. Below Detectable Limits

TABLE XXIX

CYCLIC OXIDATION BEHAVIOR OF PHASE II DOPED RENE' 100 ALLOYS

Alloy No.	Nominal Composition w/o	150 Hrs/2000°F(a) Total Δ wt. (mg/cm²)	Spalling Δ wt. (mg/cm²)	Max Metal Loss mils/side(b)
36	Rene' 100 base	+1.74	3.13	-1.5
37	Rene' 100 (Less V)	+3.37	6.87	-2.7
38	Rene' 100 + 0.11Gd + 0.2Mn	+1.59	3.85	-1.7
39	Rene' 100 (Less V) + 0.11Gd + 0.2Mn	+2.21	3.13	-2.5
40	Rene' 100 + 0.10Gd	+1.91	3.28	-1.5
41	Rene' 100 + 0.23Gd	+1.77	3.93	-3.4
42	Rene' 100 + 0.02Y + 0.09Th + 0.25Mn	+2.65	6.09	-4.2
43	Rene' 100 + 0.07Gd + 0.02Th + 0.25Mn	+2.32	3.74	-2.0
44	Rene' 100 (Less V) + 0.07Gd + 0.02Th + 0.25Mn	+2.34	2.79	-2.0

Alloy No.	Nominal Composition w/o	500 Hrs/1800°F(c) Total Δ wt. (mg/cm²)	Spalling Δ wt. (mg/cm²)	Max Metal Loss mils/side(b)
36	Rene' 100 base	1.31	1.03	-1.6
37	Rene' 100 (Less V)	2.28	2.38	-3.2
38	Rene' 100 + 0.11Gd + 0.2Mn	1.23	0.64	-3.2
39	Rene' 100 (Less V) + 0.11Gd + 0.2Mn	1.77	0.77	-3.8
40	Rene' 100 + 0.10Gd	1.26	0.70	-2.0
41	Rene' 100 + 0.23Gd	1.59	0.80	-2.0
42	Rene' 100 + 0.02Y + 0.09Th + 0.25Mn	1.60	1.31	-3.9
43	Rene' 100 + 0.07Gd + 0.02Th + 0.25Mn	1.40	0.53	-2.4
44	Rene' 100 (Less V) + 0.07Gd + 0.02Th + 0.25Mn	0.97	1.04	-7.4

(a) Two - 25 hour cycles and one - 100 hour cycle, each cooled to room temperature

(b) Average of 3 measurements to an accuracy of ± 0.5 mil

(c) Five - 100 hour cycles

TABLE XXX

COMPARISON OF HOT CORROSION RESISTANCE OF DROP CAST AND INVESTMENT CAST DOPED RENE' 100 ALLOYS

(1725±25°F/50 hr @ 100 ppm Salt)*

Alloy No.	w/o Addition	Cast Form(a)	Metal Loss (mils/dia)(b) Gross	Total	General Appearance
--	U-700	W	- 0.0	- 3.6	V. Good - Tan Oxide
14	Rene' 100 Base	D.C.	-52.8	-56.8	V. Poor - Massive Growth
15	0.13Y	D.C.	- 0.6	- 4.5	Good - Blk Oxide
15	0.13Y	I.C.	-29.8	-32.6	Fair - Spalling
16	0.24Y	D.C.	- 0.4	- 5.4	Good - Blk Oxide
16	0.24Y	I.C.	- 0.0	- 2.7	Good - Blk Oxide
17	0.20Gd	D.C.	-35.4	-37.7	V. Poor - Massive Growth
17	0.20Gd	I.C.	-27.9	-32.1	V. Poor - Massive Growth
18	0.53Gd	D.C.	- 6.5	- 8.2	Good - Blk Oxide
18	0.53Gd	I.C.	-12.6	-15.3	Fair-- Spalling
22	0.24La	D.C.	- 5.0	-11.9	Good - Blk Oxide
22	0.24La	I.C.	-16.5	-17.7	V. Poor - Massive Growth
23	0.20Th	D.C.	- 1.5	- 5.1	V. Good - Tan Oxide
23	0.20Th	I.C.	- 0.7	- 3.2	V. Good - Tan Oxide
27	0.25La + 0.2Mn	D.C.	- 0.4	- 2.2	Good - Blk Oxide
27	0.25La + 0.2Mn	I.C.	-11.2	-12.9	V. Poor - Massive Growth
28	0.015La + 0.38Mn	D.C.	- 2.1	- 5.1	Fair - Spalling
28	0.015La + 0.38Mn	I.C.	-12.9	-14.2	V. Poor - Massive Growth
30	0.12La + 0.18Th + 0.25Mn	D.C.	- 7.0	-10.3	Fair - Spalling
30	0.12La + 0.18Th + 0.25Mn	I.C.	-15.2	-16.7	V. Poor - Massive Growth
32	0.07Y + 0.16Th + 0.24Mn	D.C.	- 9.5	- 6.9	Good/Fair - Blk Oxide
32	0.07Y + 0.16Th + 0.24Mn	I.C.	-20.2	-22.2	V. Poor - Massive Growth

---

* Alloys 14-18 and 22-32 were tested separately - Alloys 22-32 may have been 25&50°F below temperature.

(a) W = wrought; D.C. = Drop Cast; I.C. = Investment Cast

(b) Average of 3 readings where gross is massive oxide formation and total loss includes internal oxidation and/or sulfidation

TABLE XXXI

SUMMARY OF REACTION PRODUCTS FORMED ON VARIOUS DOPED RENÉ 100 ALLOYS AFTER 1000 HRS. EXPOSURE AT 1600°F

Alloy	Oxidation[b] Resistance	Reaction Products[a]
14	6	NiO(s)(a_o=4.19Å)+Spinel(m)(a_o=8.33Å)+$NiTiO_3$(m)
25	7	NiO(vs)(a_o=4.19Å)+Spinel(w)(a_o=8.32Å)+$NiTiO_3$(w)
27	4	NiO(s)(a_o=4.19Å)+$NiTiO_3$(mw)+Spinel(w)(a_o=8.32Å)
28	1	NiO(s)(a_o=4.19Å)+$NiTiO_3$(mw)+Spinel(w)(a_o=8.32Å)+TiO_2(vw)
29	5	NiO(s)(a_o=4.19Å)+$NiTiO_3$(mw)+Spinel(mw)(a_o=8.32Å)+Al_2O_3(vw)
30	3	NiO(vs)(a_o=4.19Å)+Spinel(w)+$NiTiO_3$(w)
32	2	NiO(s)(a_o=4.19Å)+$NiTiO_3$(m)+Spinel(w)(a_o=8.32Å)

(a) Determined employing diffractometer traces in situ, compared to standard ASTM cards and listed in order of decreasing intensity.

(b) Relative oxidation resistance considering total weight change data.

s: strong, m: medium, w: weak, v: very

TABLE XXXII

SUMMARY OF REACTION PRODUCTS FORMED ON VARIOUS DOPED RENÉ 100 ALLOYS AFTER 1000 HRS. EXPOSURE AT 1800°F

CONTINUOUS

Alloy	Oxidation Resistance[b]	Type X-Ray	Reaction Products[a]
14	4	(c)	Matrix(s)(a_0=3.57 Å)+Spinel(m)(a_0=8.34Å)+$NiTiO_3$(m) NiO(w)+TiO_2(vw)
14	-	(d)	Spinel(vs)(a_0=8.30Å)+$NiTiO_3$(w)
25	7	(c)	Spinel(s)(a_0=8.2Å)+NiO(m)(a_0=4.17Å)+Matrix(m)(a_0=3.56Å) +Al_2O_3(w)
26	9	(c)	Matrix(vs)(a_0=3.54Å)+Spinel(m)(a_0=8.27Å)+Al_2O_3(w) +TiO_2(vw)
26	-	(d)	Spinel(vs)(a_0=8.30Å)+NiO(s)(a_0=4.2Å)+$NiTiO_3$(vw)
27	1	(c)	Spinel(s)(a_0=8.27Å)+$NiTiO_3$(ms)+Matrix(m)(a_0=3.57Å)
28	2	(c)	Spinel(s)(a_0=8.34Å)+NiO(m)(a_0=4.17Å)+Matrix(m)(a_0=3.57Å) +$NiTiO_3$(m)
29	3	(c)	Spinel(s)(a_0=8.34Å)+NiO(s)(a_0=4.21Å)+Matrix(m)(a_0=3.56Å) +$NiTiO_3$(m)
30	6	(c)	Matrix(vs)(a_0=3.57Å)+Spinel(s)(a_0=8.27Å)+$NiTiO_3$(vw)
31	8	(c)	Matrix(m)+Spinel(m)+$NiTiO_3$(w)+TiO_2(w)+Al_2O_3(w)
31	-	(d)	Spinel(s)(a_0=8.34Å)+NiO(ms)(a_0=4.20Å)+$NiTiO_3$(vw)
32	5	(c)	Spinel(m)(a_0=8.34Å)+NiO(m)(a_0=4.18Å)+Matrix(m)(a_0=3.57Å) $NiTiO_3$

CYCLIC[e]

14	3	(b)	Matrix(vs)(a_0=3.57Å)+NiO(s)(a_0=4.18Å)+$NiTiO_3$(m)+Spinel(vw)
16	1	(b)	NiO(s)(a_0=4.18Å)+Matrix(ms)(a_0=3.57Å)+$NiTiO_3$(m)+Spinel(m) (a_0=8.35Å)
17	2	(b)	NiO(vs)(a_0=4.18Å)+Matrix(ms)(a_0=3.57Å)+$NiTiO_3$(m) +Spinel(m)(a_0=8.37Å)
23	4	(b)	NiO(m)(a_0=4.20Å)+Matrix(m)(a_0=3.54Å)+$NiTiO_3$(m)+Spinel(m) (a_0=8.38Å)+TiO_2(vw)+Al_2O_3(vw)
25	5	(b)	Matrix(vs)(a_0=3.53Å)+NiO(s)(a_0=4.18Å)+Spinel(ms)(a_0=8.35Å) +$NiTiO_3$(m)+Al_2O_3(vw)

(a) Determined from ASTM cards and listed in order of decreasing intensity.
(b) Relative resistance considering total weight change and spalling resistance.
(c) Diffractometer trace of oxides in situ.
(d) Diffractometer trace of spalled oxides.
(e) 10 - 100 hour cycles, cooling to room temperature after each hold period

s: strong, m: medium, w: weak, v: very

TABLE XXXIII

SUMMARY OF REACTION PRODUCTS FORMED ON PHASE II ALLOYS

AFTER EXPOSURE AT 1800° AND 2000°F

Alloy No.	Oxidation Resistance(b)	Type X-ray	Reaction Products(a)
			1800°F/100 hrs (Isothermal)
36	3	c	Matrix + $NiTiO_3$ + Spinel + TiO_2
40	2	c	Matrix + 2 Spinels + $NiTiO_3$ + TiO_2
43	1	c	Matrix + 2 Spinels + $NiTiO_3$ + TiO_2
44	4	c	Matrix + $NiTiO_3$ + 2 Spinels
			1800°F/500 hrs (Cyclic)
36	2	c	Matrix + Spinel
37	5	c	Matrix + Spinel + $NiTiO_3$
37	5	d	Spinel + $NiTiO_3$
40	1	c	Matrix + $NiTiO_3$ + 2 Spinels
43	3	c	Matrix + $NiTiO_3$ + Spinel
44	4	c	Matrix + $NiTiO_3$ + 2 Spinels + NiO
			2000°F/100 hrs (Isothermal)
36	3	c	Matrix + Spinel + Al_2O_3 + $NiTiO_3$ + TiO_2
40	1	c	Matrix + Al_2O_3 + Spinel + $NiTiO_3$
43	2	c	Matrix + Al_2O_3 + Spinel + TiO_2
44	4	c	Matrix + $NiTiO_3$ + Spinel + Al_2O_3
			2000°F/150 hrs (Cyclic)
36	1	c	Matrix + Al_2O_3 + Spinel + NiO + TiO_2
36	1	d	Spinel + $NiTiO_3$
40	2	c	Matrix + Al_2O_3 + Spinel + $NiTiO_3$ + TiO_2
40	2	d	Spinel + NiO
43	4	c	Matrix + Spinel + $NiTiO_3$
44	3	c	Matrix + Spinel + $NiTiO_3$ + Al_2O_3

(a) Listed in order of decreasing intensity

(b) Relative resistance

(c) Diffractometer trace of oxides in situ

(d) Diffractometer trace of spalled oxides

TABLE XXXIV

TENSILE PROPERTIES OF DOPED RENE' 100 ALLOYS AT 1300°F

Alloy No.	Doping Additions (w/o)	UTS (KSI)	AVG UTS (KSI)	0.2% YS (KSI)	AVG 0.2% YS (KSI)	Elong %	AVG % Elong	R.A. %	AVG % R.A.
36	R'100 Base	138.5	134.5	120.0	121.6	3.6	2.7	8.8	8.0
36	R'100 Base	130.5		123.2		1.8		7.2	
37	R'100 (Less √)	133.9	133.2	112.8	115.1	3.9	3.6	8.7	7.2
37	R 100 (Less √)	132.5		117.3		3.2		5.6	
38	0.11 Gd + 0.2 Mn	139.5	140.1	123.4	120.7	2.4	2.6	9.4	7.9
38	0.11 Gd + 0.2 Mn	140.7		118.0		2.7		6.4	
39	(Less √) + 0.11 Gd + 0.2 Mn	137.6	134.0	*	117.0	3.2	2.3	5.6	5.6
39	(Less √) + 0.11 Gd + 0.2 Mn	130.3		117.0		1.3		5.6	
40	0.10 Gd	140.3	141.2	122.1	122.1	3.9	4.2	5.6	6.4
40	0.10 Gd	142.0		*		4.5		7.1	
41	0.23 Gd	139.6	137.4	122.0	122.6	3.0	2.9	6.3	6.0
41	0.23 Gd	135.2		123.1		2.7		5.6	
42	0.02 Y + 0.095 Th + 0.25 Mn	143.3	138.8	121.0	122.3	3.3	2.7	7.1	6.0
42	0.02 Y + 0.095 Th + 0.25 Mn	134.3		123.5		2.1		4.8	
43	0.07 Gd + 0.02 Y + 0.25 Mn	138.7	136.9	126.0	126.6	2.7	2.5	7.1	7.1
43	0.07 Gd + 0.02 Y + 0.25 Mn	135.0		127.1		2.2		7.1	
44	0.07 Gd + 0.02 Y + 0.25 Mn	134.0	134.1	116.0	117.5	1.8	2.4	6.4	6.4
44	0.07 Gd + 0.02 Y + 0.25 Mn	134.1		119.0		3.0		6.3	

* Extensometer slipped - could not compute

TABLE XXXV

STRESS RUPTURE OF PHASE II ALLOYS AT 1500°F/80 KSI

Alloy No.	Alloy	Heat No.	Spec. No.	Life (hrs.)	R of A (%)	Elong. (%)	P C=20
36	Base	S948	6	1.7	2.5	0.764	39.6
37	Base (Less V)	S949	27	9.6	4.3	2.42	41.05
38	0.11 W/O Gd + 0.2 W/O Mn	S950	48	2.1	2.7	1.13	39.81
39	(Less V) + 0.11 W/O Gd + 0.2 W/O Mn	S951	69	4.5	4.0	2.50	40.5
40	0.10 W/O Gd	S952	90	14.6	3.9	2.18	41.41
41	0.23 W/O Gd	S953	111	14.6	3.2	2.35	41.41
42	0.02 W/O Y + 0.095 W/O Th + 0.25 W/O Mn	S954	132	2.6	2.6	1.14	40.01
43	0.07 W/O Gd + 0.02 W/O Y + 0.25 W/O Mn (less V)	S955	153	4.0	2.5	1.44	40.4
44	0.07 W.O Gd + 0.02 W/O Y + 0.25 W/O Mn	S956	174	6.1	4.8	1.67	40.65

(A) Stress was 79,624 Psi

TABLE XXVI

STRESS-RUPTURE OF PHASE II ALLOYS AT 1500°F/68 KSI

Alloy No.	Alloy	Heat No.	Spec. No.	Life (hrs.)	R of A (%)	Elong. (%)	C_{ρ} =20
36	Base		AF3	183.8	6.4	2.7	43.6
		S848	*AF8	136.2	2.9	7.1	43.55
37	Base (Less V)		AF24	127.96	8.7	4.6	43.3
		S949	*AF29	99.5	7.0	3.38	43.1
38	0.11 W/O Gd + 0.2 W/O Mn		AF45	118.2	6.4	2.7	43.25
		S950	*AF50	108.1	4.0	2.05	43.2
39	(Less V) + 0.11 W/O Gd + 0.2 W/O Mn	S951	AF66	64.93	7.9	4.6	42.75
40	0.10 W/O Gd		AF87	190.7	10.8	5.3	43.62
		S952	*AF92	31.7	1.8	0.76	42.15
41	0.23 W/O Gd	S953	AF108	108.7	6.4	3.6	43.15
42	0.02 W/O Y + 0.095 W/O Th + 0.25 W/O Mn	S954	AF129	80.03	4.8	2.08	42.9
43	0.07 W/O Gd + 0.02 W/O Y + 0.25 W/O Mn		AF150	140.99	9.5	4.2	43.2
		S955	*AF155	131.9	5.7	3.0	43.35
44	(Less V) + 0.07 W/O Gd + 0.02 W/O Y + 0.25 W/O Mn	S956	AF171	62.7	5.6	4.15	42.8

* Denotes alternate testing source

TABLE XXXVII

STRESS-RUPTURE OF PHASE II ALLOYS AT 1800°F/27.5 KSI

Alloy No.	Alloy	Heat No.	Spec. No.	Life (hrs.)	R of A (%)	Elong. (%)	ρ C=20
36	Base	S948	AF5	28.6	10.3	3.3	48.5
37	Base (Less V)	S949	AF26	19.5	18.3	12.5	48.05
38	0.11 W/O Gd + 0.2 W/O Mn	S950	AF47	27.7	5.5	2.91	48.4
39	(Less V) + 0.11 W/O Gd + 0.2 W/O Mn	S951	AF68	5.3	8.8	3.01	46.81
40	0.10 W/O Gd	S952	AF89	9.8	3.0	1.34	47.01
41	0.23 W/O Gd	S953	AF110	15.4	4.0	1.69	47.9
42	0.02 W/O Y + 0.095 W/O Th + 0.25 W/O Mn	S954	AF131	30.3	9.5	5.63	48.55
43	0.07 W/O Gd + 0.02 W/O Y + 0.25 W/O Mn	S955	AF152	17.4	2.6	1.67	48.0
44	(Less V) + 0.07 W/O Gd + 0.02 W/O Y + 0.25 W/O Mn	S956	AF173	5.8	5.2	3.49	46.9

TABLE XXXVIII

STRESS-RUPTURE OF PHASE II ALLOYS AT 1800°F/20 KSI

Alloy No.	Alloy	Heat No.	Spec. No.	Life (hrs.)	R of A (%)	Elong. (%)	C_P =20
36	Base		AF2	119.7	17.7	7.75	49.9
		S948	*AF7	228.3	15.7	10.4	50.5
37	Base (Less V)		AF23	72.0	13.2	13.75	49.4
		S949	*AF28	137.9	19.3	8.86	50.0
38	0.11 W/O Gd + .2 W/O Mn		AF44	58.3	3.5	2.5	49.15
		S950	*AF49	156.9	5.8	4.39	50.15
39	(Less V) + 0.11 W/O Gd + .2 W/O Mn	S951	AF65	48.6	0.0	3.23	49.0
40	0.10 W/O Gd		AF86	100.9	4.0	4.07	49.75
		S952	*AF91	165.6	5.0	4.96	50.2
41	0.23 W/O Gd	S953	AF107	66.7	4.01	3.92	49.3
42	0.02 W/O Y + 0.095 W/O Th + 0.25 W/O Mn	S954	AF128	87.6	4.0	5.0	49.6
43	0.07 W/O Gd + 0.02 W/O Y + 0.25 W/O Mn		AF149	75.9	5.6	4.3	49.42
		S955	*AF154	152.8	7.0	3.84	50.15
44	(Less V) 0.07 W/O Gd + 0.02 W/O Y + 0.25 W/O Mn	S956	AF170	26.3	3.2	1.85	48.4

* Denotes alternate testing source

Inco 713 C | Inco 713 C (La + Mn) | IN-100 | IN-100 (La)

Rene' 63 | Rene' 63 (La + Mn) | Rene' 80 | Rene' 80 (La + Mn)

Figure 1: Effect of Minor Element Additions on Hot Corrosion Behavior. Exposed 50 hrs/1700°F (1.8% Salt Solution of 90% NaCl + 10% $NaSO_4$ Ingested at 100 ppm)

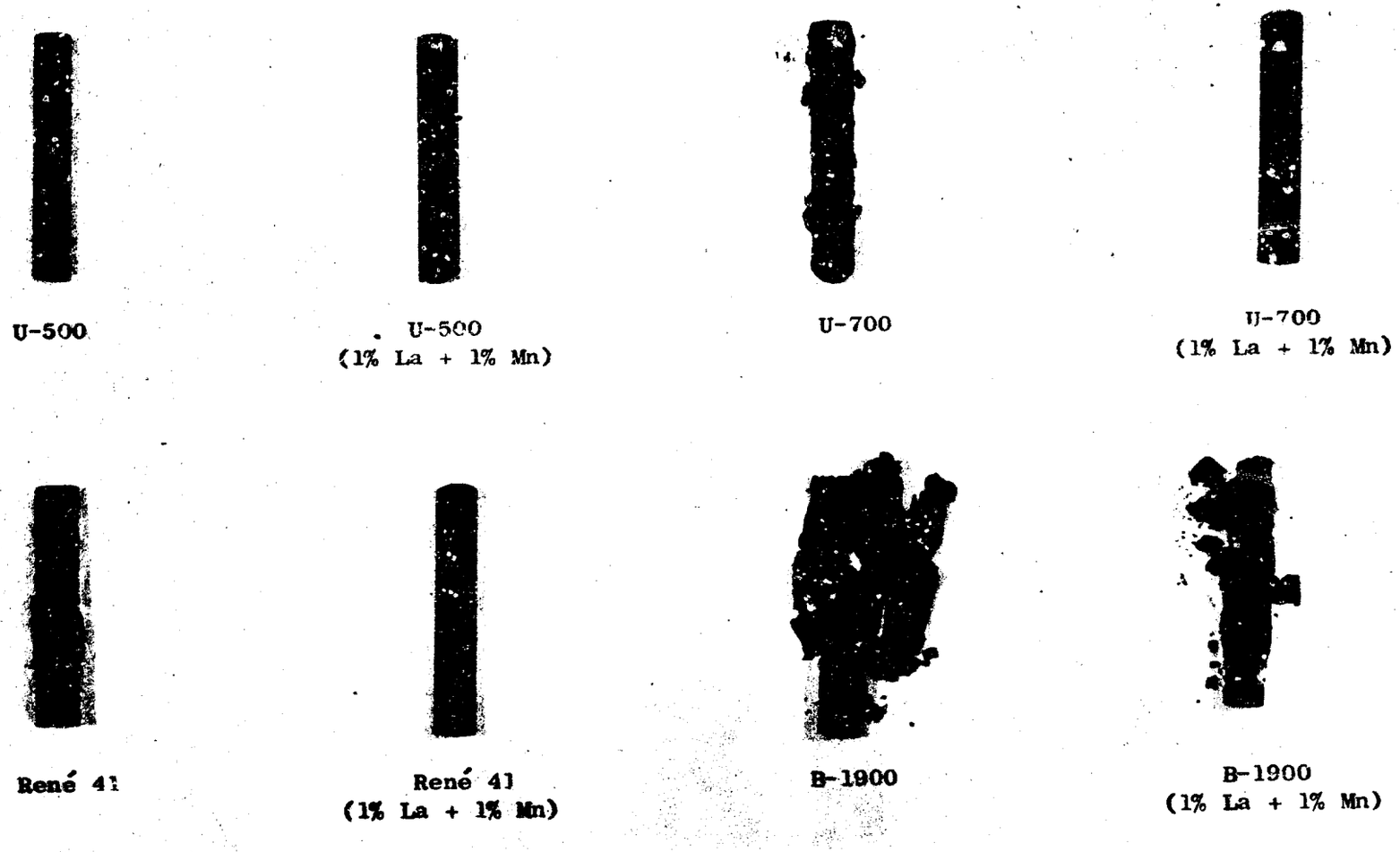

Figure 2: Effect of Minor Element Additions on Hot Corrosion Behavior, Exposed 50 Hrs/1700°F C67051935
(1.6% Salt Solution of 90% NaCl + 10% $NaSO_4$ Ingested at 100 ppm)

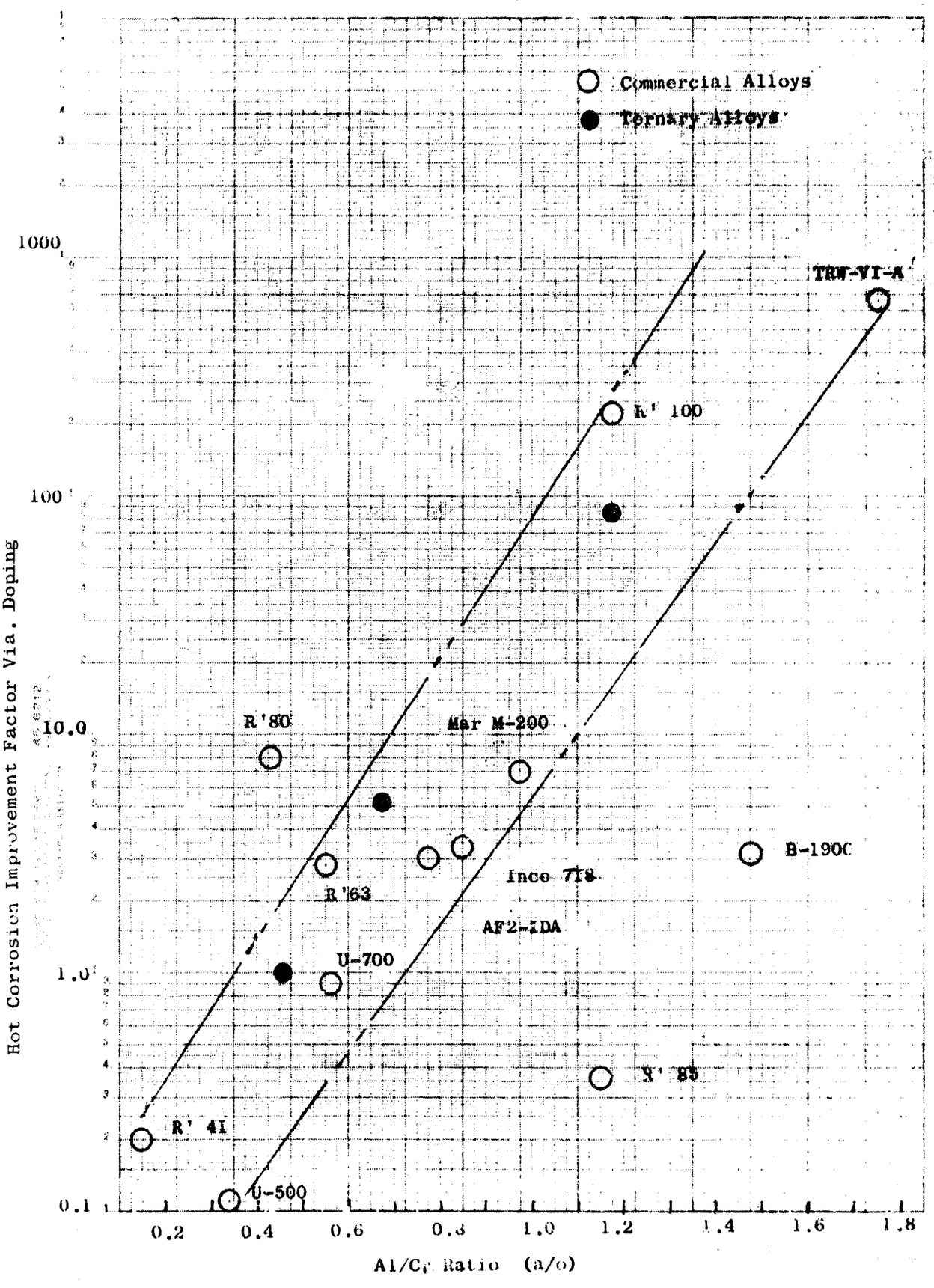

Figure 3: Relation Between Al/Cr Ratio in Alloy and Benefit Derived from Doping

250X N1729

Undoped René 100
(-68.4 Mils/Dia. Loss)

250X N1740

René 100 + 0.12 La + 0.80 Mn
(-55.8 Mils/Dia. Loss)

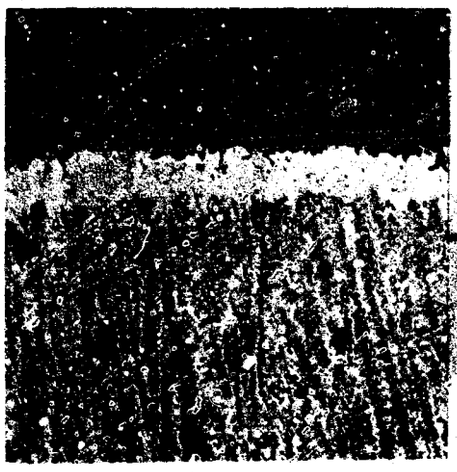

250X N1741

René 100 + 0.31 La + 0.8 Mn
(-0.2 Mil/Dia. Loss)

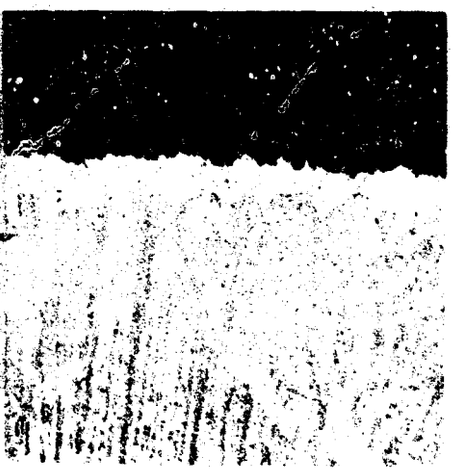

250X N1736

René 100 + 0.56 La + 0.8 Mn
(-0.3 Mils/Dia. Loss)

Figure 4:

EFFECT OF La CONCENTRATION ON THE HOT CORROSION RESISTANCE OF CHILL-CAST RENE' 100 AFTER 50 HRS. EXPOSURE AT 1700°F

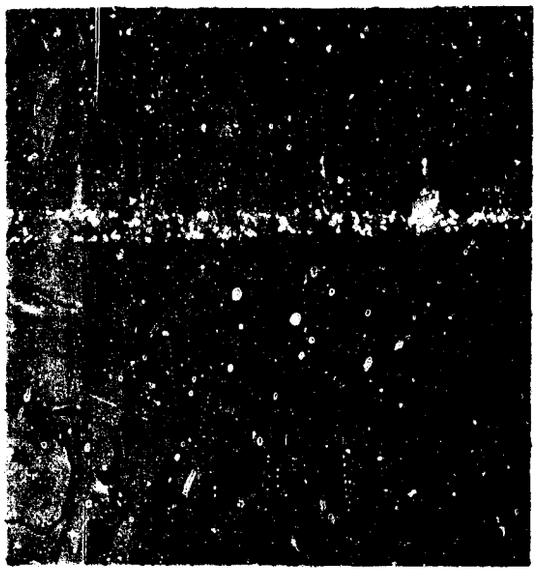

N4607

(a) Ni-Gd Master Alloy

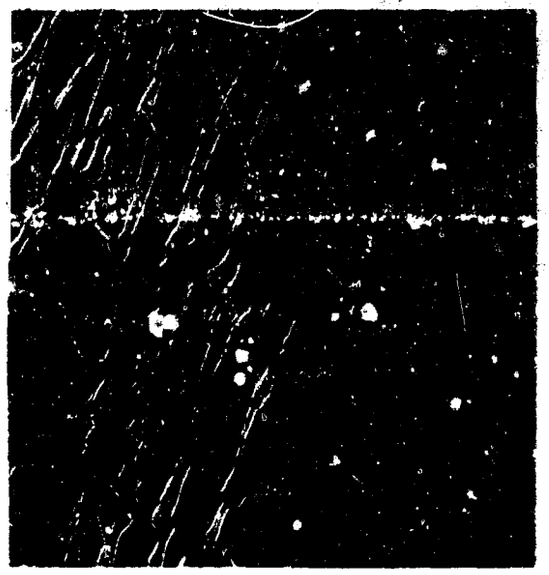

N4606

(b) Same As (a) Polarized Depicts Ni_5Gd-Ni Eutectic In Matrix of Ni_5Gd.

N4605

(c) Ni-Sm Master Alloy

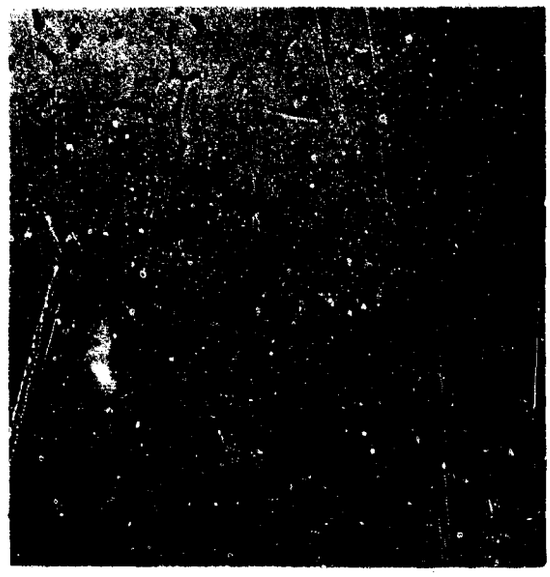

N4609

(d) Ni-Mischmetal Master Alloy

Figure 5 Metallographic Appearance of Hypereutectic Ni_5 R.E. Alloys. Electrolytic Etch in Mixed Acids. 500X.

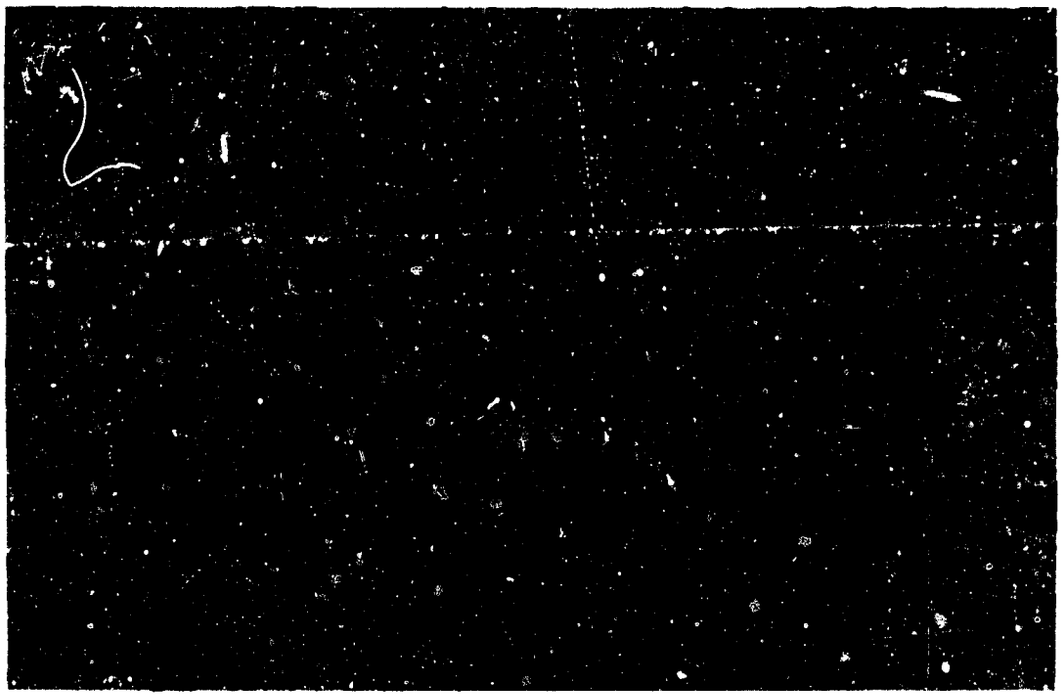

(a) Massive Inclusions (Carbonitrides) 0.14 w/o (250X) N5748

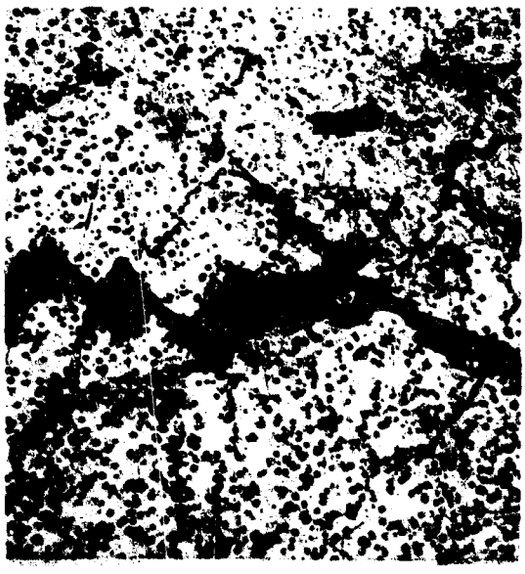

N5713

(b) Edge Cracking - 0.42 Ce (50X)

N5752

(c) Grain Boundry Tearing 0.42 w/o La (250X)

Figure 6 Examples of Problems Encountered with Doped AF 2-IDA Extrusions

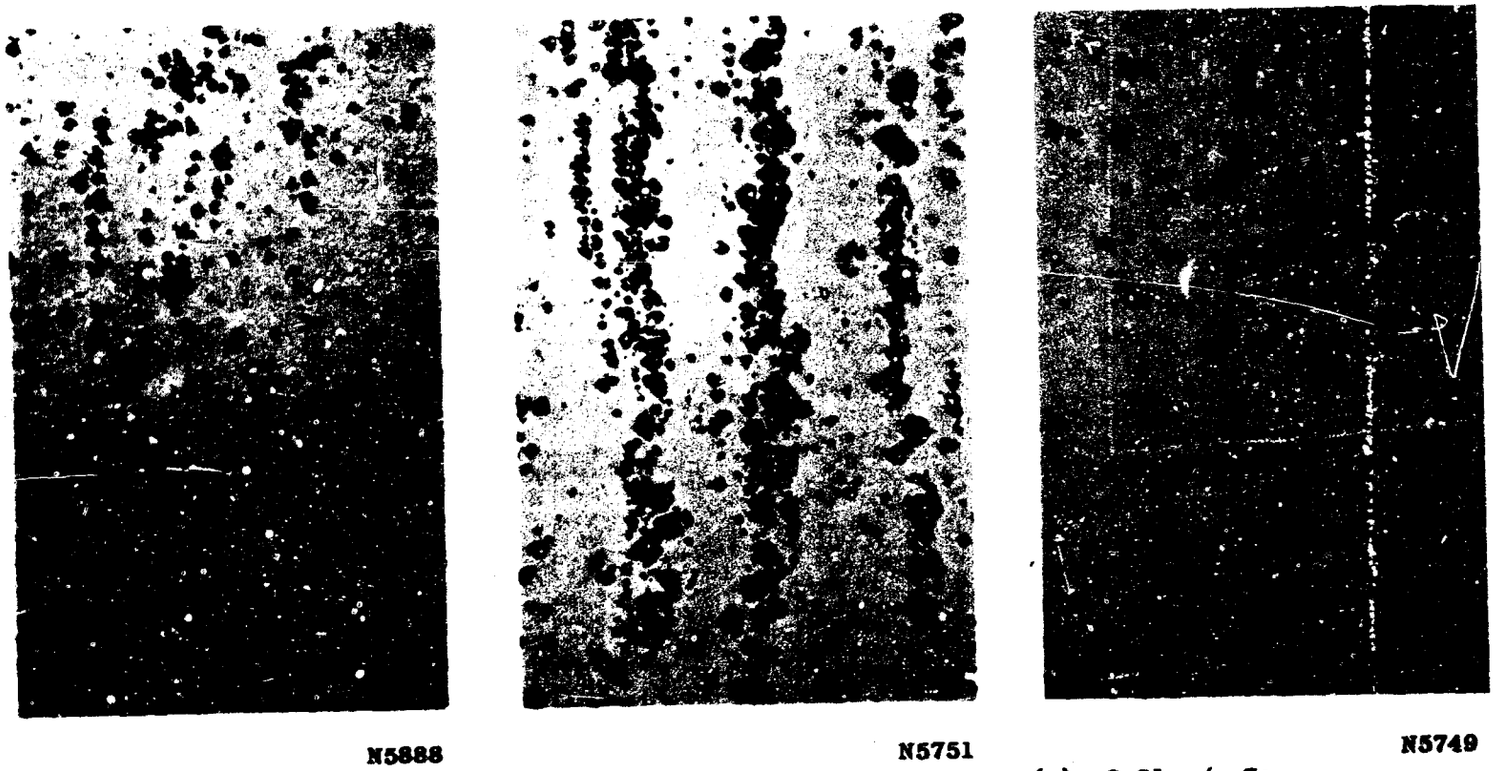

N5888 N5751 N5749

(a) Undoped (b) 0.23 w/o Gd (c) 0.21 w/o Ce

Figure 7 Typical Examples of Stringering and Inclusions Found in As-Extruded Unitemp AF 2-IDA Alloys. Note Massive Carbonitrides and Oxide Inclusions As Polished 250X.

N5757

(a) 0.21 w/o Ce

N5755

(b) 0.42 w/o Ce

N5762

(c) 0.23 w/o Gd

N5761

(d) 0.46 w/o Gd

Figure 8 General Microstructures of Doped Unitemp AF 2-IDA. As Extruded (Long.) Electrolytic Etch 500X.

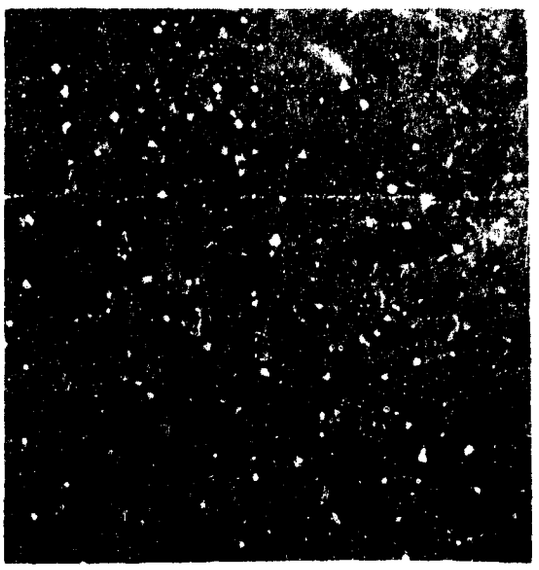

P1307

(a) AF2-1DA base as-extruded
Note: Fine carbides and absense of primary γ'

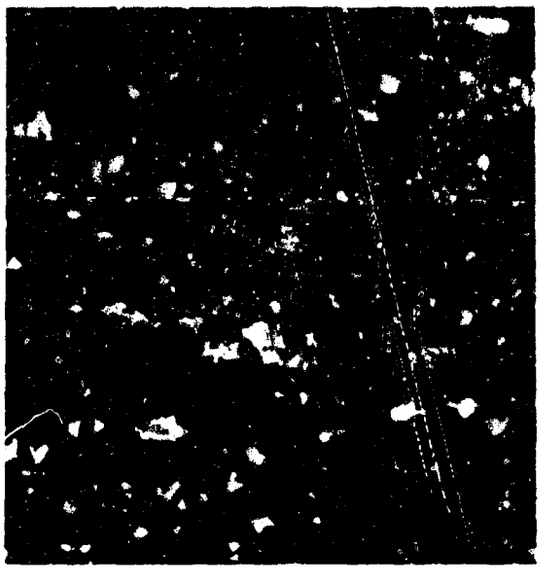

P1348

(b) AF2-1DA +.20 w/o La + 79 w/o Mn As-extruded. Note: Relatively massive carbides and primary γ'

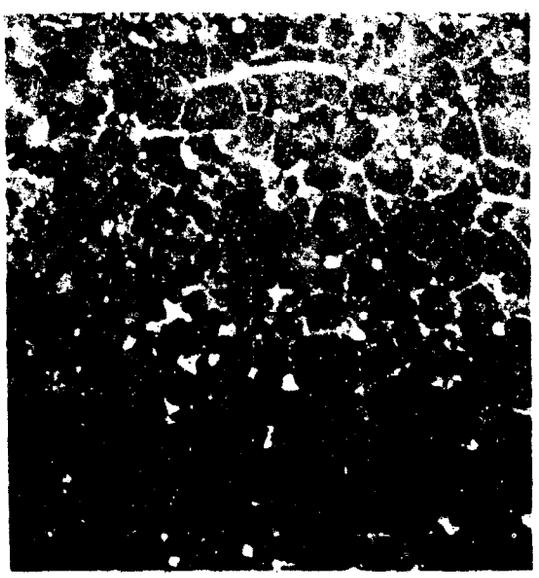

P1346

(c) AF2-1DA + .11 w/o Y + .81 w/o Mn As-extruded.

P1345

(d) AF2-1DA + .28 w/o Y + .75 w/o Mn As-extruded. Note: Larger carbide size than (c)

Figure 9: General as-extruded microstructure of AF2-1DA alloys with various dopant additions (500X). Etch - 8:1 H_3PO_4 in H_2O.

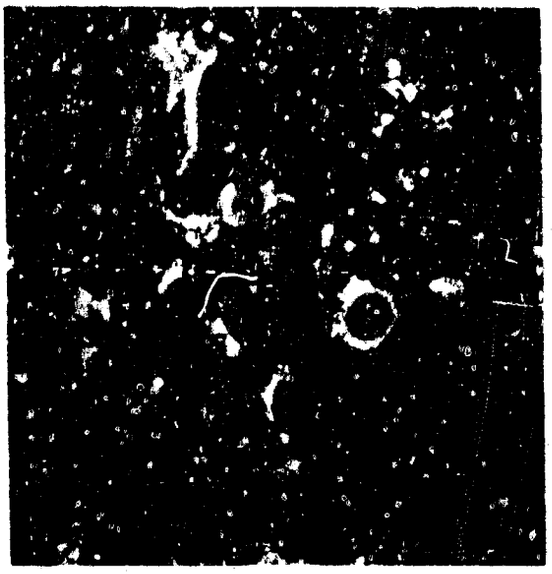

P1325

(a) #10 - AF2-1DA + .38 w/o Th + .8 w/o Mn As cast Note: Segregation of Th Rich phase (arrow)

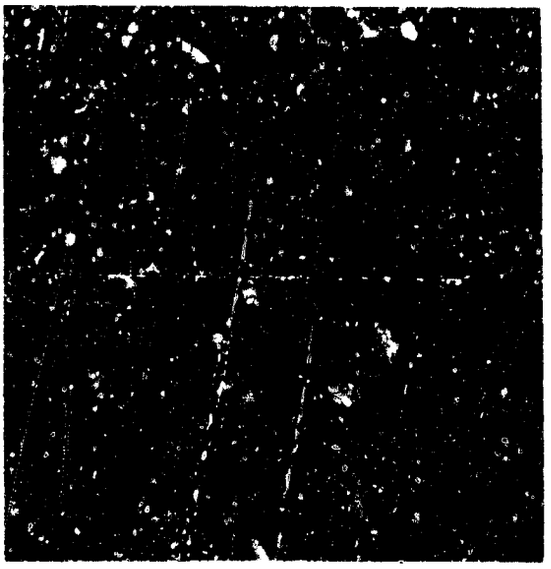

P1326

(b) #10 - As extruded Note: Fine structure and microfissures.

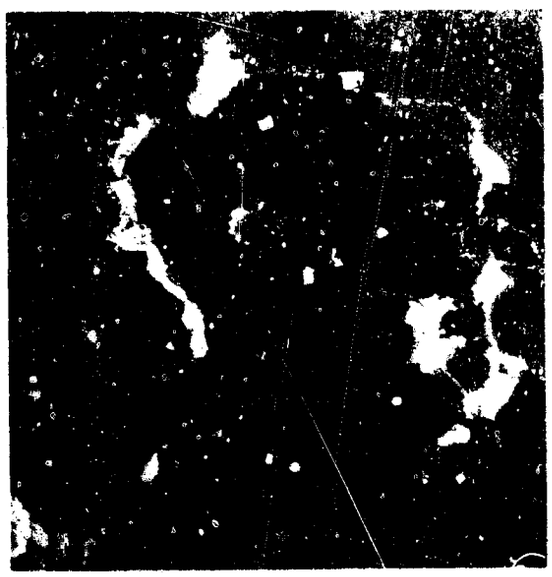

P1323

(c) #14 AF2-1DA + .22 w/o Gd +.9 w/o Mn As cast. Note:Segregation of Gd rich phase (arrow).

P1324

(d) #4 - As extruded. Note: Fine structure

Figure 10: Effect of primary working on the microstructure of typical doped AF2-1DA alloys (500X) Etch - 8:1 H_3PO_4 in H_2O

(a) Relation Between Rare-Earth and Carbides

(b) Relation Between Rare-Earth and γ-γ' Eutectic Nodules

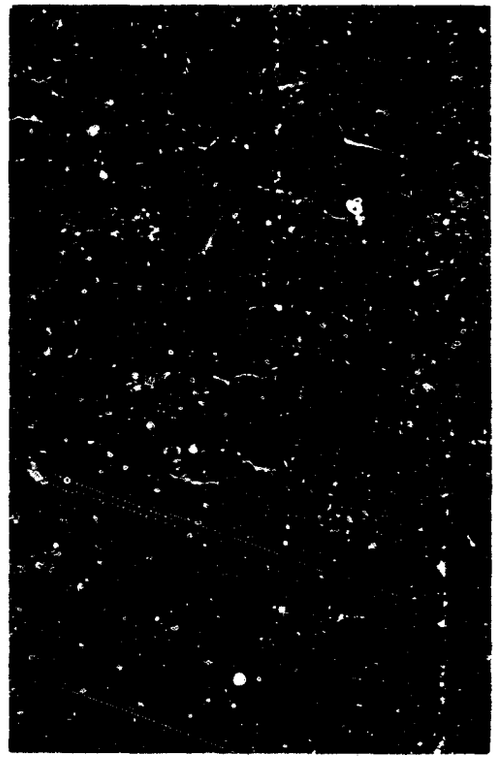

(c) Relation Between Rare-Earth, Carbides and γ-γ' Eutectic Nodules

Figure 11: As-Cast AF 2-IDA Doped with 0.23 W/O Gd + 0.8 W/O Mn Showing Morphology of Gd Containing Phase (Heavily Shadowed). 5000X

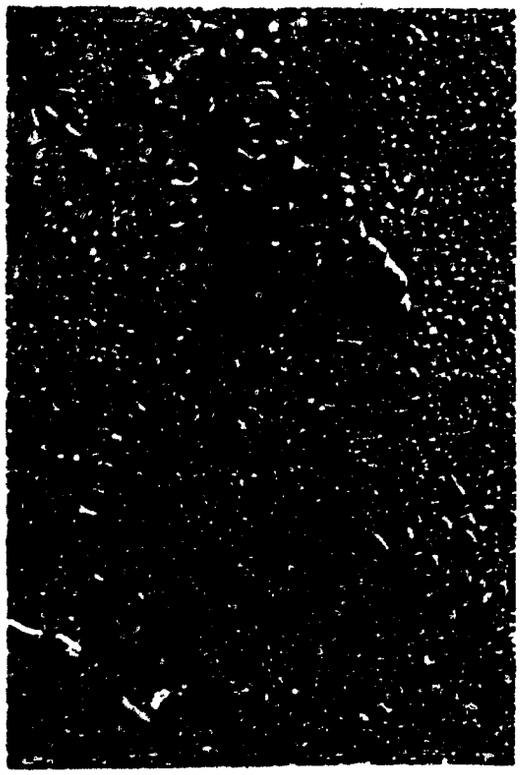

(a) Note Relatively Blocky Rare-Earth Phase

(b) Note Rare-Earth Phase Within Carbides and Grain Boundries

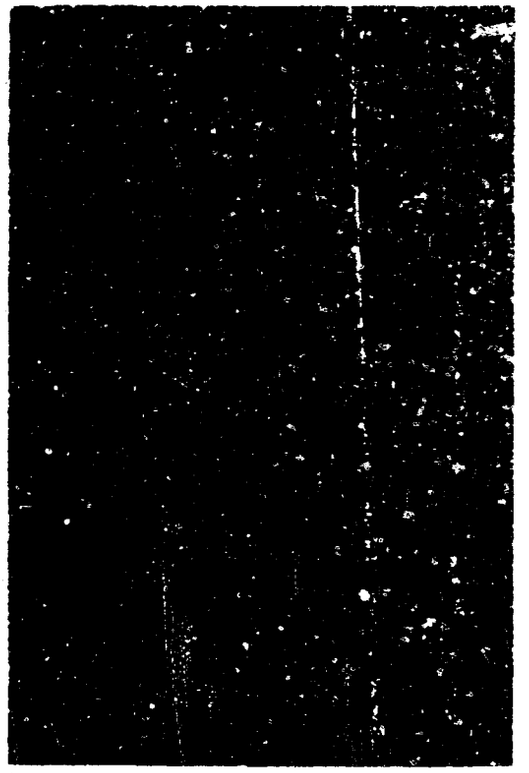

(c) Note Partial Break-Up of γ-γ' Eutectic and Rare-Earth Phase

Figure 12: Microstructure of AF 2-IDA Doped with 0.23 W/O Gd and 0.8 W/O Mn After Extrusion (Arrows Show Rare-Earth Phase). 5000X

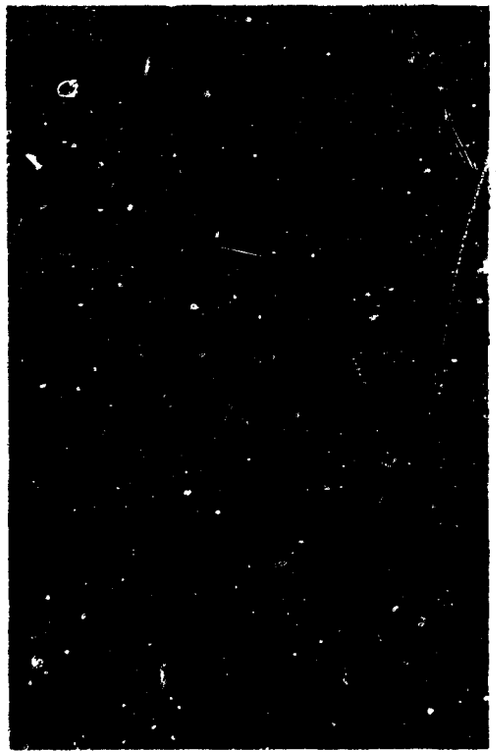

P3430

(a) As-Cast

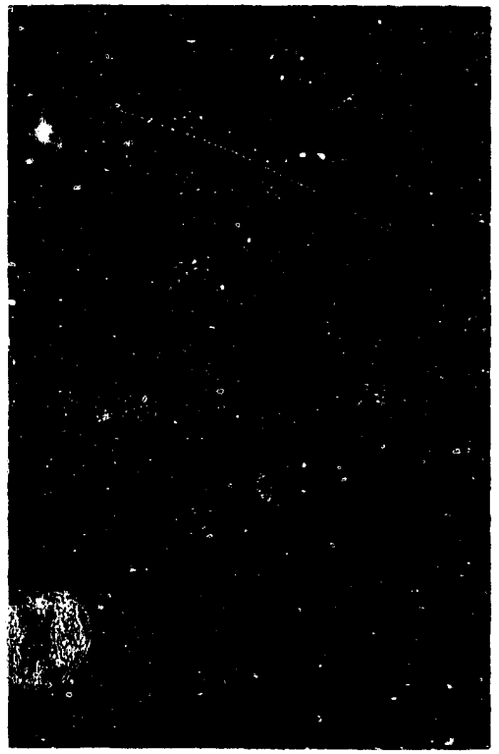

P3429

(b) Extruded at 2025°F with 9:1 Ratio

P3425

(c) Rod Rolled ≈ 10% at ?000°F

Figure 13: Effect of Processing on Microstructure of AF 2-IDA Doped with 0.23 W/O Gd + 0.8 W/O Mn Etched in 8:1 H_3PO_4:H_2O (250 X)

C67082415

(a) 0.14 w/o Y - Hot Cracks

C6782416

(b) 0.42 Ce - Gas Entrapment

Figure 14 Doped B-100 Castings Illustrating Casting Difficulties. Full Size.

C67082419

(a) 0.21 W/O La - Sound Casting

C67082828

(b) 0.14 W/O Y - Non Uniform Grain Size

Figure 15: Doped Rene' 100 Castings Illustrating Casting Difficulties. Full Size.

N2694

(a) Rare-Earth Phase (Arrows) In Bright Field

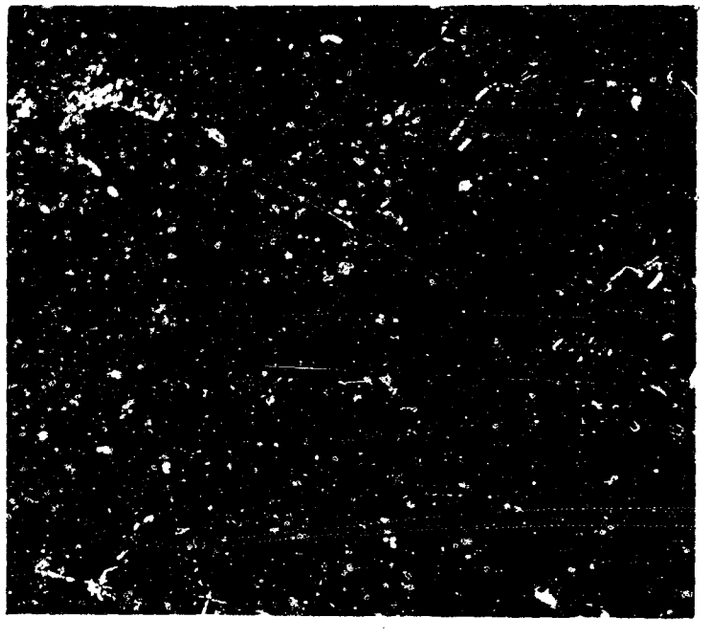

N2695

(b) Optical Activity of Rare-Earth Phase in Polarized Light

Figure 16: Appearance of La Rich Phase From As-Cast Rene' 100 Doped with 0.6 W/O La. As Polished 500X

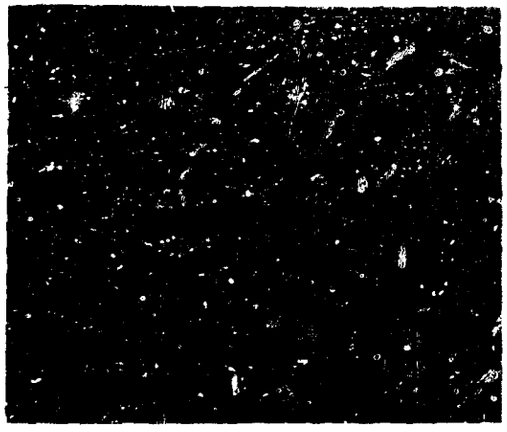

N9176

(a) Undoped René 100

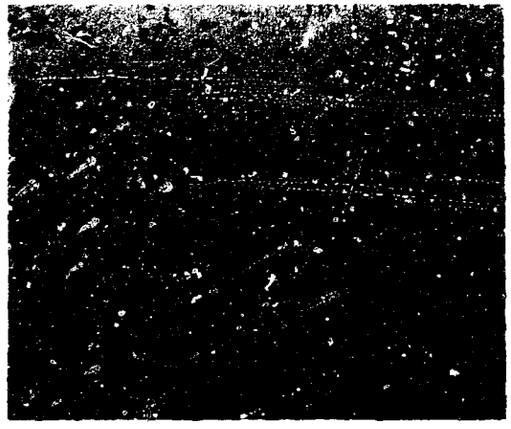

N9177

(b) R-100 + .09 a/o Y

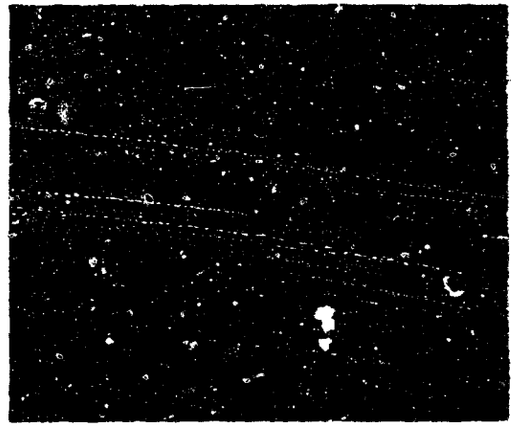

N9178

(c) R-100 +.17 a/o Y - Note R.E. phase and Massive carbides

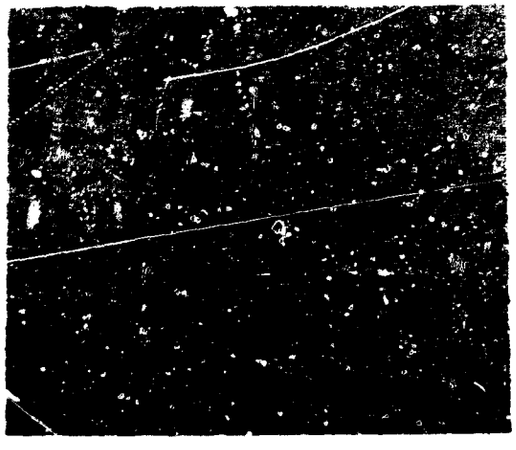

N9180

(d) R-100 +.23 a/o Gd - Note R.E. containing phase in g.b.

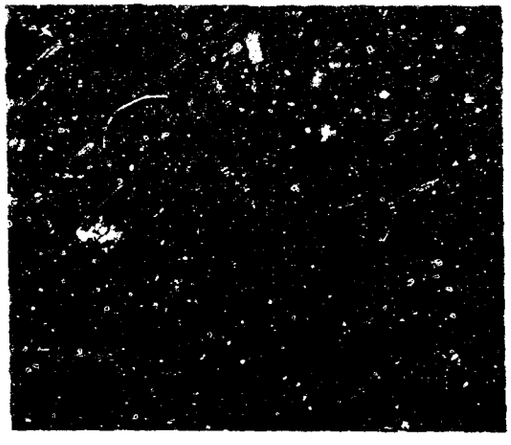

N9182

(e) R-100 + .12 a/o La

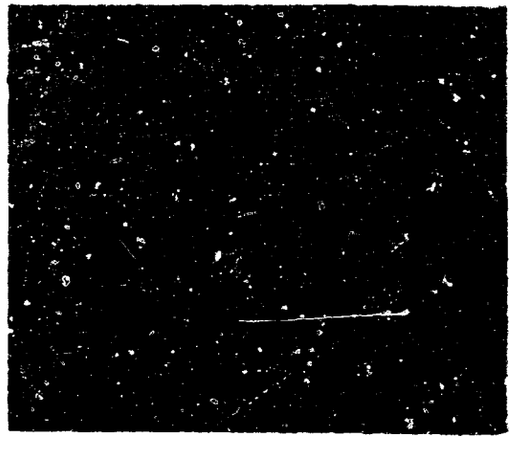

N9187

(f) R-100 + ~.2 a/o MM - Note R.E. phase in g.b.

Figure 17: Effect of reactive metal additions on the general microstructure of as cast René 100. (150X Unetched)

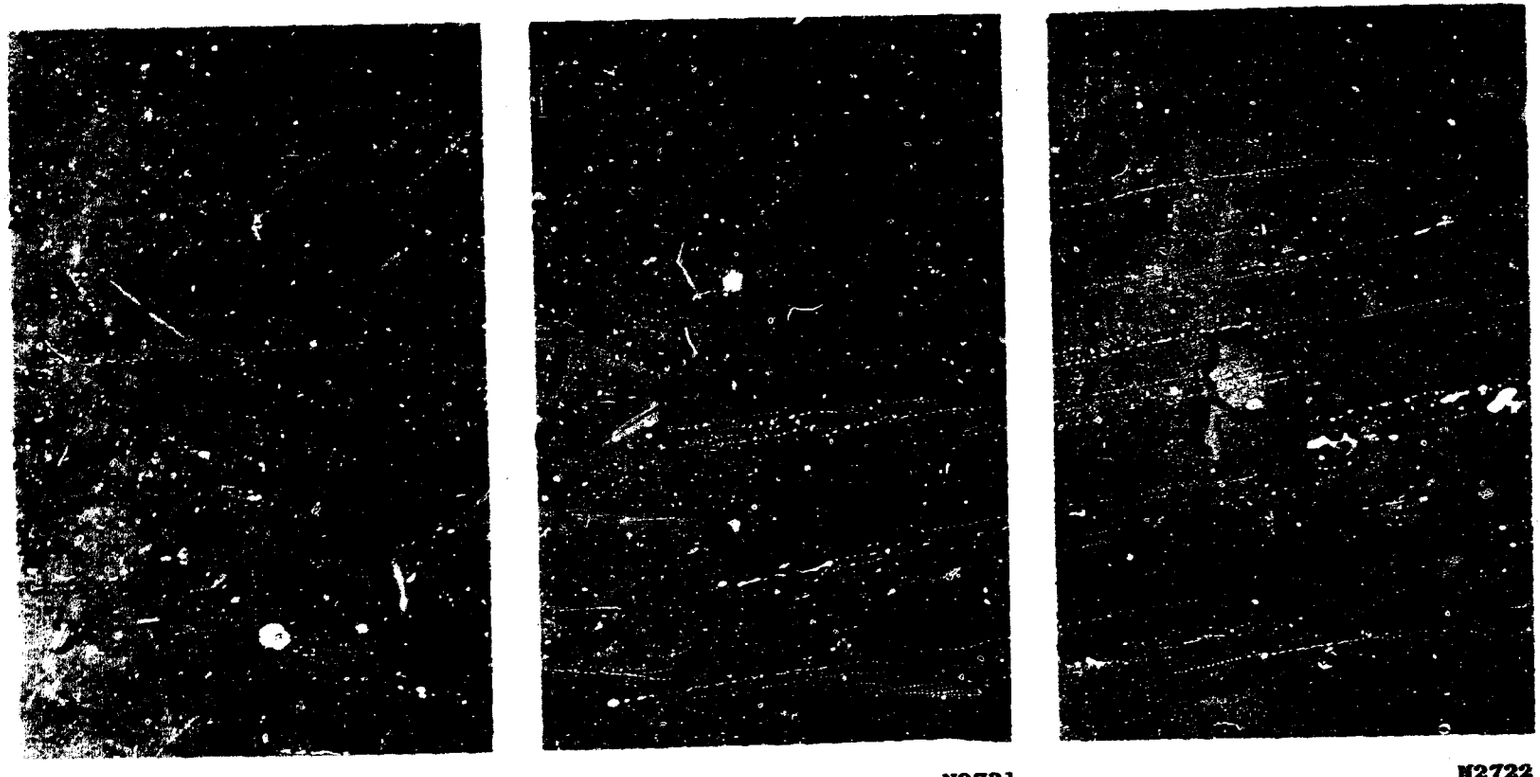

N2720 N2721 N2722

(a) As Polished (b) Light Etch (c) Heavier Etch

Figure 18: Morphology of La Rich Phase (Arrow) In Cast R-100 With 0.6 w/o La. Note: Hardness of La Phase, Association with Grain Boundries and Primary γ' Nodules, and Attack by Acid Etch. Dilute Schantz Etch - 250X.

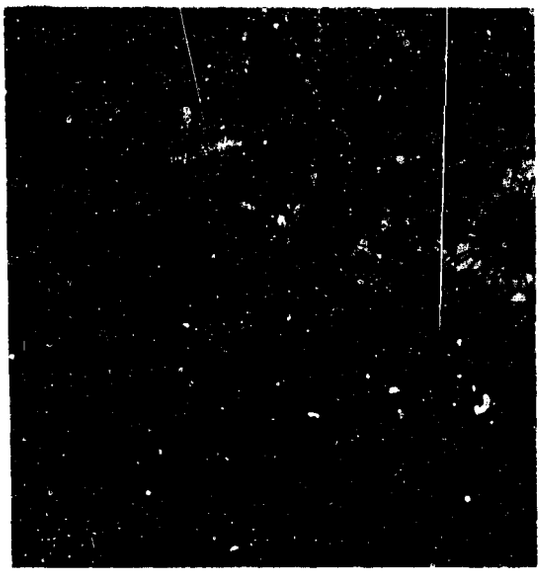

P1316

(a) #14 René 100 Base

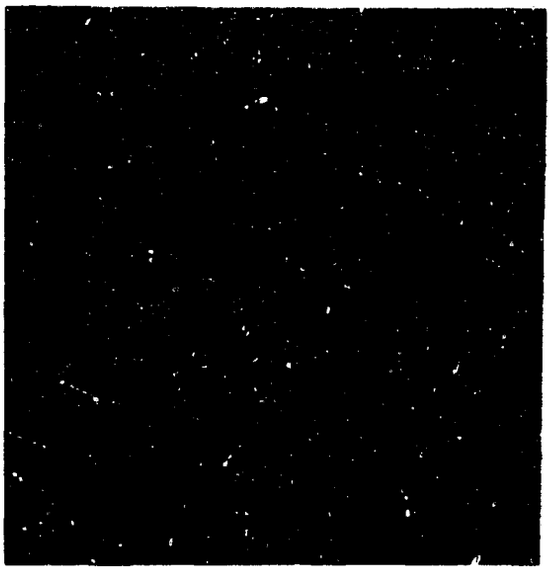

P1322

(b) #16 R-100 + 0.17 a/o Y
Note: Massive Y containing phase (arrow)

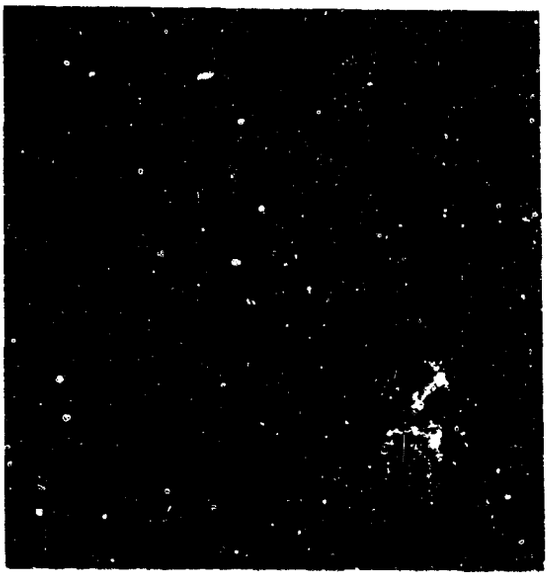

P1320

(c) #18 R-100 + 0.23 a/o Gd
Note: Massive Gd containing phase (arrow)

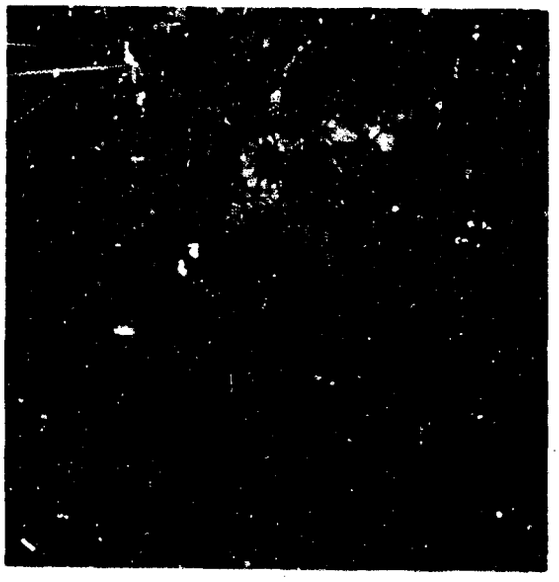

P1321

(d) #19 R-100 + 0.09 a/o Ce
Note: Relatively fine structure

Figure 19: As cast microstructure of various doped René 100 alloys (500X) Etch - 8:1 H_3PO_4 in H_2O

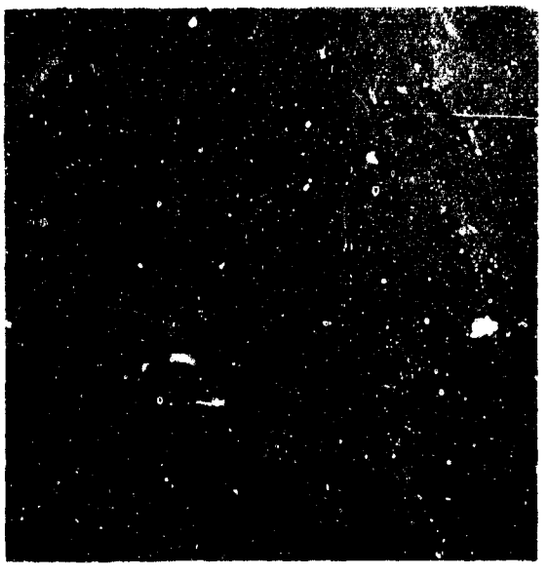

P1315

(a) #22 - R-100 + 0.12 a/o La
Note: La Rich Phase (Arrow)

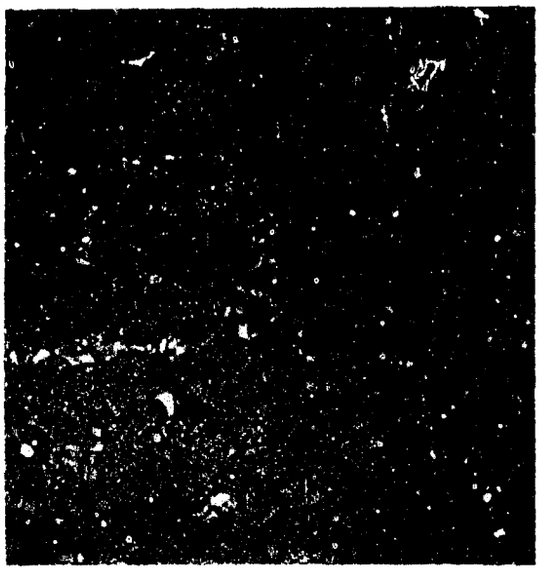

P1317

(b) #28 - R-100 + 0.38 w/o Mn
Note: Blocky carbides and absense of Primary γ'

P1314

(c) #29 - R-100 + .15 a/o La + .68 w/o Mn

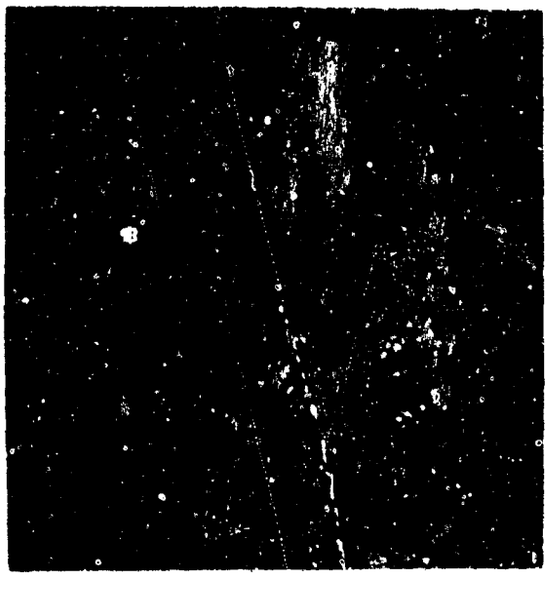

P1319

(d) #32 - R-100 + .05 a/o Y + .05 a/o Th + .24 w/o Mn Note: Relatively fine structure

Figure 20: As-cast microstructures of various doped René 100 alloys. (500X) Etch - 8:1 H_3PO_4 in H_2O

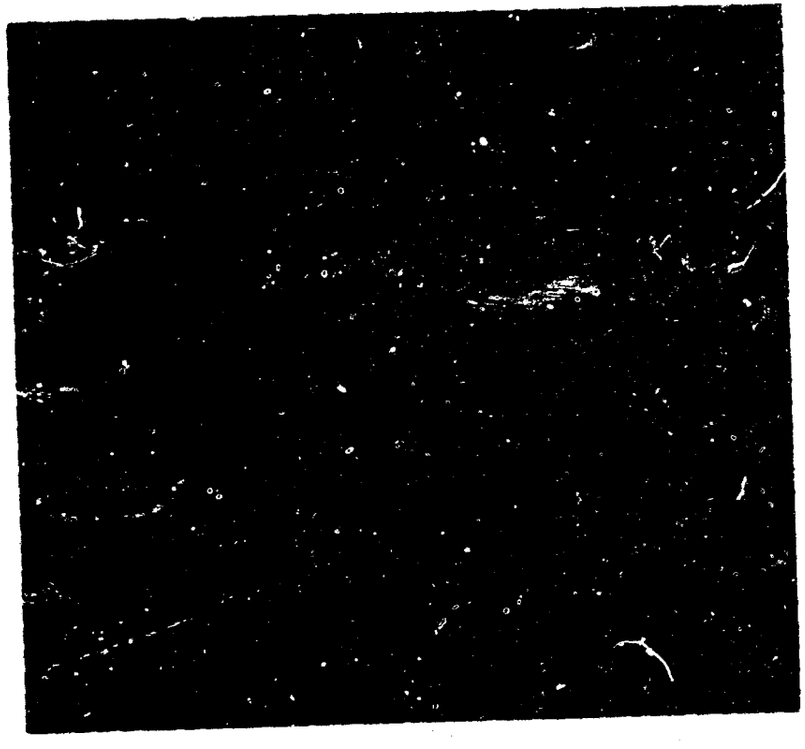

910A

(a) Shows Carbide Morphology

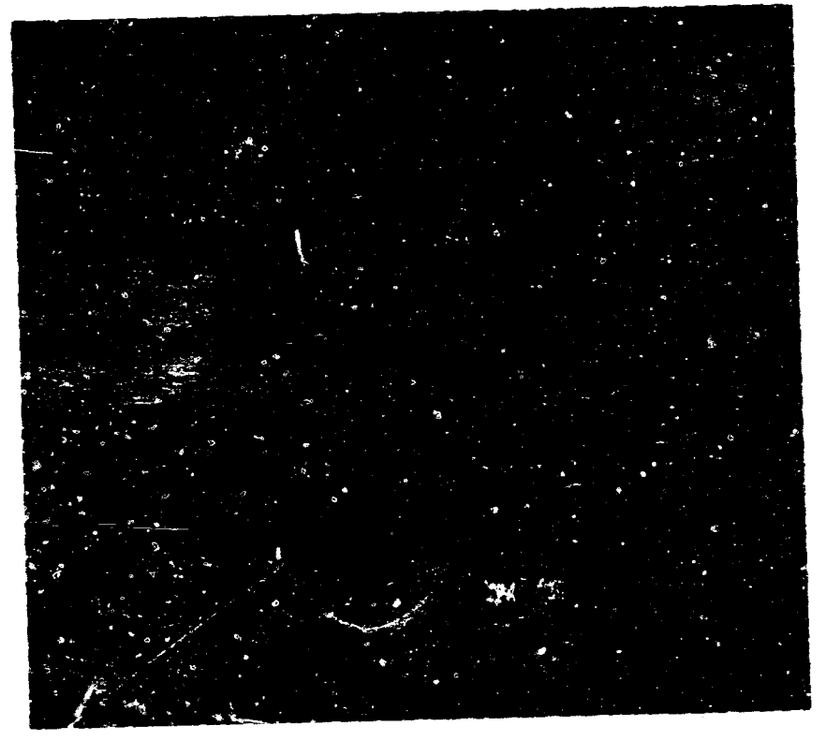

910A

(b) Shows γ-γ' Eutectic Morphology

Figure 21: Typical Electron Micrographs of Undoped Rene' 100 (5000X)

910B

(a) Rene' 100 + 0.17 A/O Y - Association Between Rare-Earth Phase (Arrow), Carbides, and γ-γ' Eutectic

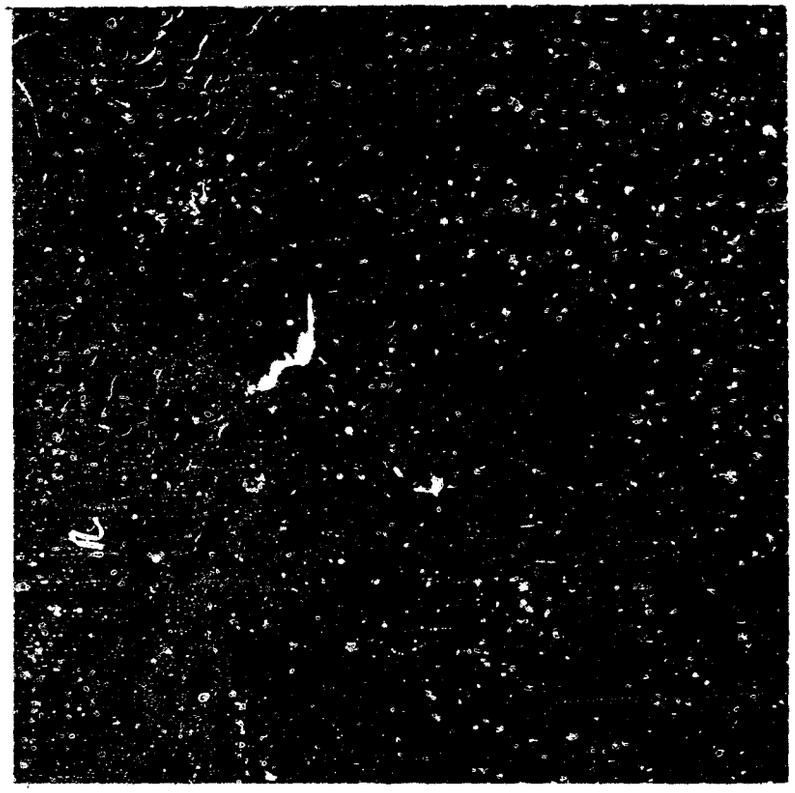

910C

(b) Rene' 100 + 0.23 A/O Gd - Association Between Rare-Earth Phase (Arrow), Carbides and Grain Boundries

Figure 22: Morphology of Rare-Earth Containing Phase (5000X)

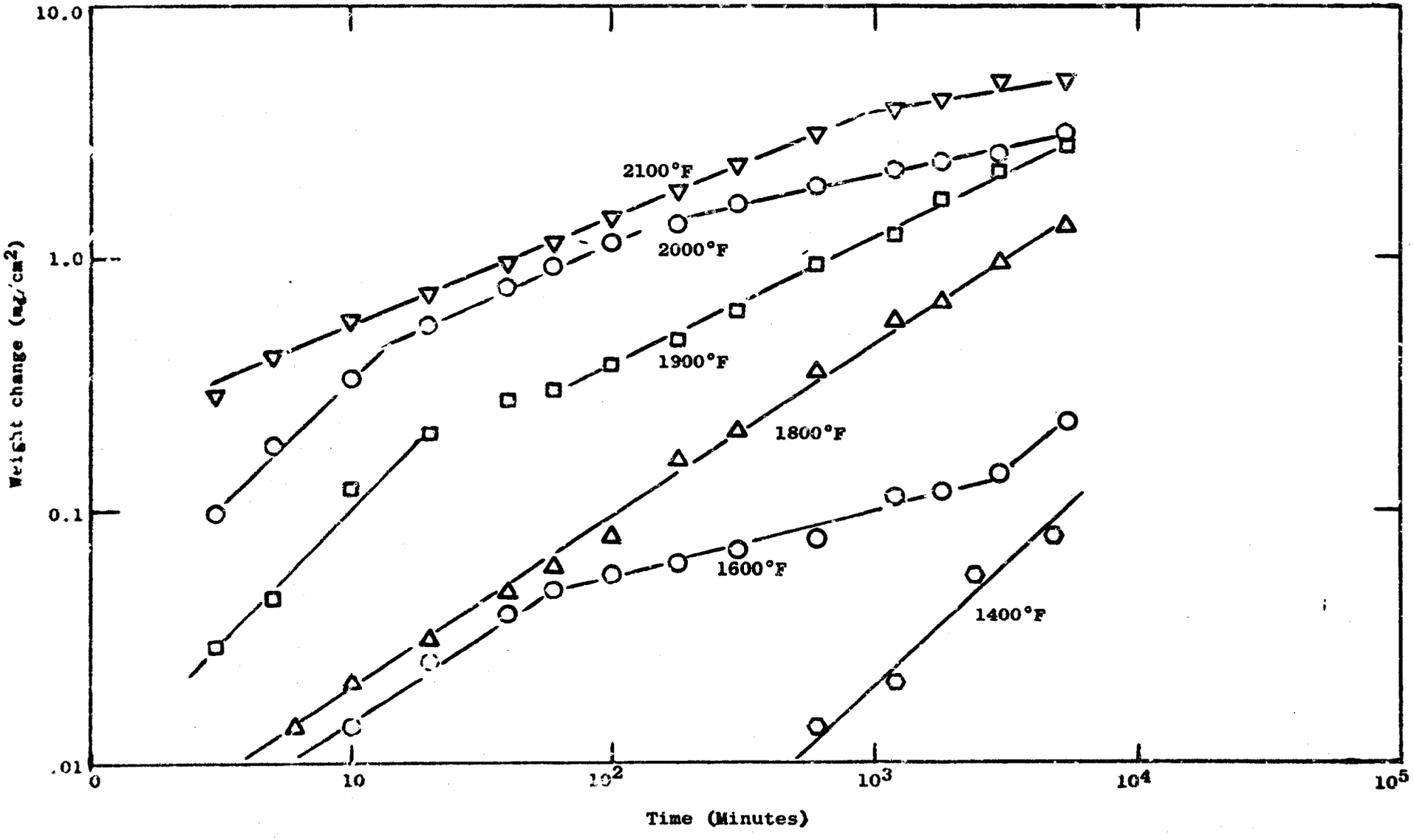

Figure 23 Typical oxidation behavior of Unitemp AF 2-1DA

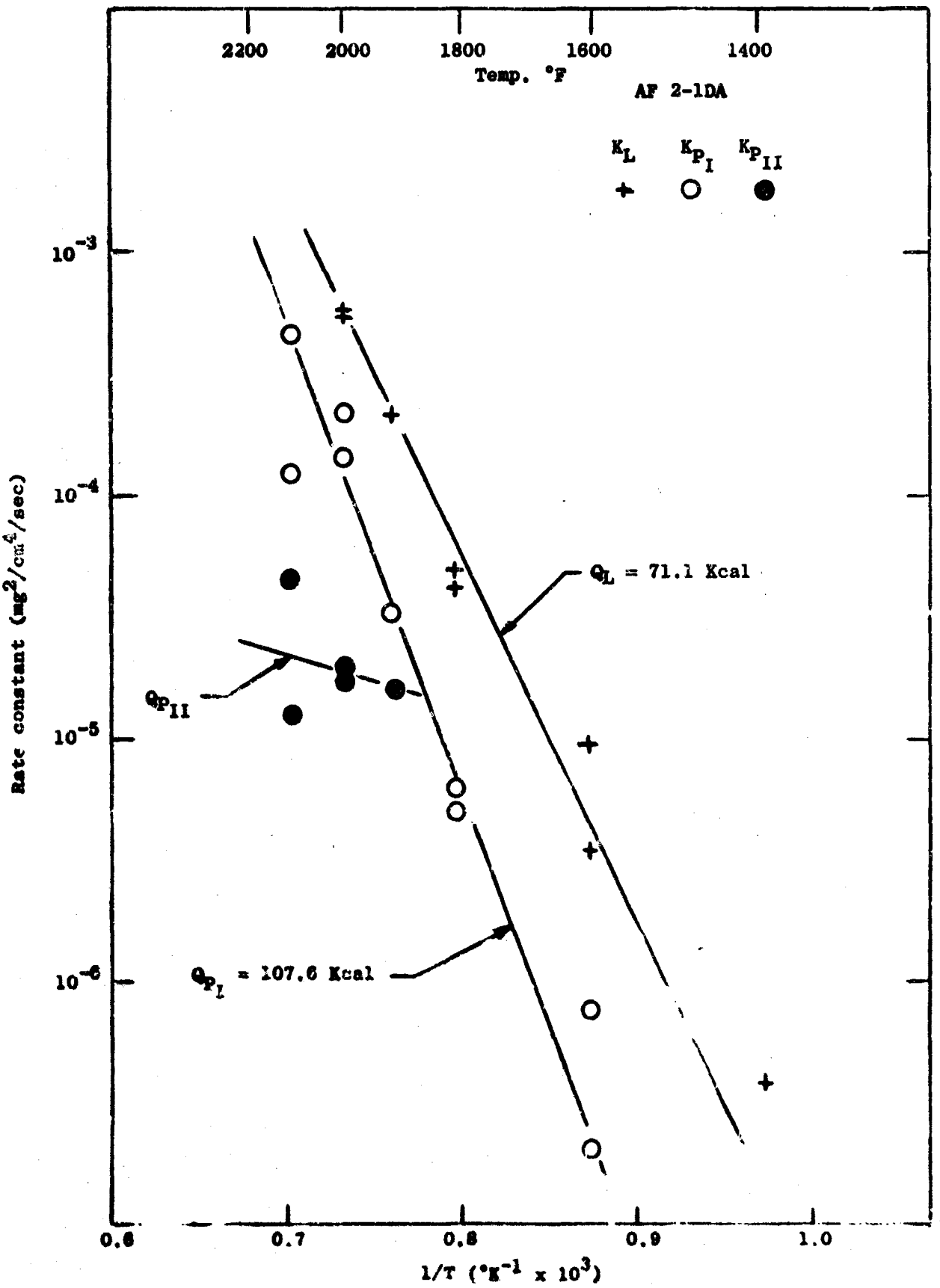

Figure 24. Arrhenius plot of the rate constants for Unitemp AF 2-1DA

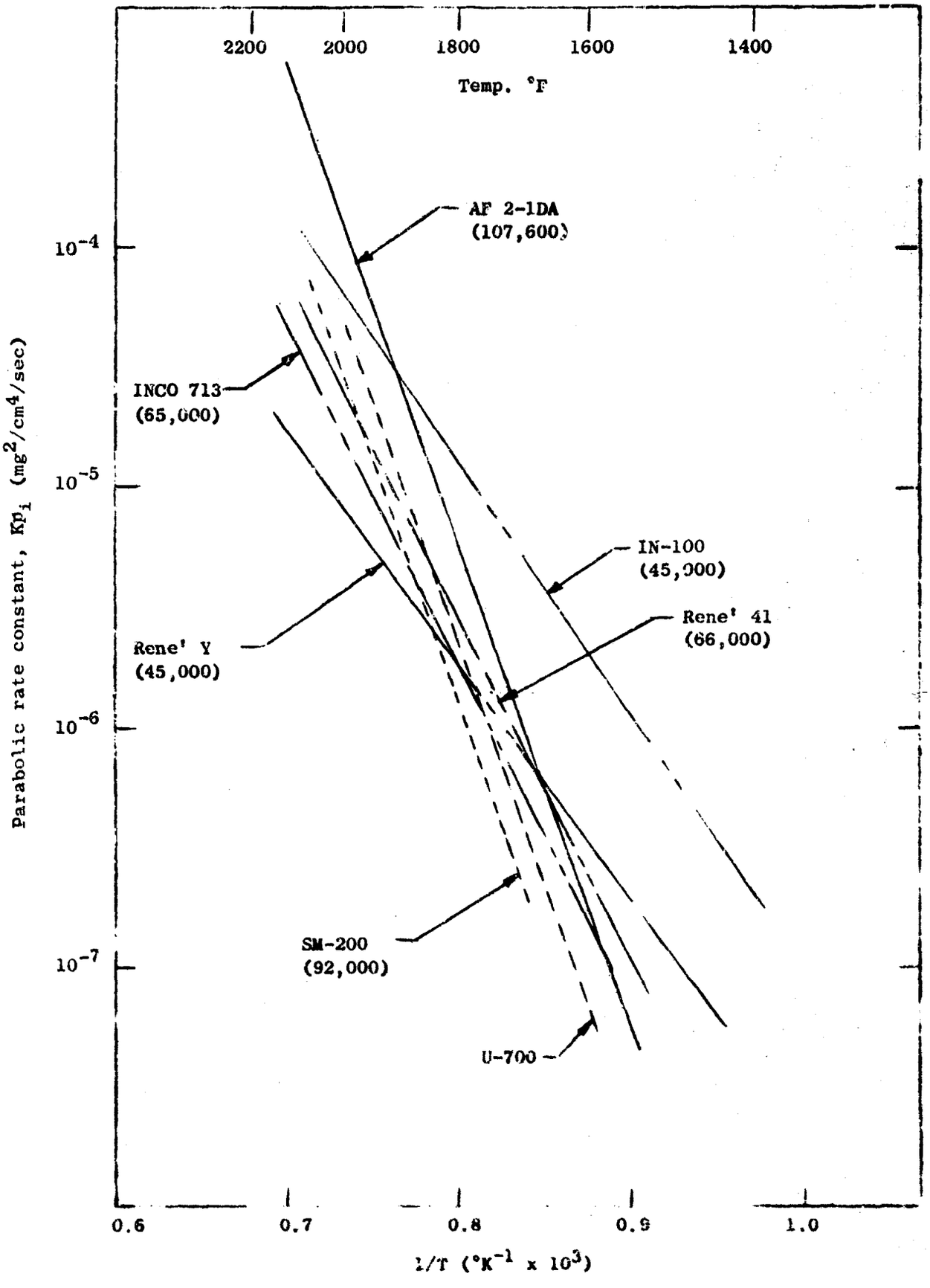

Figure 25 A comparison of the oxidation rate of Unitemp AF 2-1DA with other commercial nickel base alloys

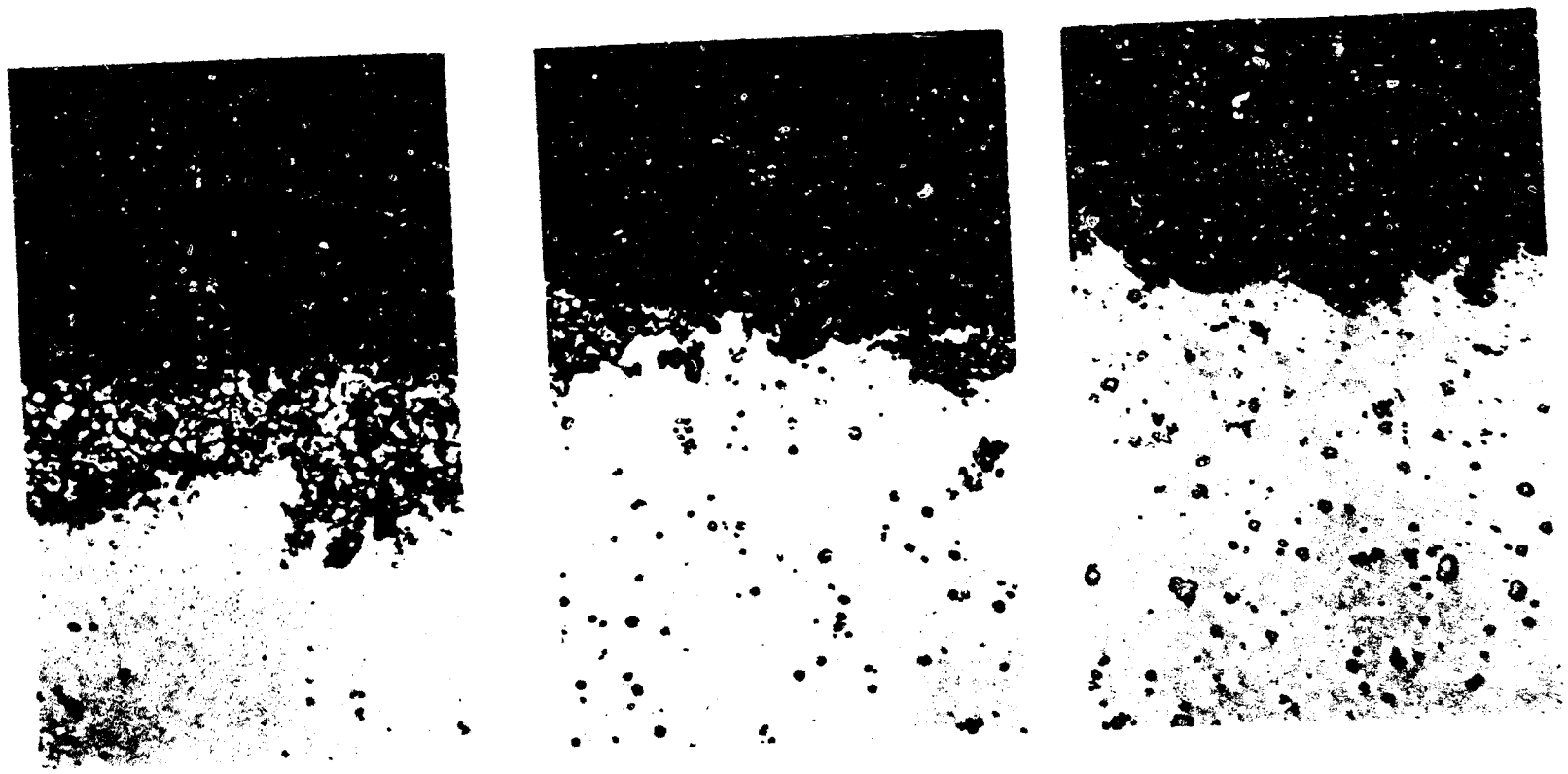

N5883

(a) Oxidized 100 Hrs. at 1800°F.

N5884

(b) Oxidized 100 Hrs. at 1900°F

N5886

(c) Oxidized 100 Hrs. at 2000°F.

Figure 26 Metallographic Appearance of Oxide Products Formed On Unitemp AF 2-IDA. Note Stability of Carbides to 2000°F. As Polished 250X 4:1 Taper.

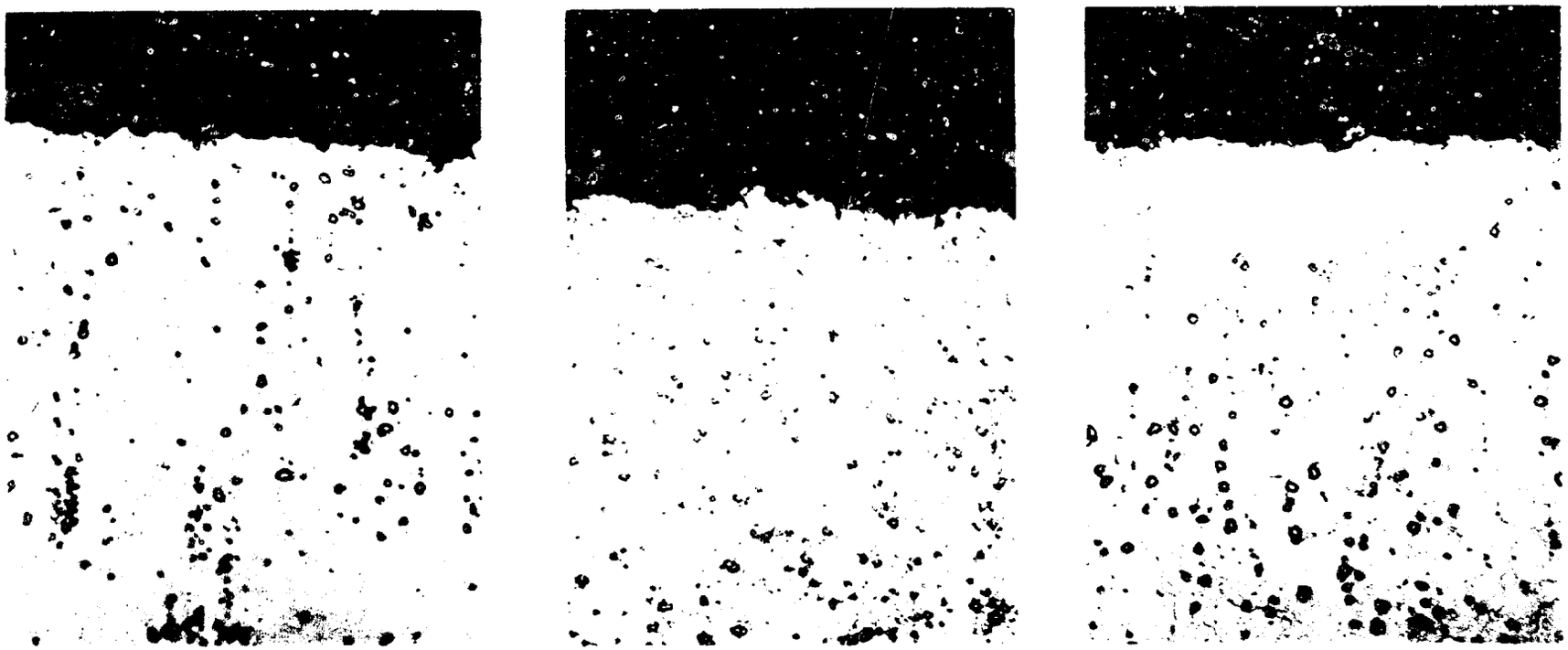

P7458 P7460 P7459

(a) Base (b) 0.08Y (c) 0.10 Gd

Figure 27:

Metallographic Appearance of Oxide Products Formed on Doped Unitemp AF 2-IDA During Cyclic Oxidation at 2000°F/175 Hours

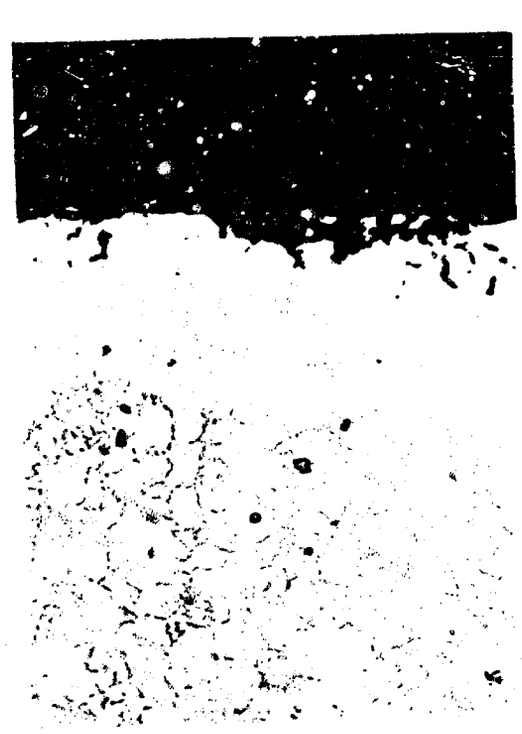

P7461

(a) Base
Note Carbide Depletion

P7463

(b) 0.08Y
Note Carbide Depletion

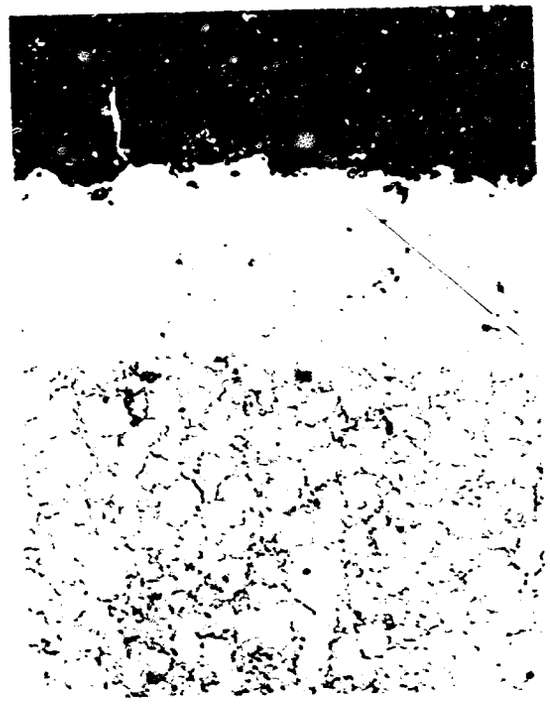

P7463

(c) 0.10 Gd
Note Carbide Depletion

Figure 28: Metallographic Appearance of Oxide Products Formed on Doped Unitemp AF 2-1DA During Cyclic Oxidation at 1800°F/1000 Hours Continuous Exposure

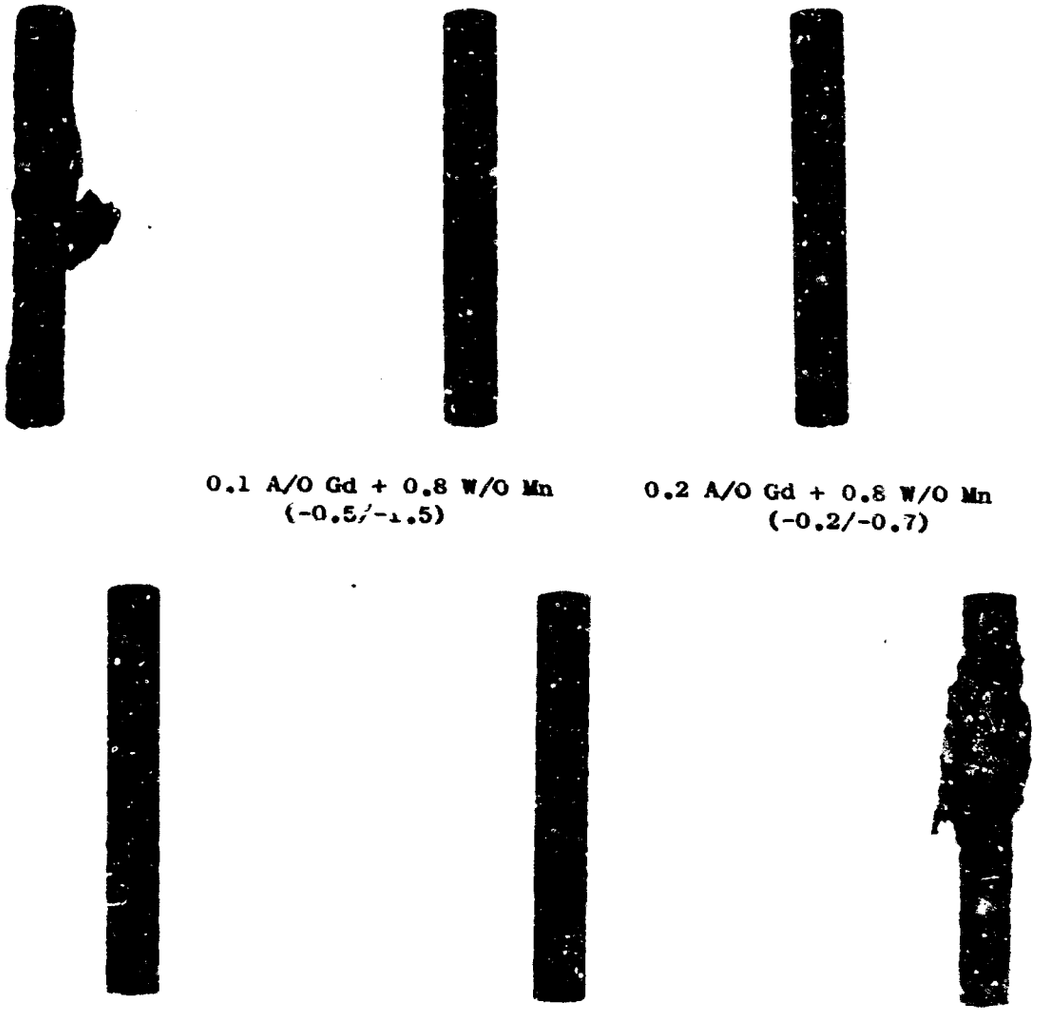

Figure 29: Hot Corrosion Appearance and Metal Loss for Various Doped AF 2-IDA Alloys. Values in Parentheses Refer to Gross and Maximum Metal Loss, Respectively.

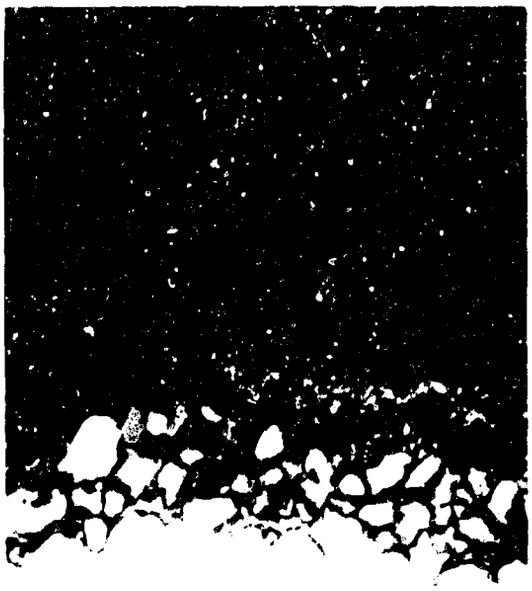

P2851

(a) AF 2-IDA Base
(-20 mils/side)

P2856

(b) AF 2-IDA + 0.1 A/O La + 0.8 W/O Mn
(-0.6 mils/side)

P2859

(c) AF 2-IDA + 0.1 A/O Th +0.8 W/O Mn
(-0.9 mils/side)

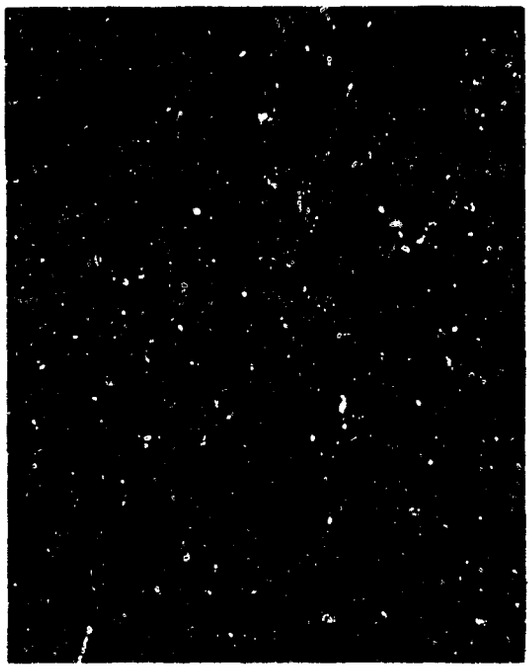

P2858

(d) AF 2-IDA + 0.2 A/O Th + 0.8 W/O Mn
(-1.3 mils/side)

Figure 30: Microstructural Appearance of Doped AF 2-IDA After Hot Corrosion Exposure of 50 Hrs./1700°F

(300 X)

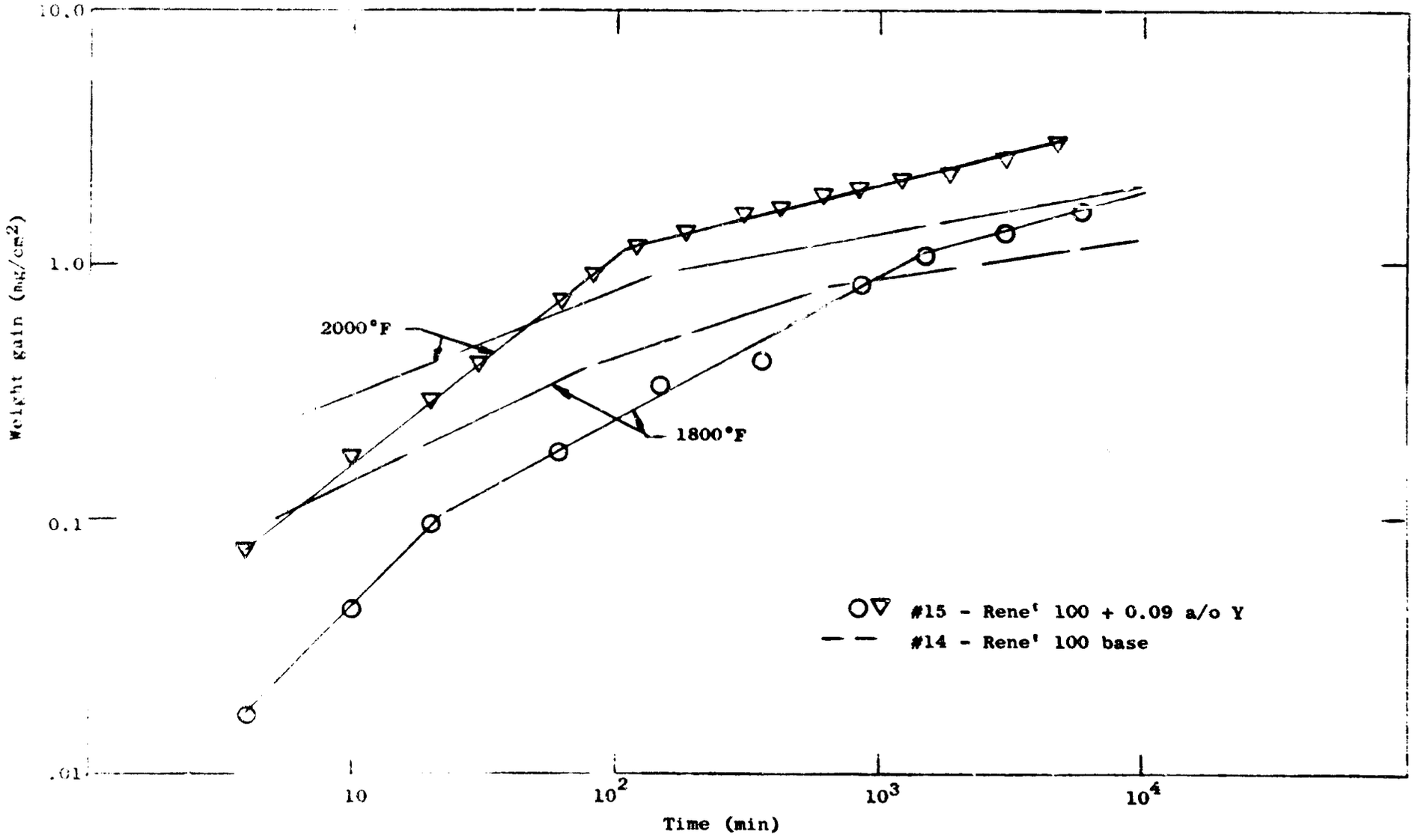

Figure 31 Effect of Yttrium additions on the oxidation Kinetics of Rene' 100

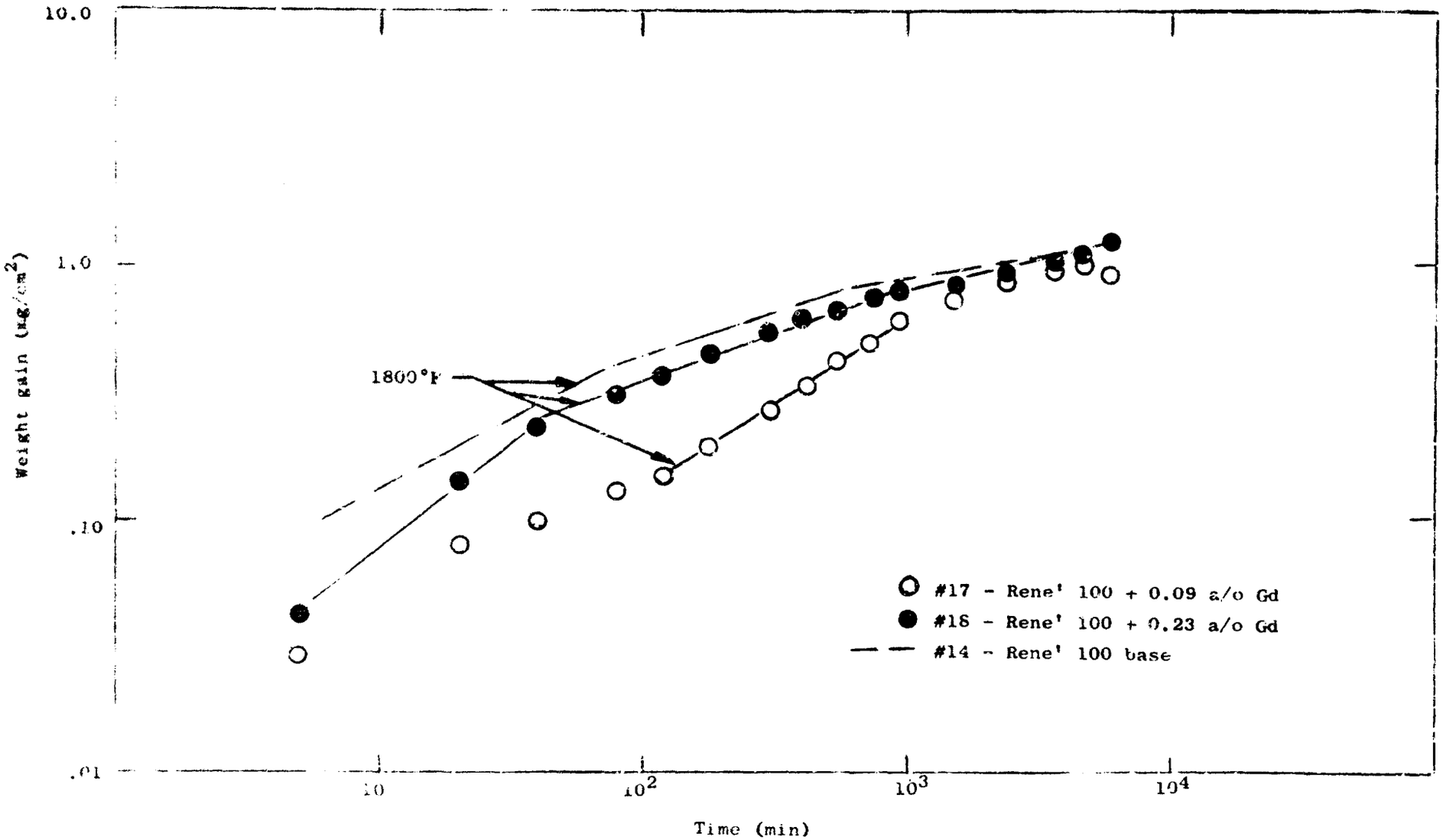

Figure 32 Effect of gadolinium additions on the oxidation kinetics of Rene' 100

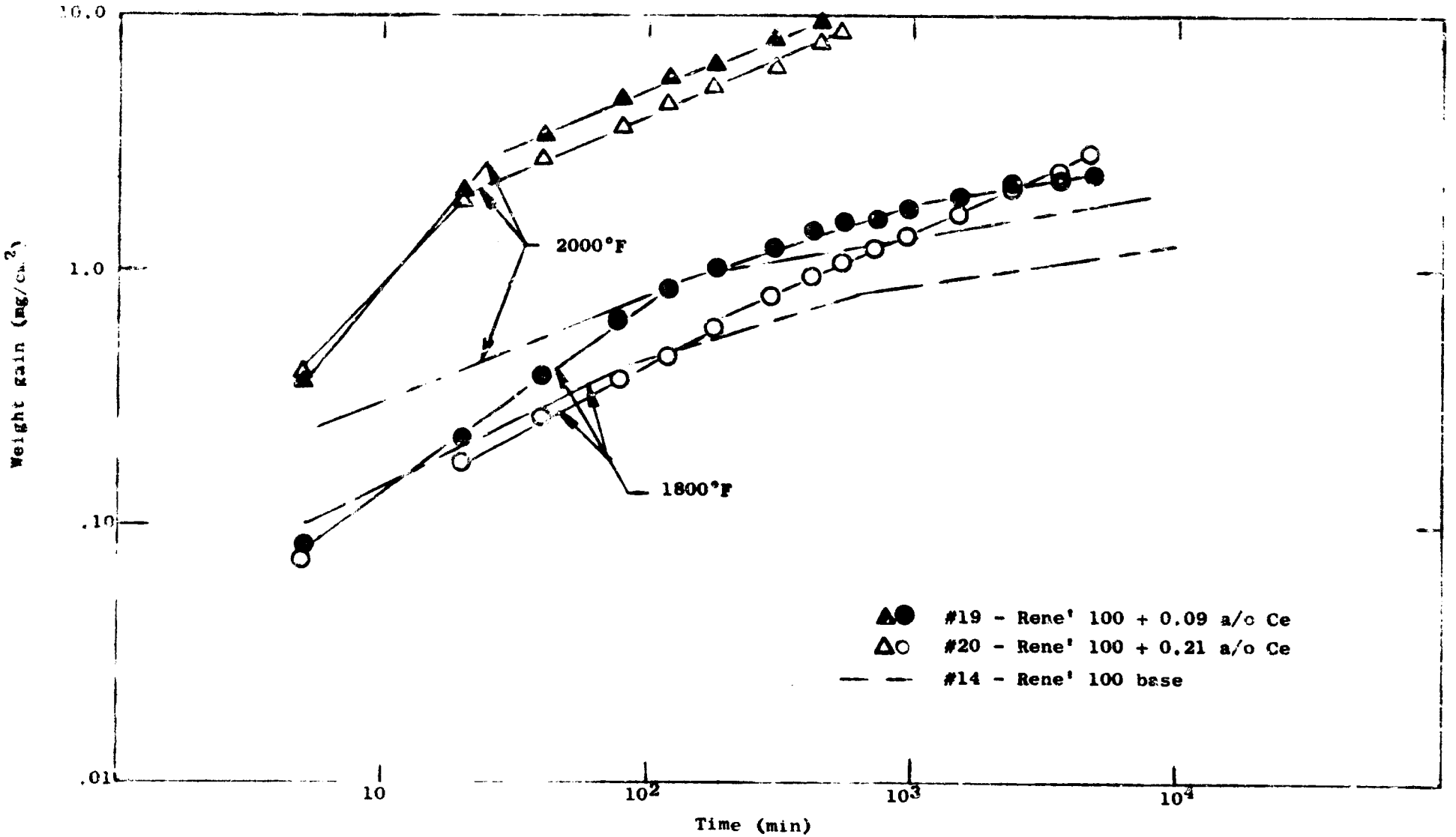

Figure 33 Effect of cerium additions on the oxidation Kinetics of Rene' 100

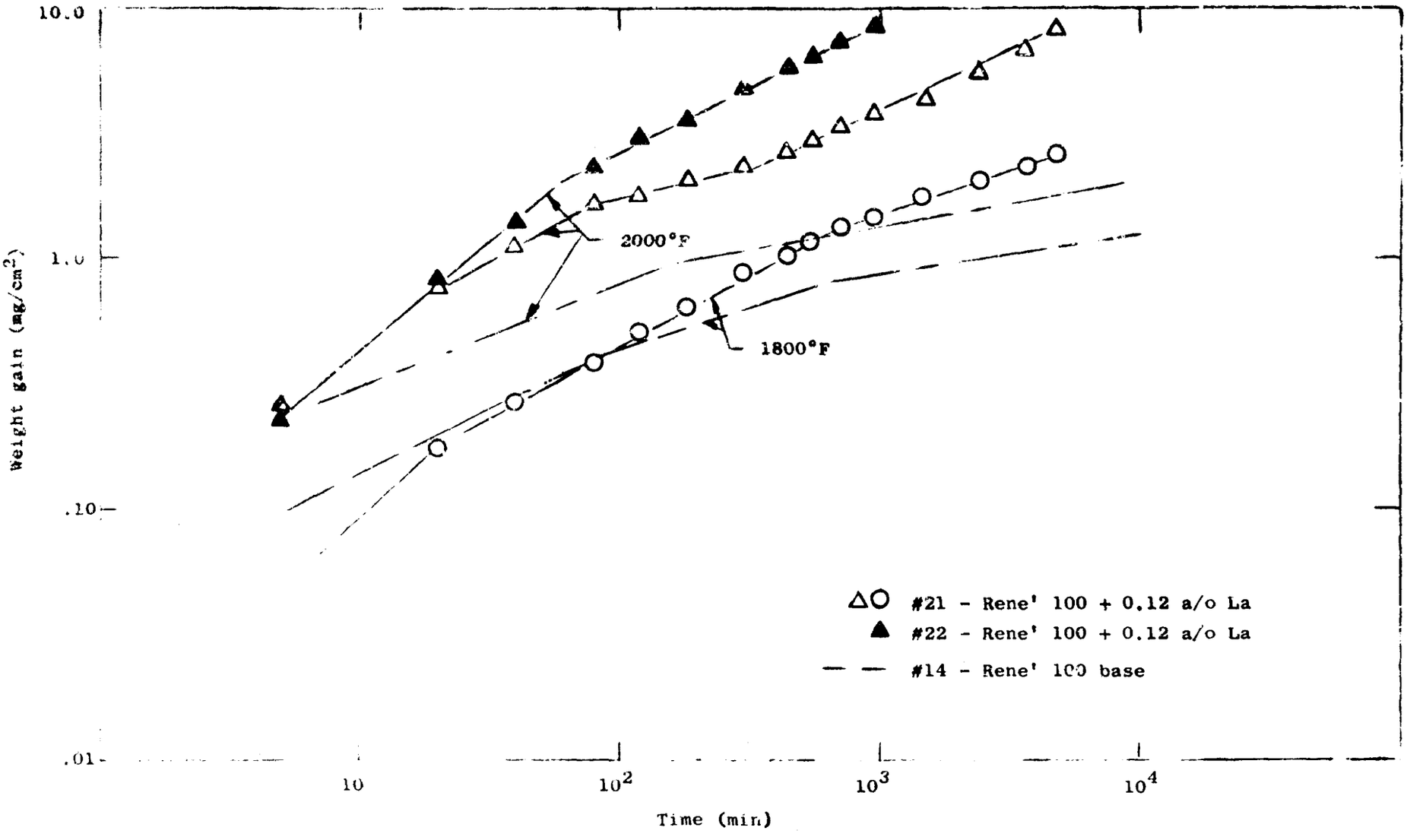

Figure 34 Effect of lanthanum additions on the oxidation rate of Rene' 100

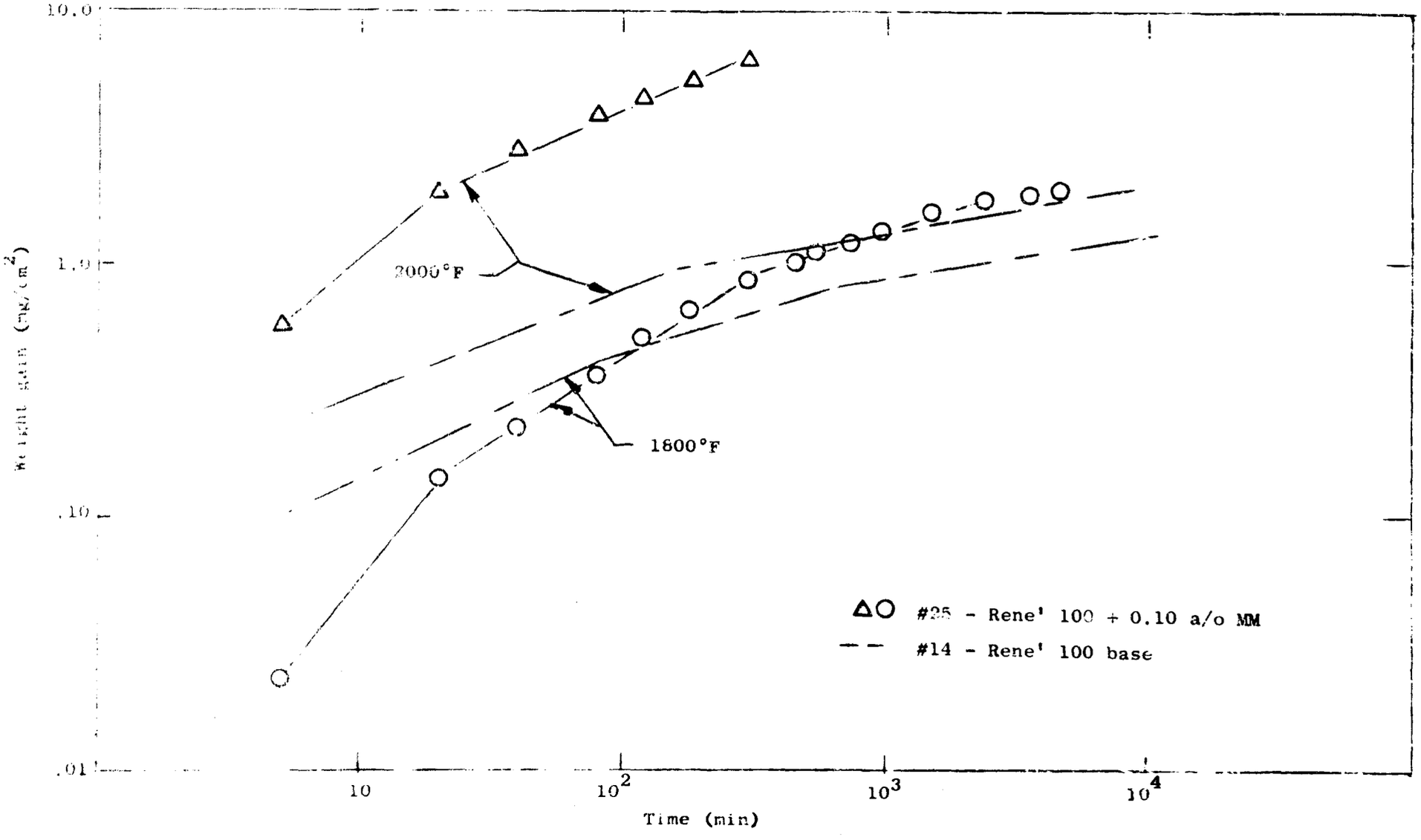

Figure 35 Effect of Mishmetal additions or the oxidation Kinetics of Rene' 100

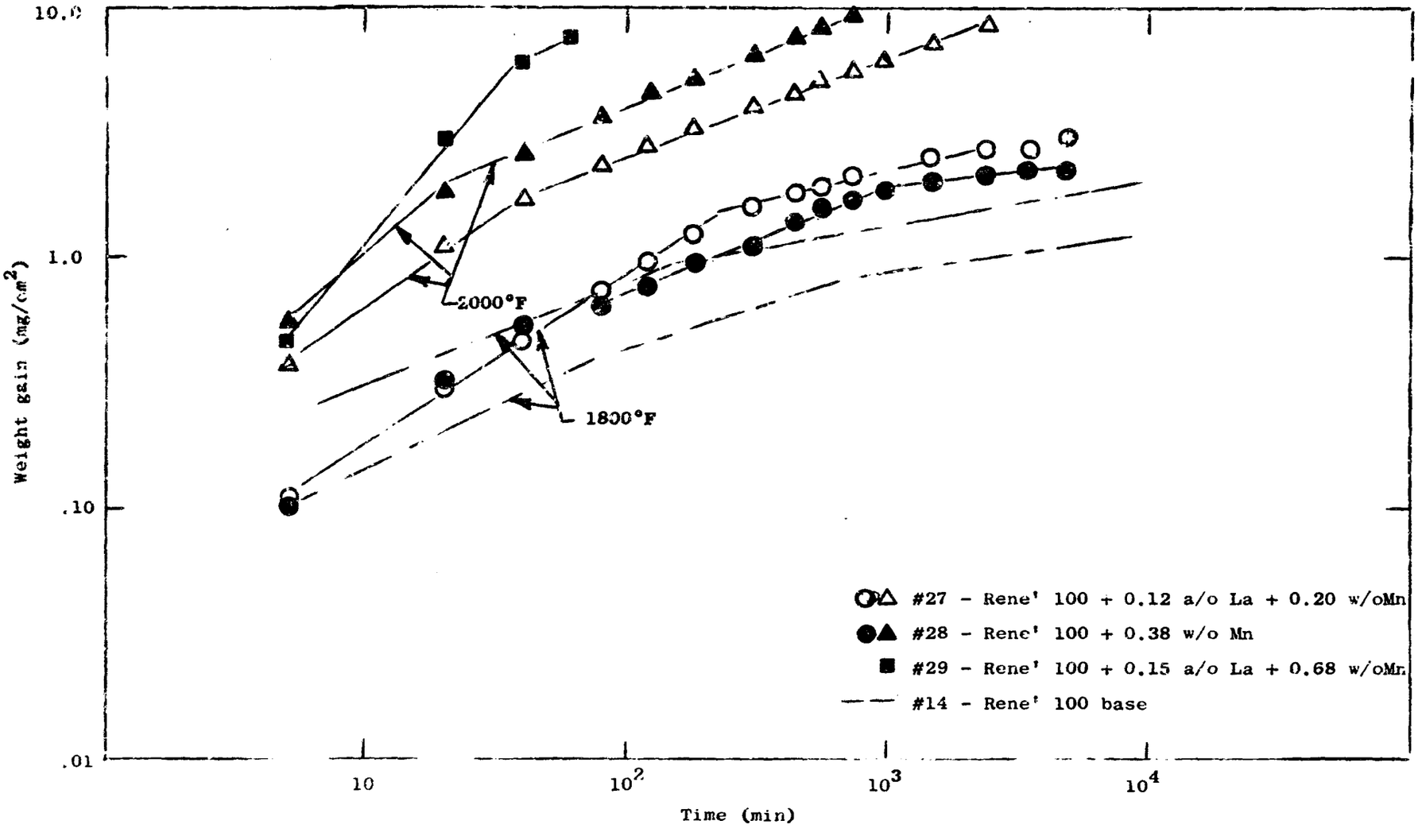

Figure 36 Effect of lanthanum and manganese additions on the oxidation Kinetics of Rene' 100

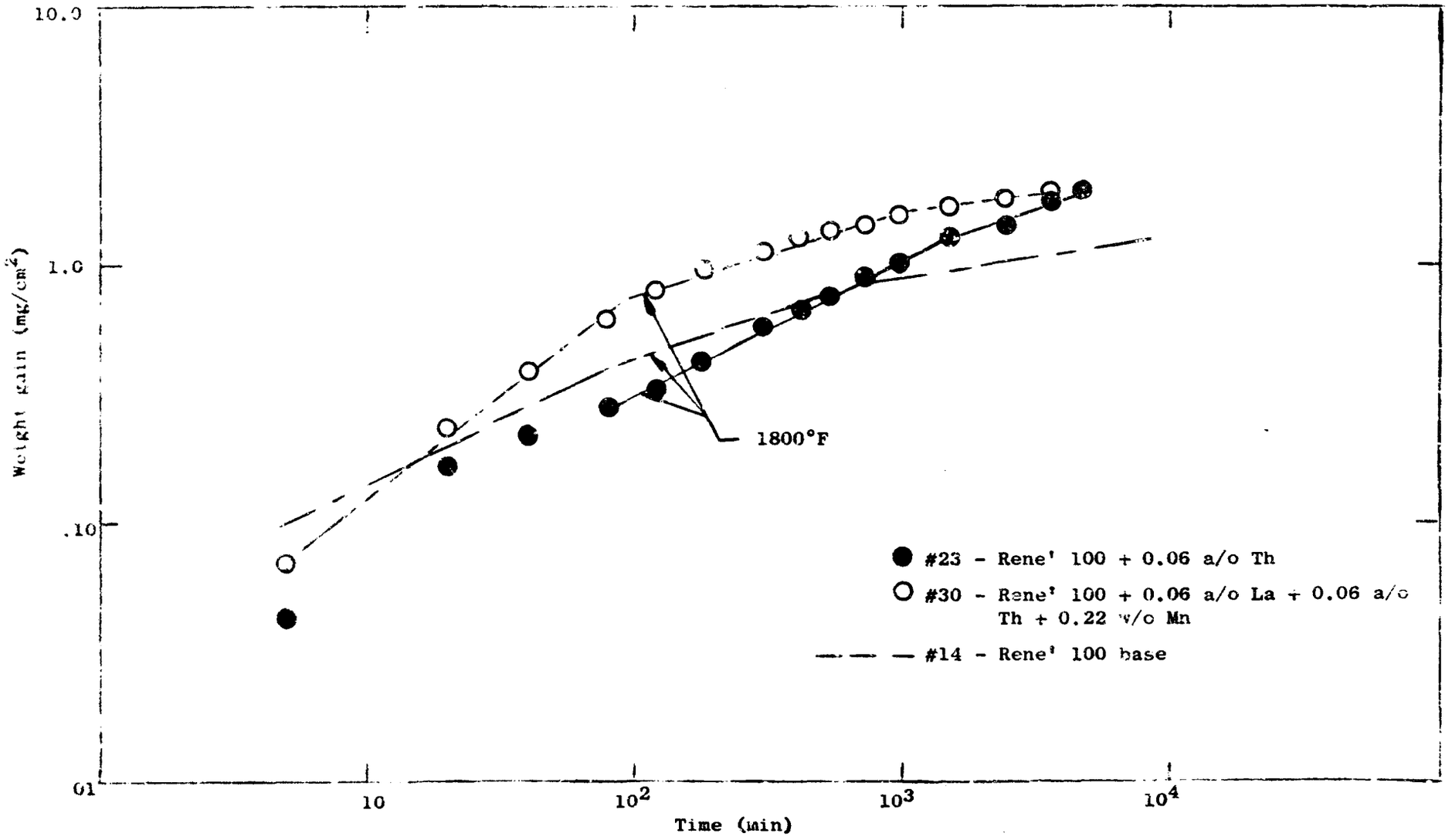

Figure 37 Effect of thorium and manganese additions on the oxidation Kinetics of Rene' 100

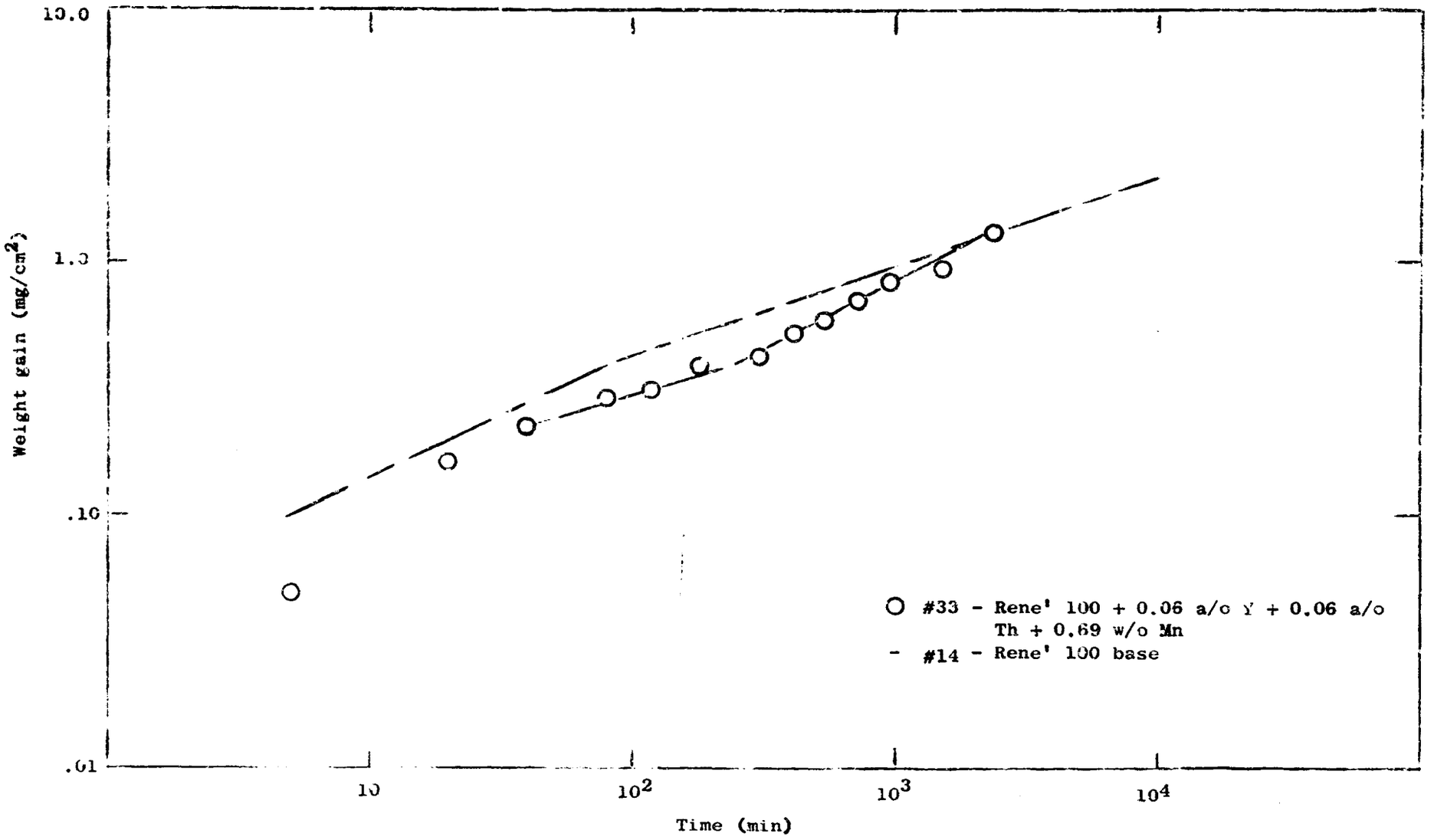

Figure 38 Effect of yttrium, thorium and manganese additions on the oxidation resistance of Rene' 100

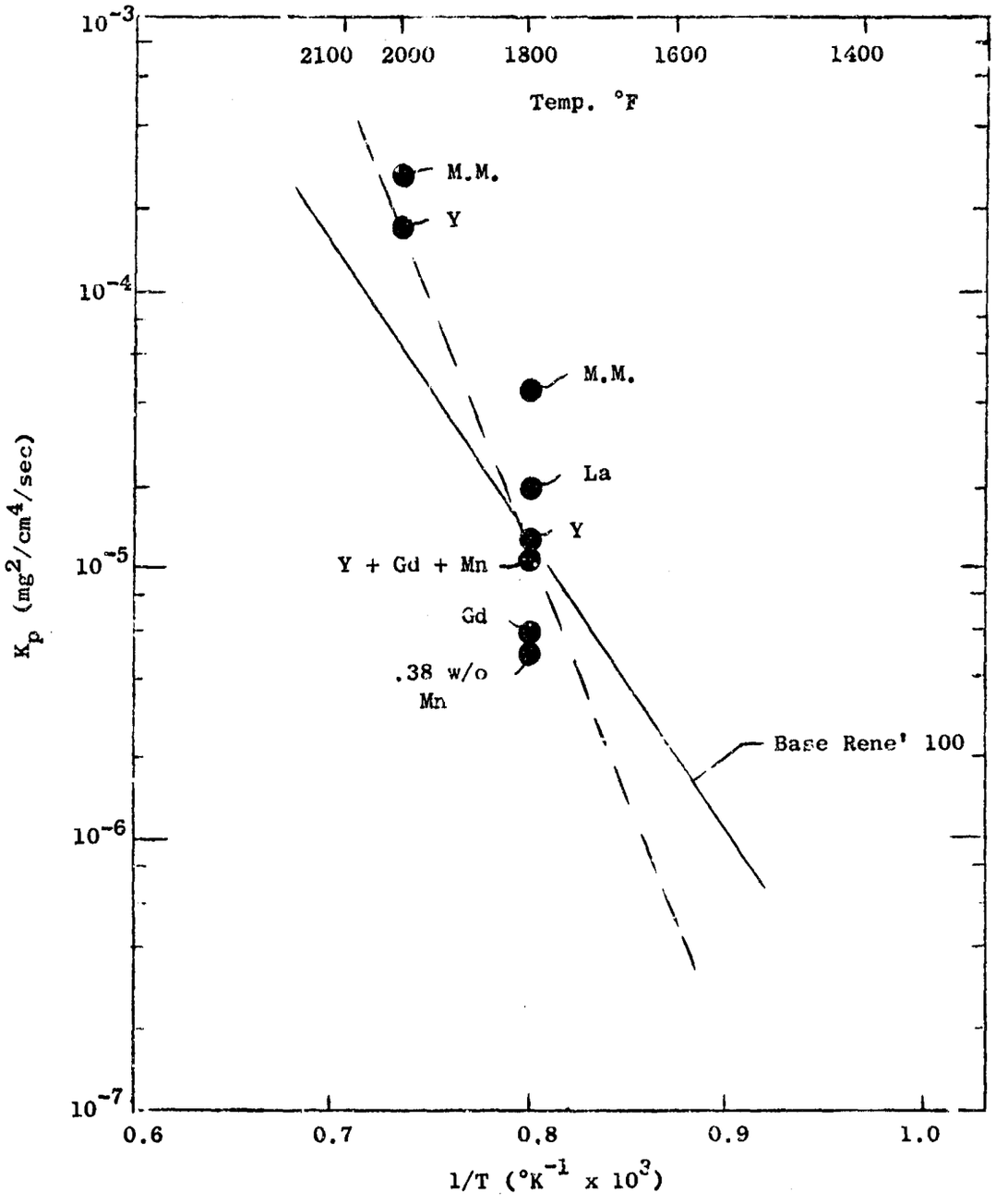

Figure 39 The effect of 0.1 atomic percent additions of various "rare-earths" on the oxidation Kinetics of Rene' 100

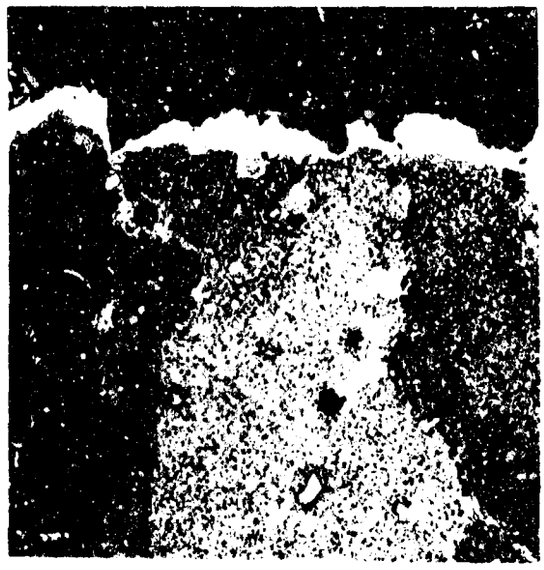

N7278

(a) René 100 + 0.12 a/o La
(100 hr/1800°F)

N7280

(b) René 100 + 0.12 a/o La
(100 hr/2000°F) - Note:
Alloy depletion and degenerate γ'

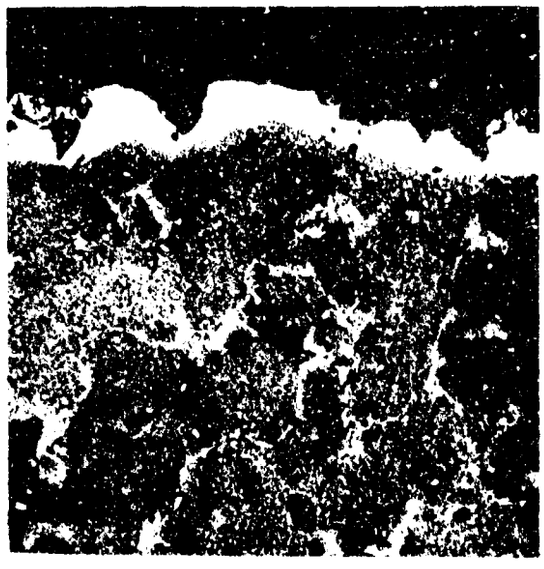

N7277

(c) René 100 + 0.21 a/o Ce
(100 hr/1800°F)

N7276

(d) René 100 + 0.09 a/o Y
(100 hr/2000°F) - Note:
Alloy depletion and degenerate γ'

Figure 40: Microstructure of oxidation reactions during continuous weight gain testing (250X Codep Etch).

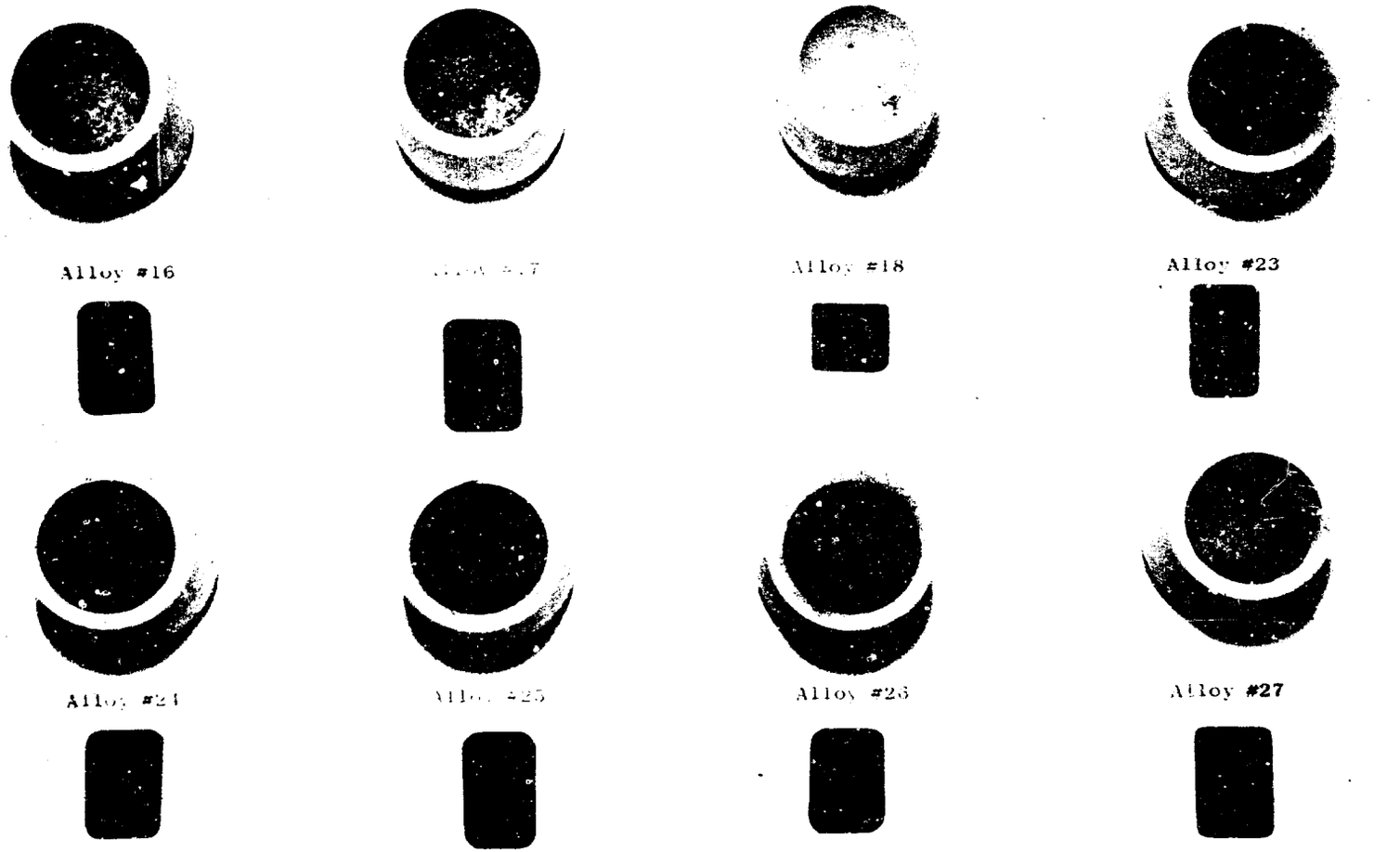

Figure 41: General appearance of doped Rene´ 100 alloys after 10-100 hour cycles at 1800°F. (Note: Alloy #18 exposed for 5-100 hour cycles.)

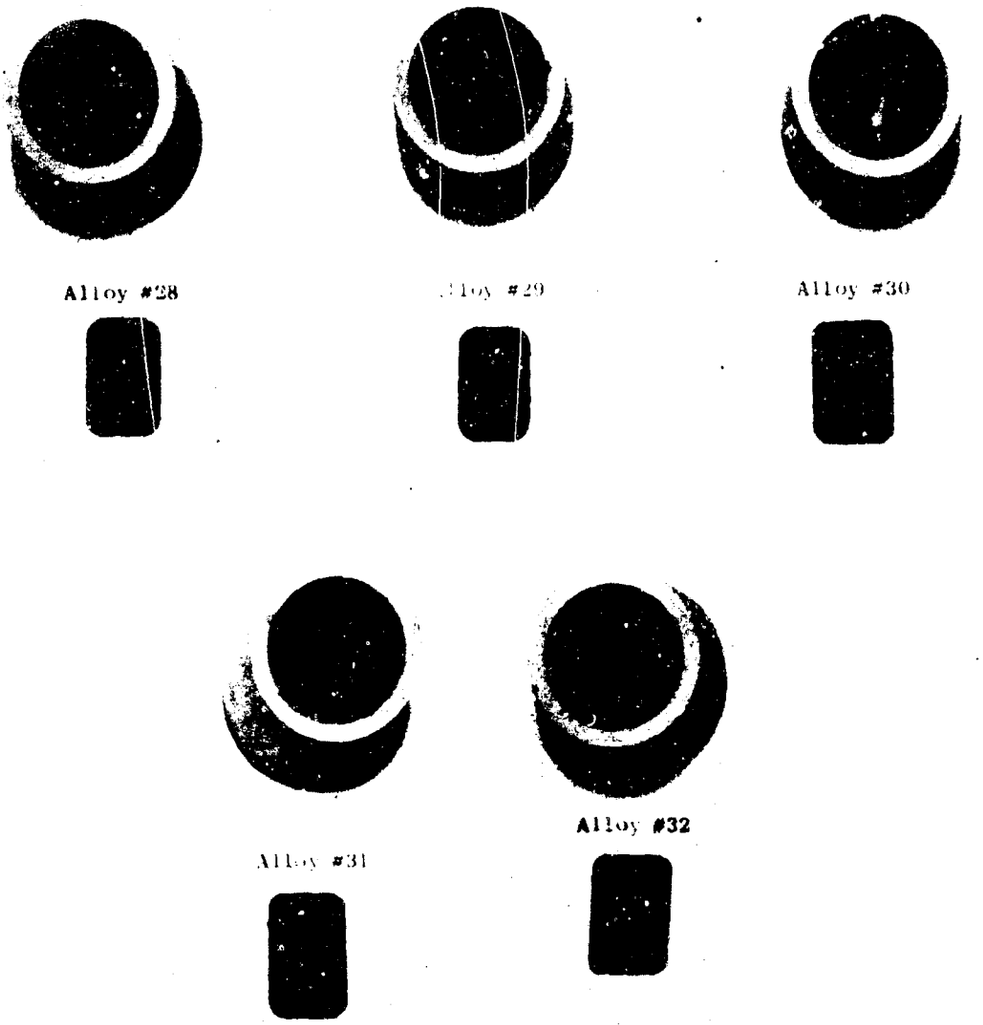

Figure 42: General appearance of doped René 100 alloys after 10-100 hour cycles at 1800°F. (Alloy #30 typifies René 100 base alloy.)

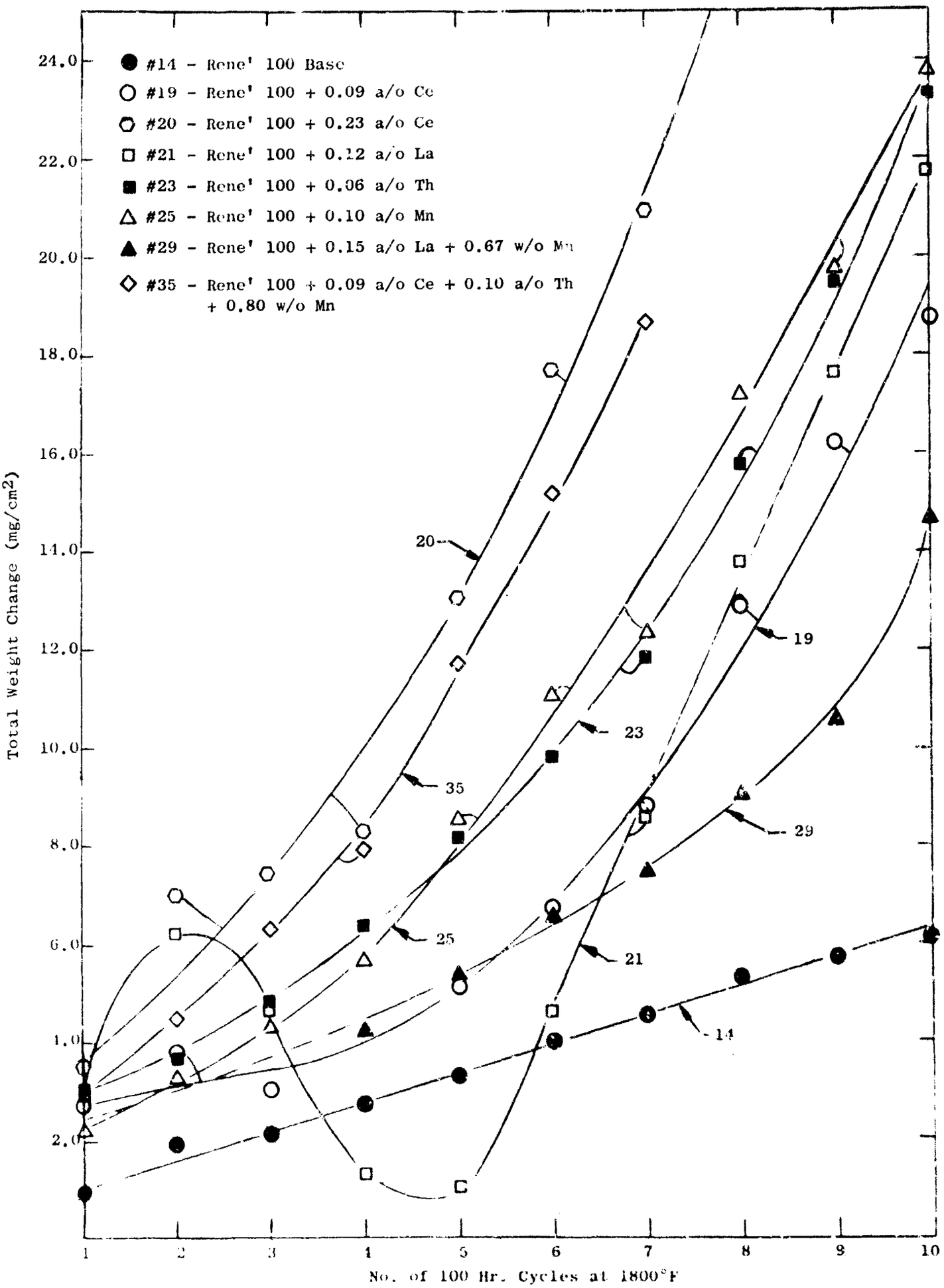

Figure 43. Thermocyclic oxidation behavior of those alloys worse than Rene' 100 at 1800°F

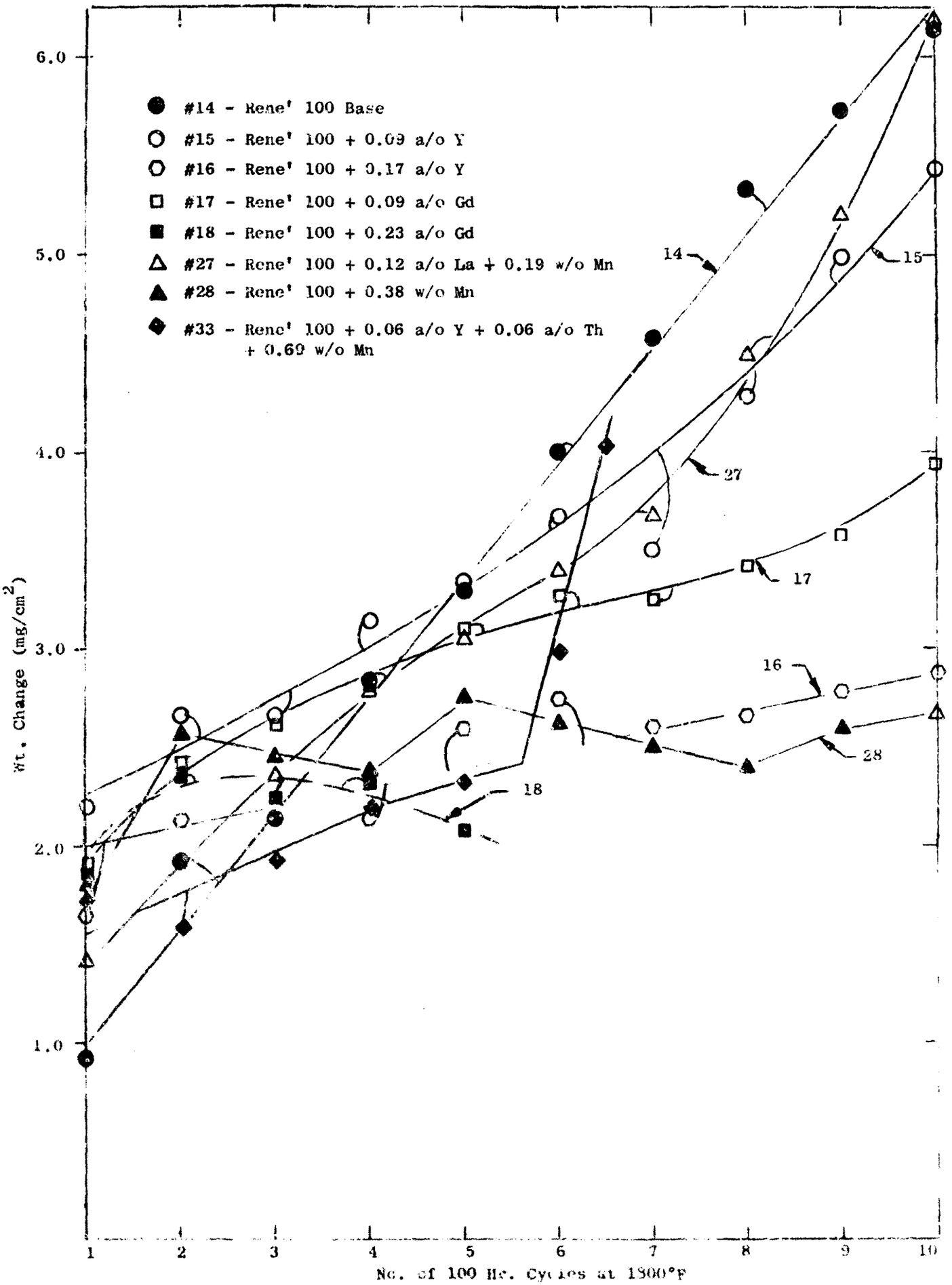

Figure 44. The cyclic oxidation behavior of those alloys better than Rene' 100 at 1800°F

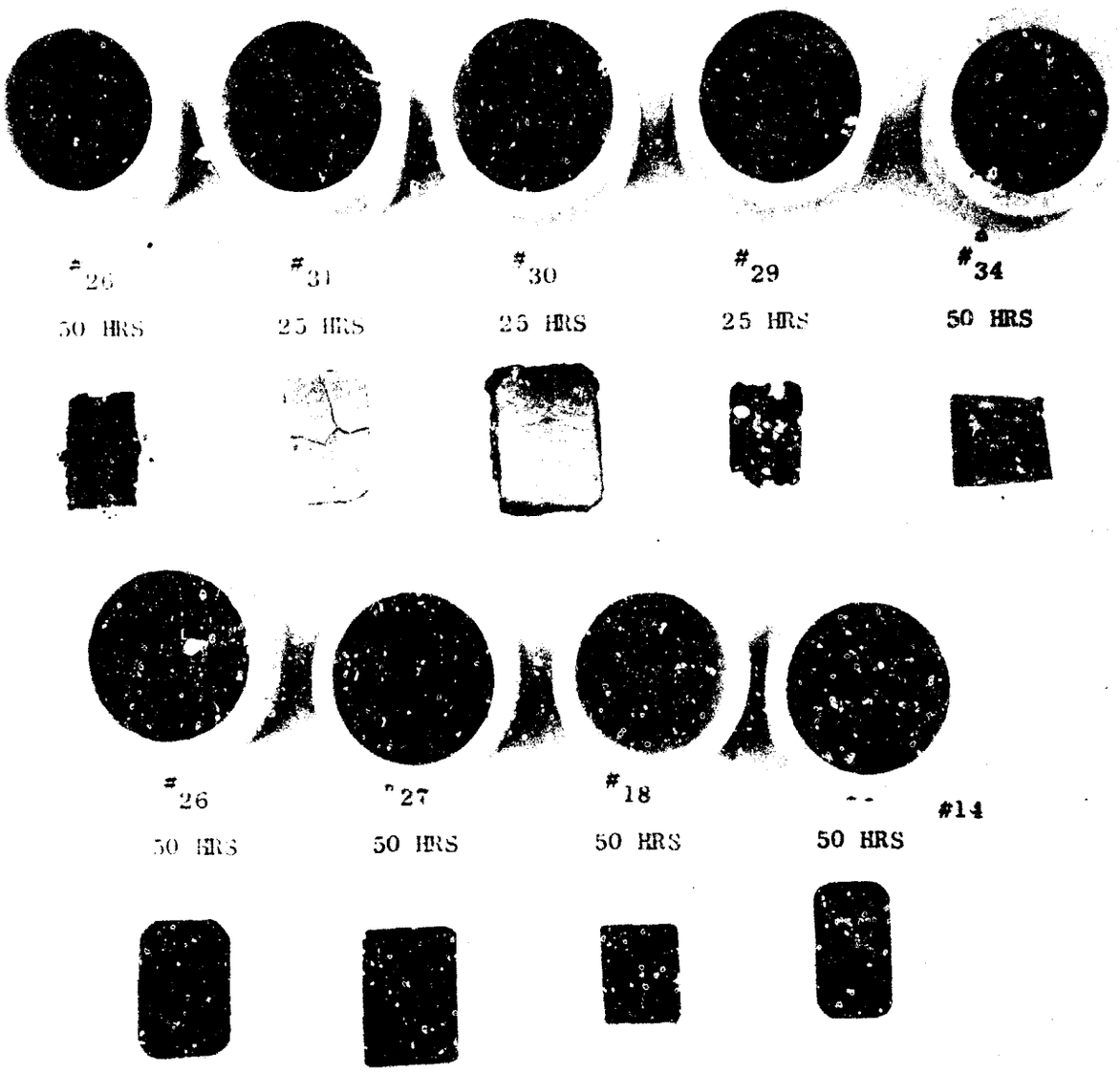

Figure 45: Differences in oxidation behavior of doped René 100 alloys during 2000 F cyclic oxidation (hours refer to total exposure in 25 hour intervals.

P1308

(a) #14 René 100 Base
Note: Multiphase Oxide

P1303

(b) #15 R-100 + .09 a/o Y

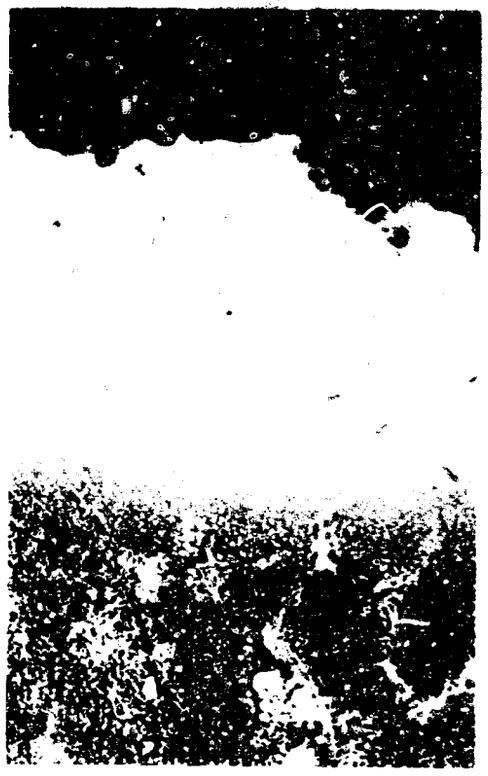

(c) #17 R-100 + 0.09 a/o Gd
Note: Absense of I.O. or subscale formation.

Figure 46: Typical microstructure of oxides formed on various doped René 100 alloys after 1000 hrs/1800°F cyclic oxidation. (500X). Etch - 8:1 H_3PO_4 in H_2O

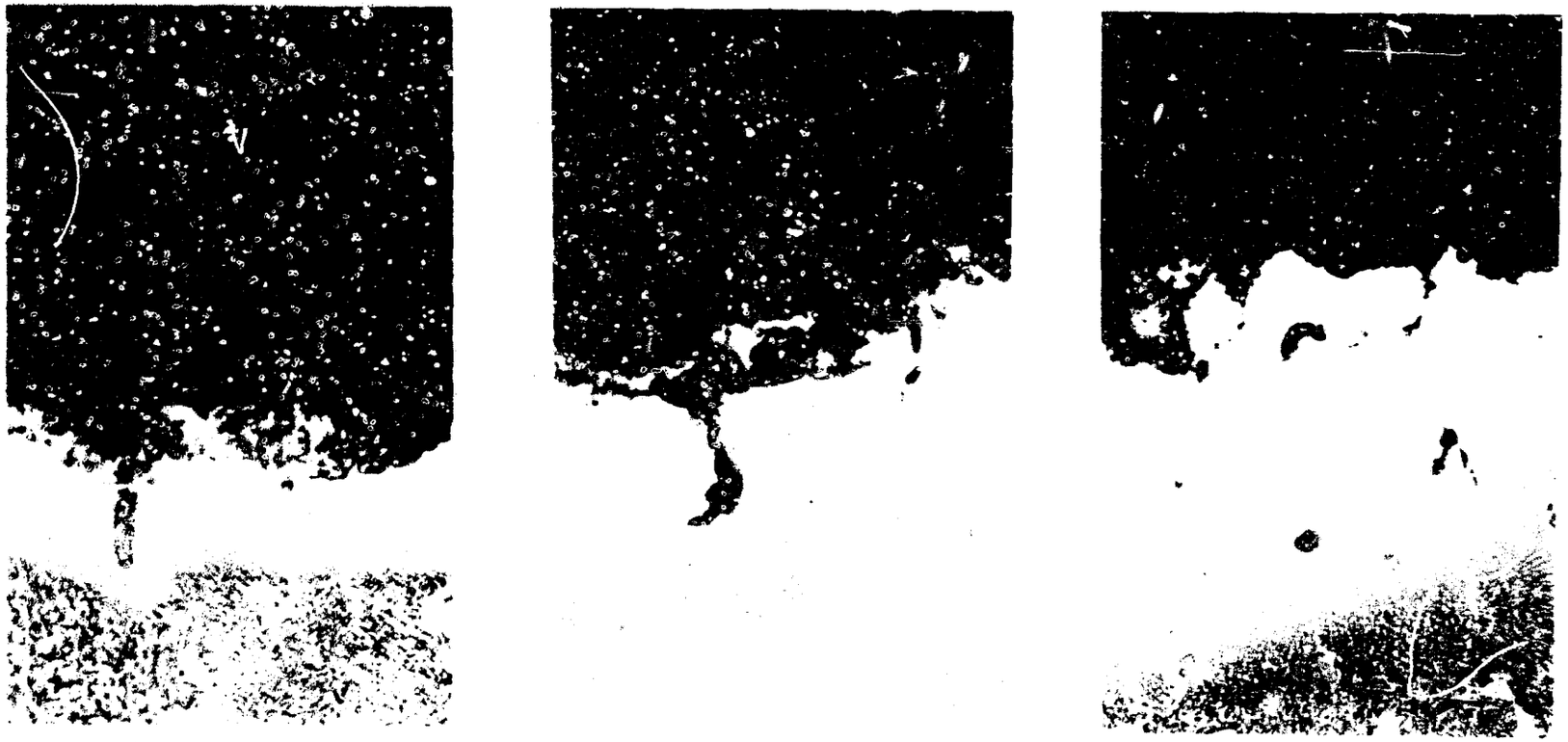

P1305

(a) #18 R-100 + 0.09 a/o Ce
Note: Duplex scale and internal oxidation.

P1302

(b) #23 R-100 + 0.06 a/o Th

P1306

(c) #27 R-100+0.12 a/o La + 0.2 w/o Mn

Figure 47: Typical microstructure of oxides formed on various doped René 100 alloys after 1000 hrs/1800°F cyclic oxidation. (500X). Etch - 8:1 H_3PO_4 in H_2O

P1309

(a) #29 R-100 + 0.15 a/c La + 0.68 w/o Mn Note: Excessive internal oxidation.

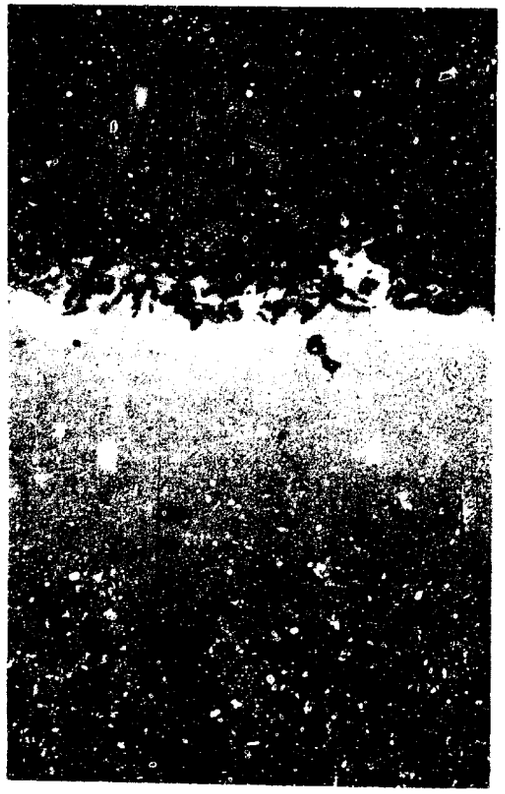

P1312

(b) #31 R-100 + .06 a/o La + .06 a/o Th + .72 w/o Mn Note: Duplex oxide scale and internal oxidation.

P1301

(c) #32 R-100 + .05 a/o Y + .05 a/o Th + .24 w/o Mn Note: Relatively dense oxide with no internal oxidation.

Figure 48: Typical microstructure of oxides formed on various doped René 100 alloys after 1000 hrs/1800°F cyclic oxidation. (500X). Etch - 8:1 H_3PO_4 in H_2O.

P1295

(a) #27 .12 a/o La + .20 w/o Mn
Note: At least three scale constituents.

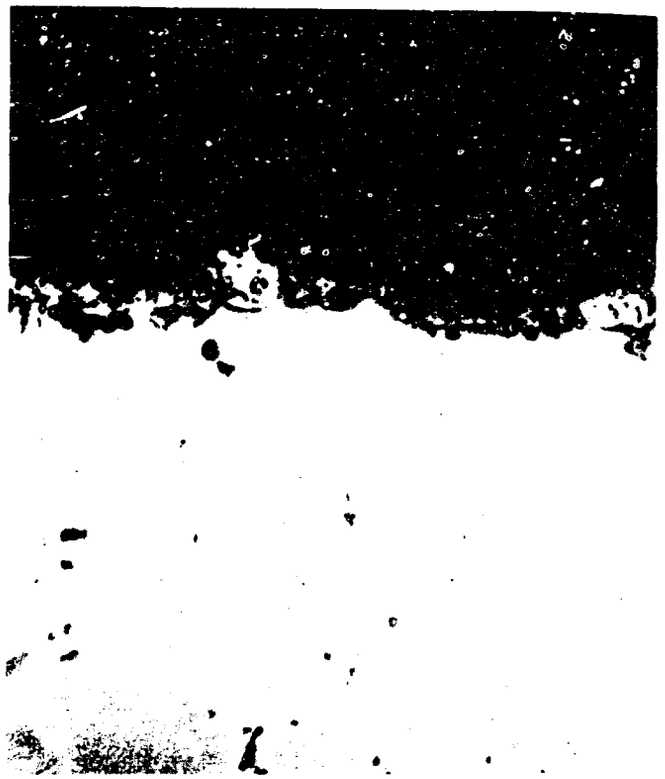

P1298

(b) #31 .06 a/o La + .06 a/o Th + .72 w/o Mn
Note: At least three different oxide phases.

Figure 49: Microstructures depicting multiphase oxide formation in the scale/subscale of doped René 100 alloys after cyclic oxidation at 1800°F. (500X) Etch - 8:1 H_3PO_4 in H_2O

P1310

(a) General Scale/I.O. Morphology
Note: Deep intergranular oxidation
(250X)

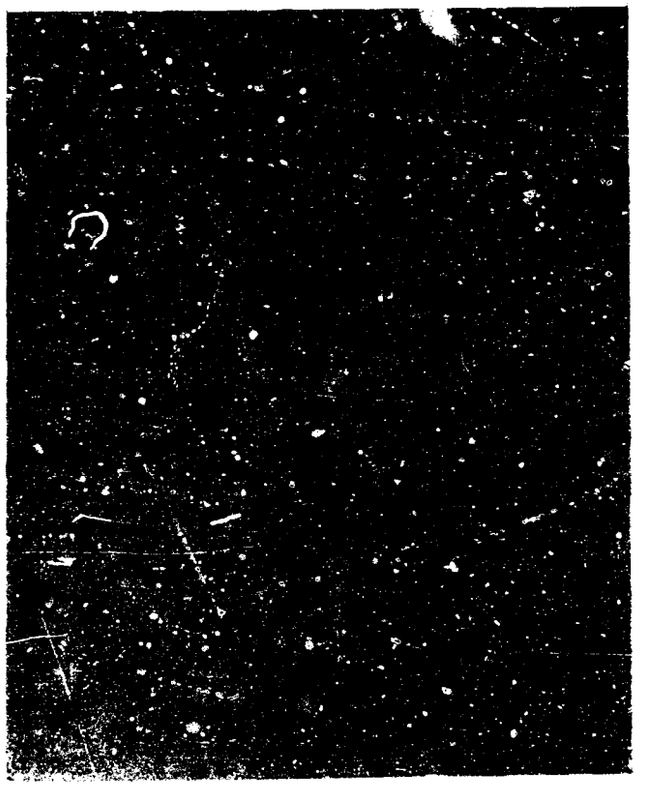

P1311

(b) Nature of intergranular oxidation
Note: La containing Ni compound (medium grey) is resistant to oxidation but secondary precipitates (presumably R.E. carbides) are prone to oxidation. (1000X).

Figure 50: Nature of oxidation reaction of René 100 alloy doped with 0.15 a/o La + 0.68 w/o Mn (Alloy #29) Cyclic exposed 1000 hr. at 1800°F. Etched - 8:1 H_3PO_4 in H_2O

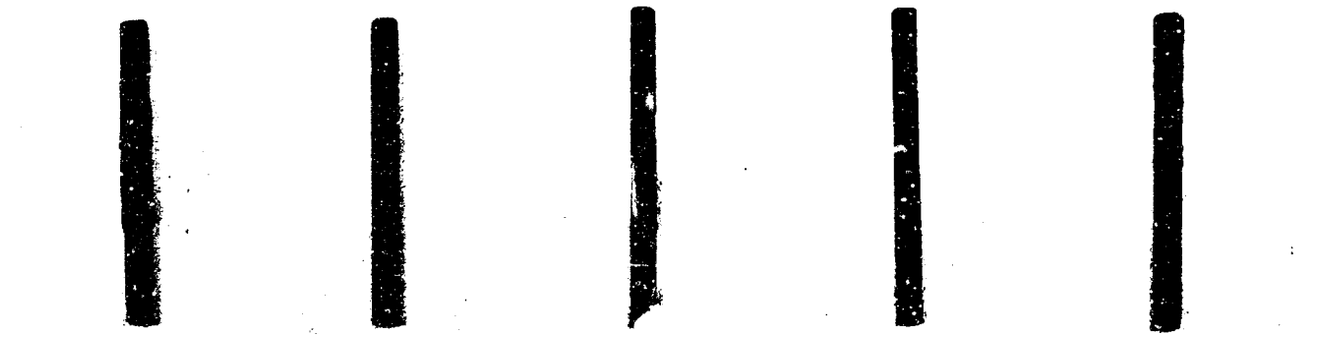

#23 0.06 a/o Th (-15.5)
#22 0.12 a/o La (-1.6)
#21 0.12 a/o La (-2.3)
#20 0.21 a/o Ce (-3.7)
#19 0.09 a/o Ce (-8.5)

#18 0.23 a/o Gd (-2.8)
#17 0.09 a/o Gd (-49.1)
#16 0.17 a/o Y (-27.0)
#15 0.09 a/o Y (-22.0)
#14 Base R-100 (-68.0)

Figure 51: Appearance of Doped R-100 hot corrosion specimens after 50 hour exposure at 1700°F (100 ppm salt). Value in parenthesis is max. depth of attack. (1X)

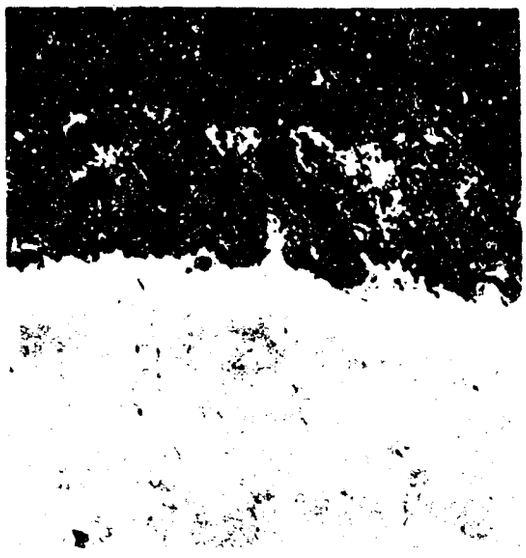

P1349

(a) #15 R-100 + 0.09 a/o Y
Note: Eutectic type sulfidation
(-22.0 mils/dia)

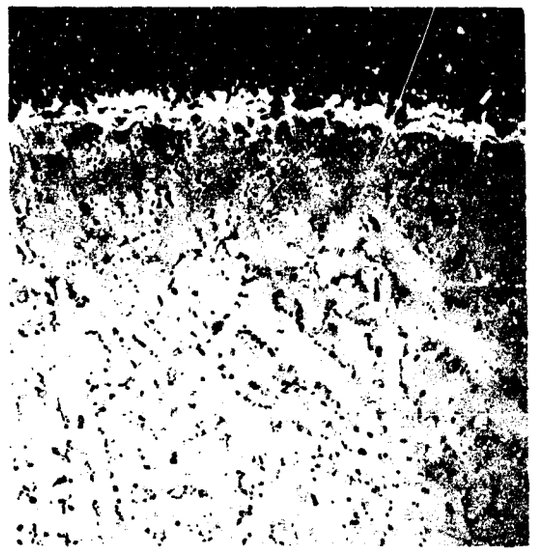

P1355

(b) #18 R-100 + 0.23 a/o Gd
Note: Heavy sulfidation below oxide
(-2.8 mils/dia)

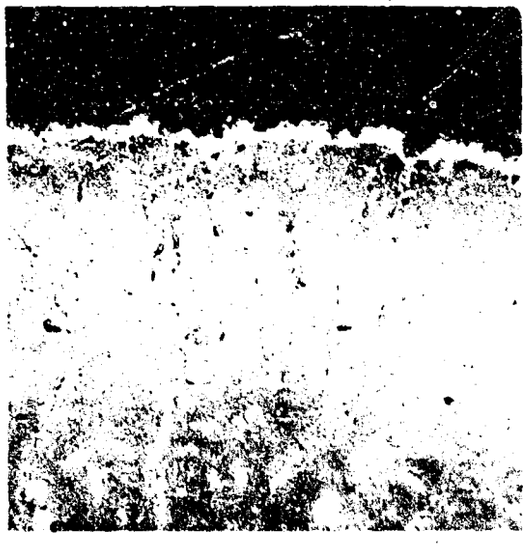

P1350

(c) #21 R-100 + 0.12 a/o La
Note: Dense protective scale
(-2.3 mils/dia)

P1354

(d) #23 R-100 + 0.06 a/o Th
Note: Heavy oxidation and massive
sulfides (-15.5 mils/dia)

Figure 52: Types of hot corrosion attack for doped René 100 alloys (100X)
Etch - 8:1 H_3PO_4 in H_2O

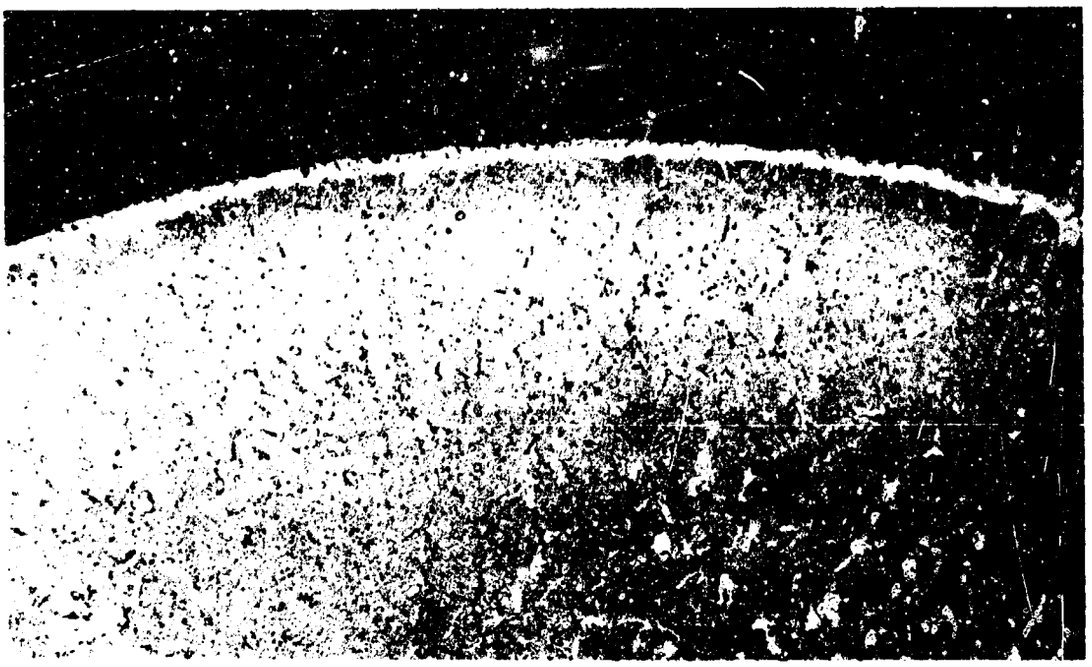

P1352

(a) General appearance of oxide scale formed on Alloy #22 R-100 + .12 a/o La (-1.6 mils/dia) (100 X).

P1353

(b) Protective nature of oxide formed on Alloy #22 Note: Fine subscale sulfides (Gray phase in alloy depletion zone) (500X).

Figure 53: Morphology of scale produced during hot corrosion testing of René 100 + 0.12 w/o La.

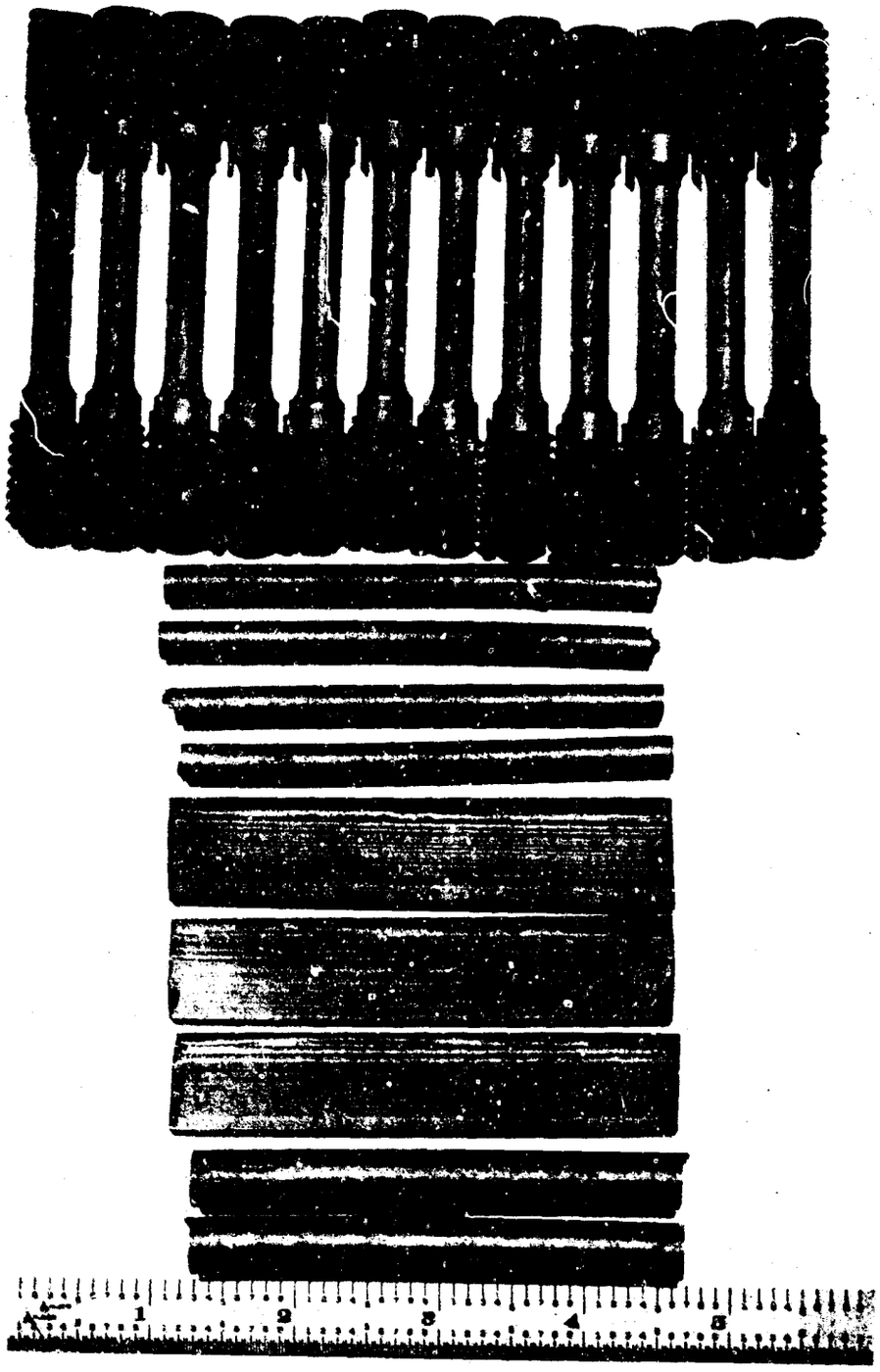

C68080610

Figure 54:
Specimens from Investment Casting

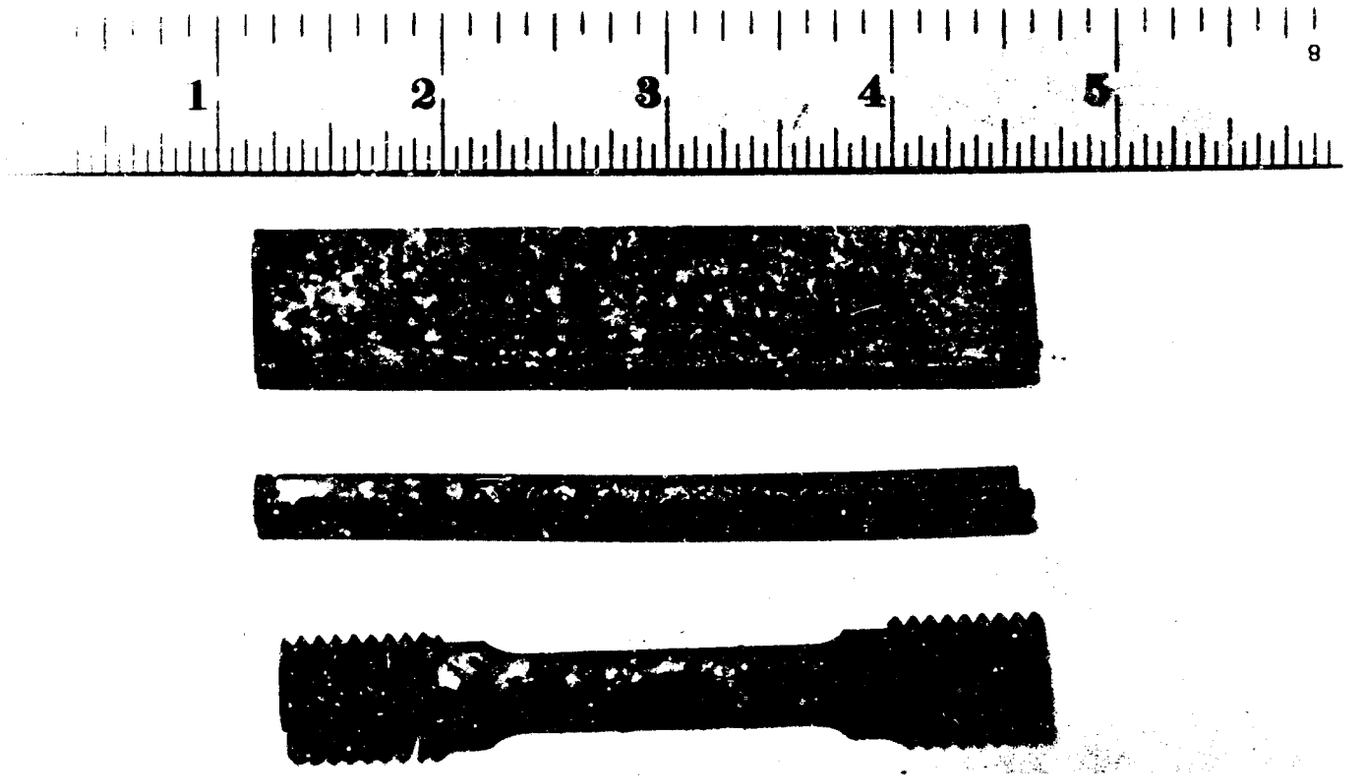

C68080610

Figure 55:

Typical Cast-To-Size Specimen Configurations. Note Grain Size Variation

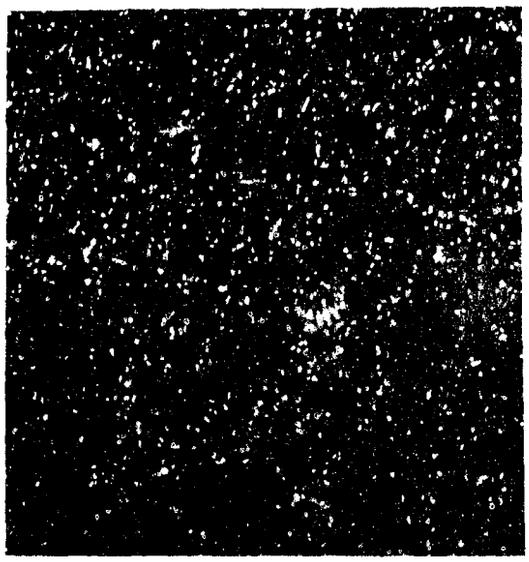

P6468

(a) Rene' 100 Base

P6469

(b) Rene' 100 (Less V) - Note Increased γ-γ' Eutectic

P6470

(c) Rene' 100 + 0.11 W/O Gd + 0.2 Mn - Note Rare-Earth Phase

P6475

(d) Rene' 100 (Less V) + 0.11 W/O Gd + 0.2 W/O Mn - Note Increase γ-γ' Eutectic

Figure 56:

Effect of Vanadium and Gadolinium Modifications on Microstructure of As-Cast Rene' 100 Both With and Without R.E. Additions. Etched in 8:1. (500X)

P6476

(a) Rene' 100 + 0.10 W/O Gd - Note Rare-Earth and γ-γ' Eutectic in Grain Boundaries

P6477

(b) Rene' 100 + 0.23 W/O Gd - Note Increased Rare-Earth and γ-γ' Eutectic in Boundaries

P6480

(c) Rene' 100 (Less V) + 0.07 W/O Gd + 0.02 W/O Y + 0.25 W/O Mn - Note Carbide Precipitation Within γ-γ' Eutectic

Figure 57:

Effects of Rare-Earth and Mn Additions on Phase Morphology. Etched in 3:1

(500X)

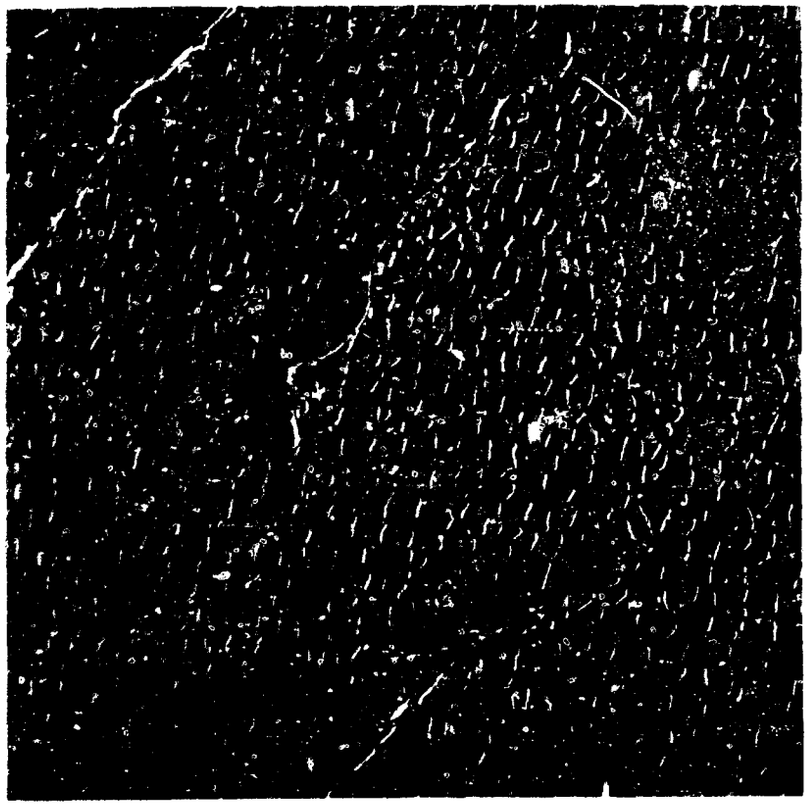

975D

(a) Typical γ' and Carbide Morphology

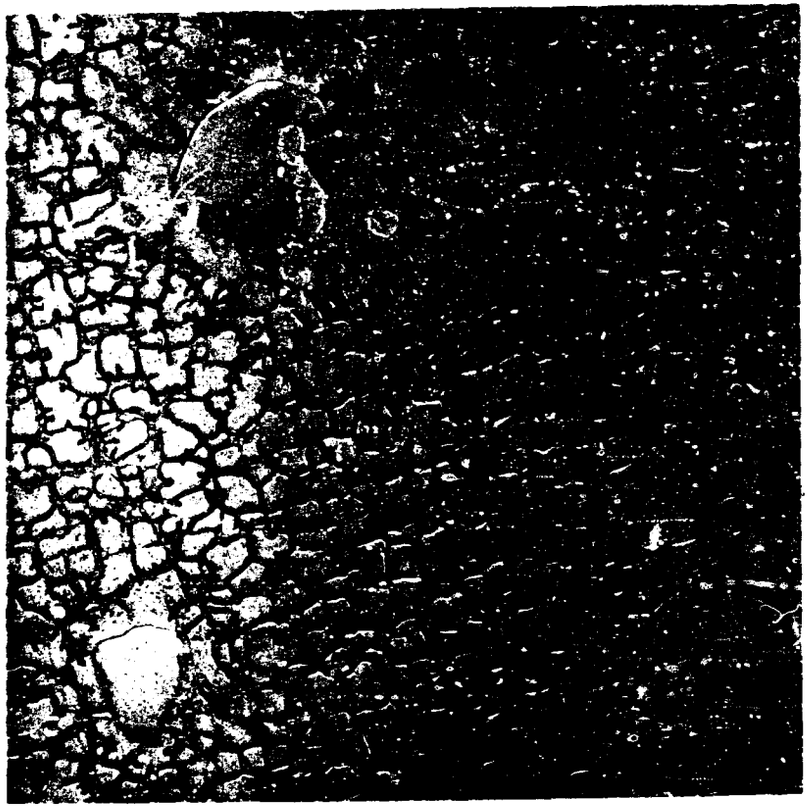

975B

(b) Typical γ-γ' Eutectic Morphology

Figure 58: Electron Microscopy Typifying Base Rene' 100.

(5000X)

975C

(a) Rene' 100 + 0.11 W/O Gd + 0.2 W/O Mn

975F

(b) Rene' 100 + 0.23 W/O Gd

Figure 59:

Typical Distribution of Rare-Earth Phase (Arrow) in Grain Boundaries.

(5000X)

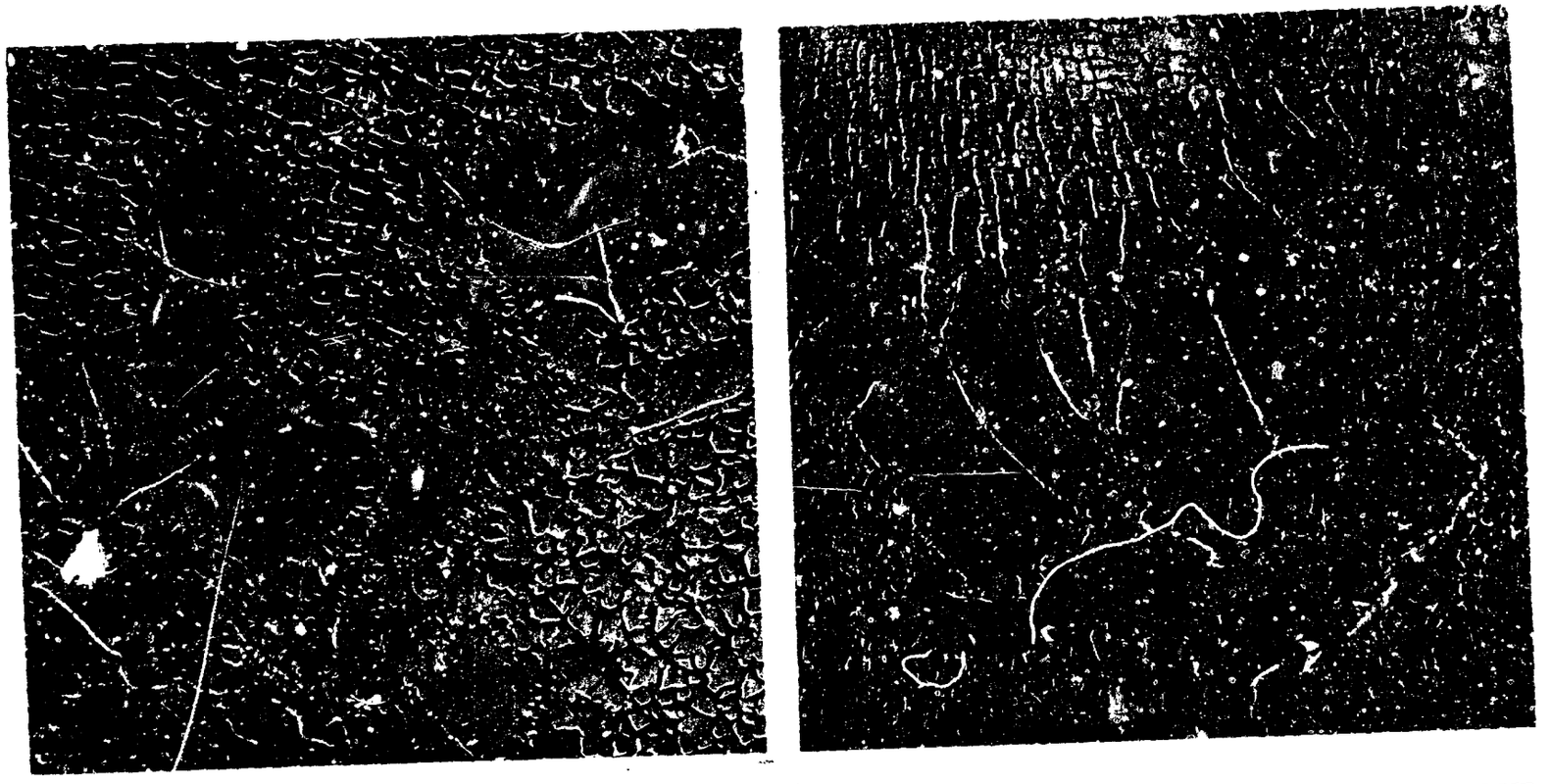

975D

975F

(a) Rene' 100 (Less V) + 0.11 W/O Gd + 0.2 W/O Mn (b) Rene' 100 + 0.23 W/O Gd

Figure 60:
Electron Photomicrographs Showing Relation Between Rare-Earth Rich Phase (Arrows) and γ-γ' Eutectic. (5000X)

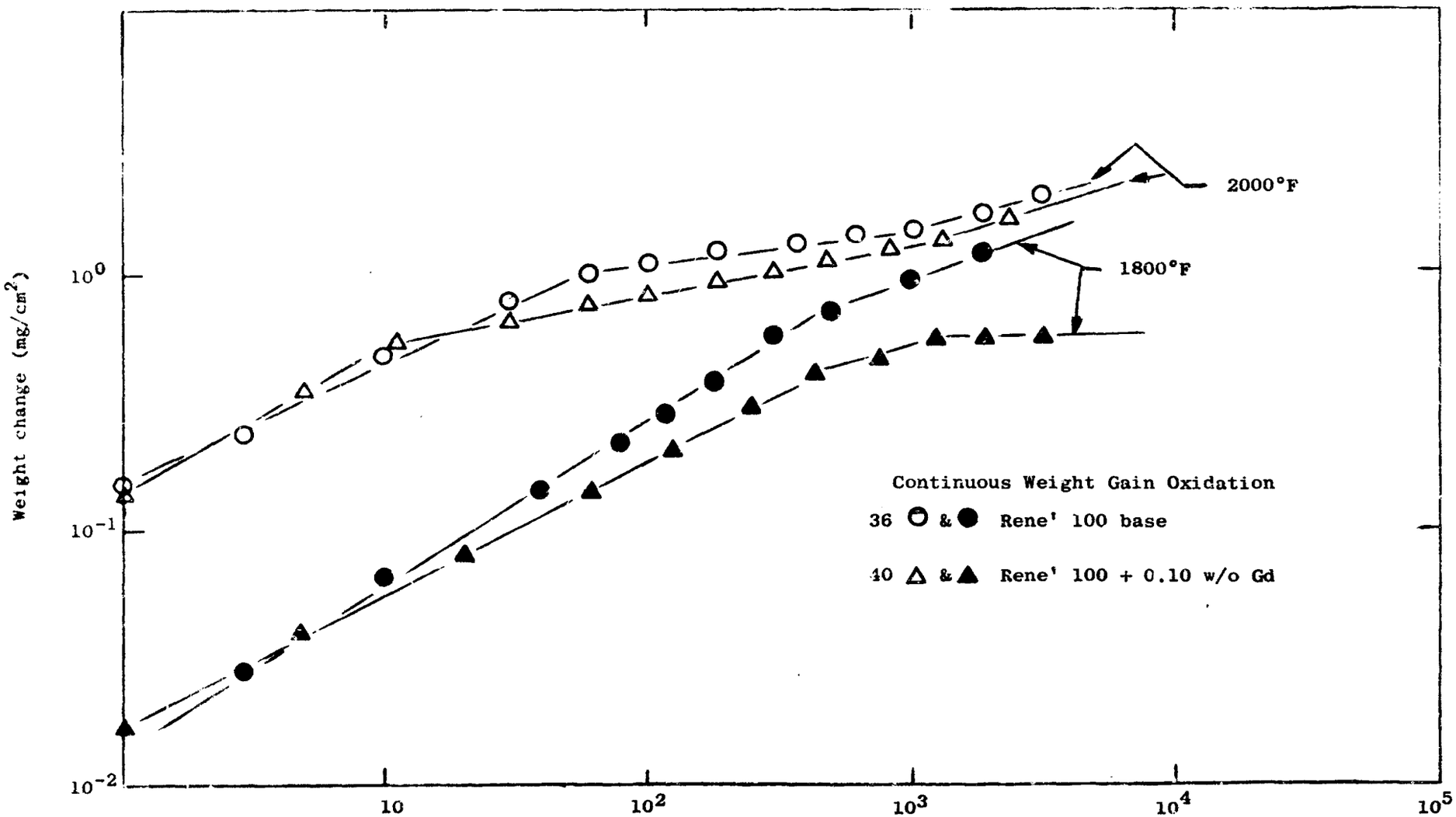

Figure 61: Continuous weight gain curves for alloys 36 and 40 at 1800° and 2000°F

J9626

(a) Alloy 36 (Base Rene' 100)

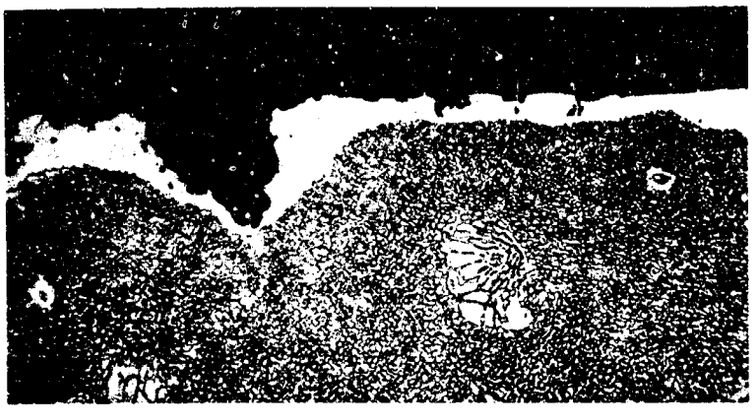

J9627

(b) Alloy 37 (Base - Less V)

J9630

(c) Alloy 40 (0.10 A/O Gd)

Figure 62 Phase II Alloys Oxidized for 500 Hrs. at 1800°F

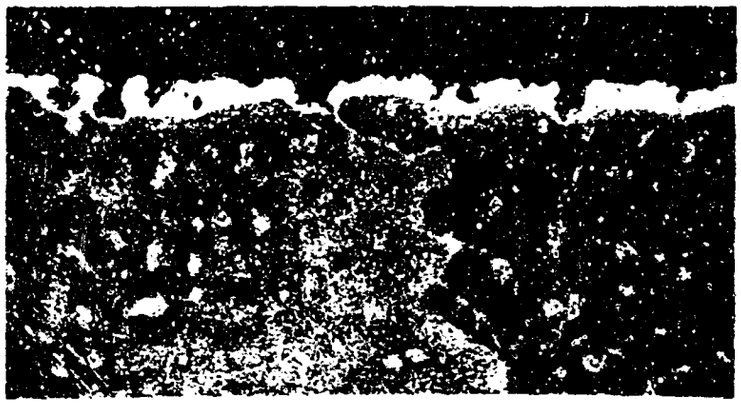

J8161

(a) Alloy 37 (Base Less V)

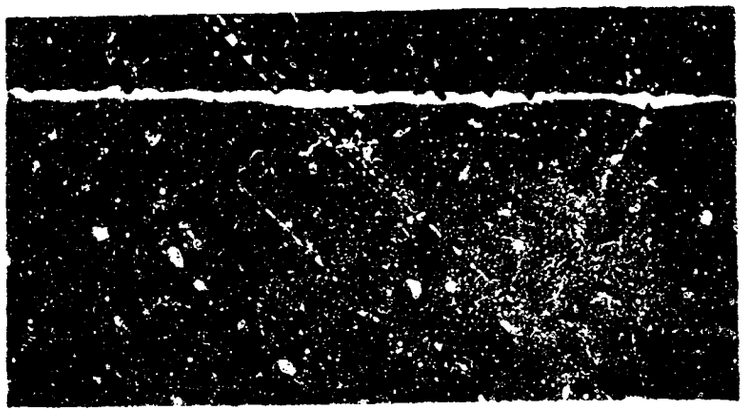

J8162

(b) Alloy 38

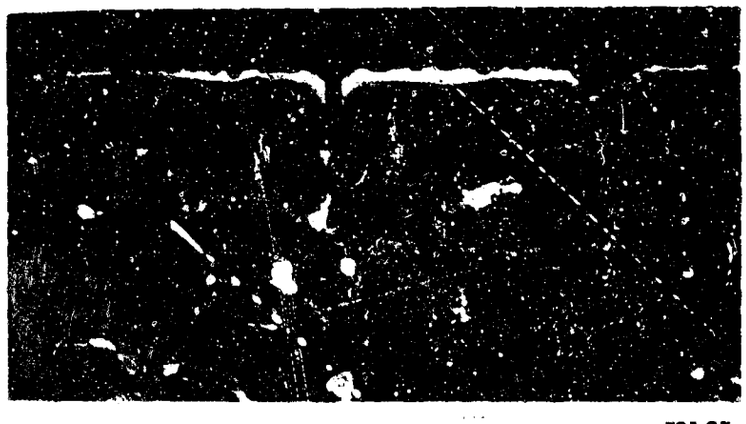

J8165

(c) Alloy 42

Figure 63:

Phase II Alloys Oxidized 150 Hrs. at 2000°F (100X)

9106

(a) Alloy 36

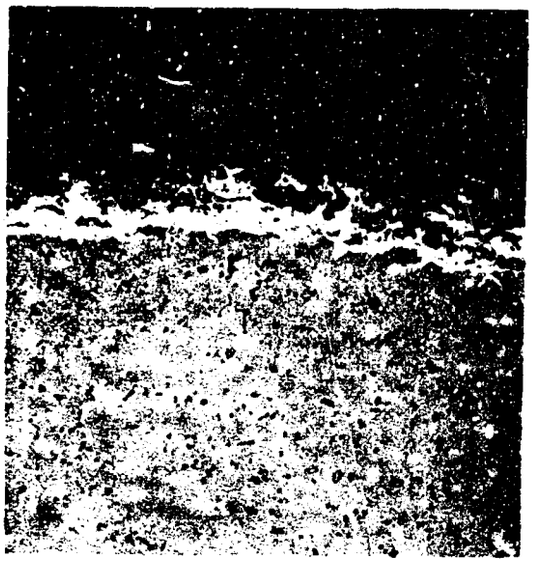

9107

(b) Alloy 37

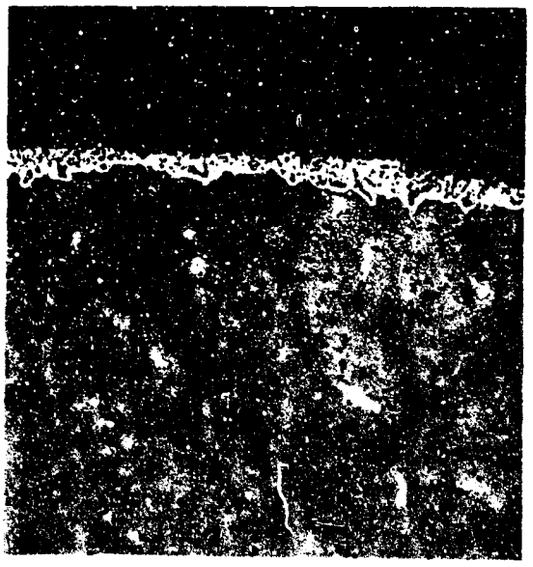

9108

(c) Alloy 38

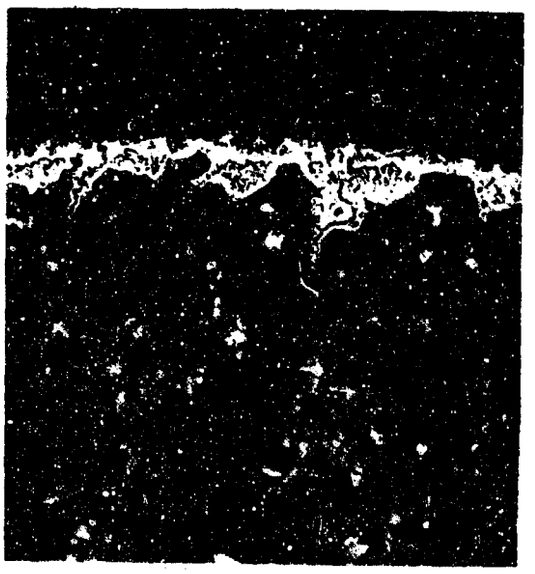

9109

(d) Alloy 39

Figure 64:

Phase II Alloys After Hot Corrosion at 1725°F/50 Hrs. (100X)

9110

(a) Alloy 40

9111

(b) Alloy 41

9112

(c) Alloy 42

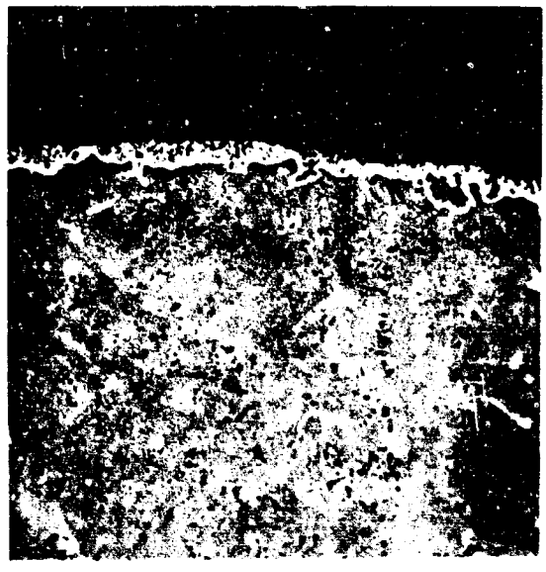

9113

(d) Alloy 43

Figure 65:

Phase II Alloys After Hot Corrosion at 1725°F/50 Hrs. (100X)

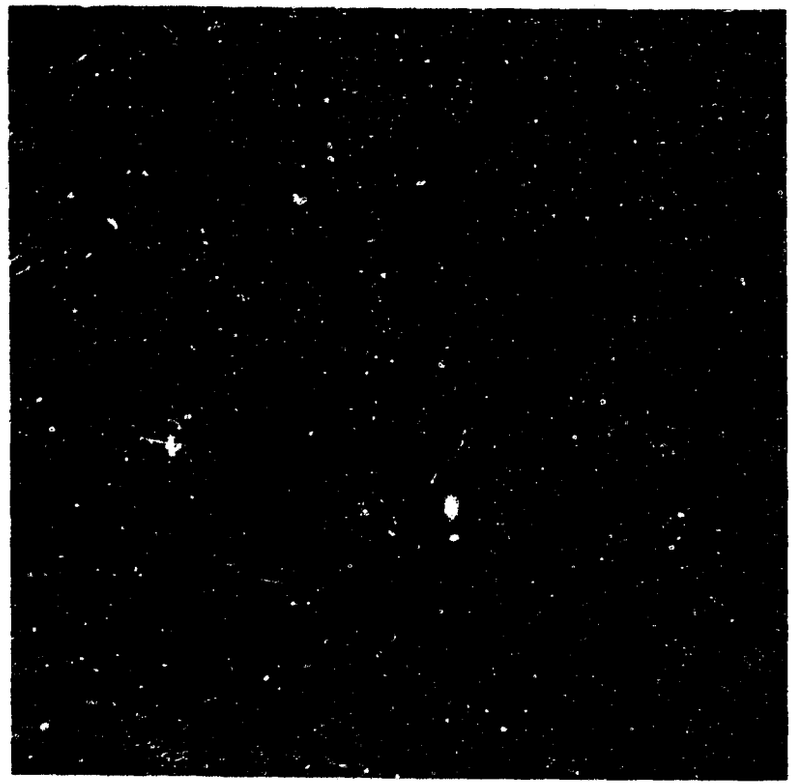

910E

(a) Rene' 100 + 0.15 A/O La + 0.68 W/O Mn Investment Cast-- Note Coarse Rare-Earth Phase.

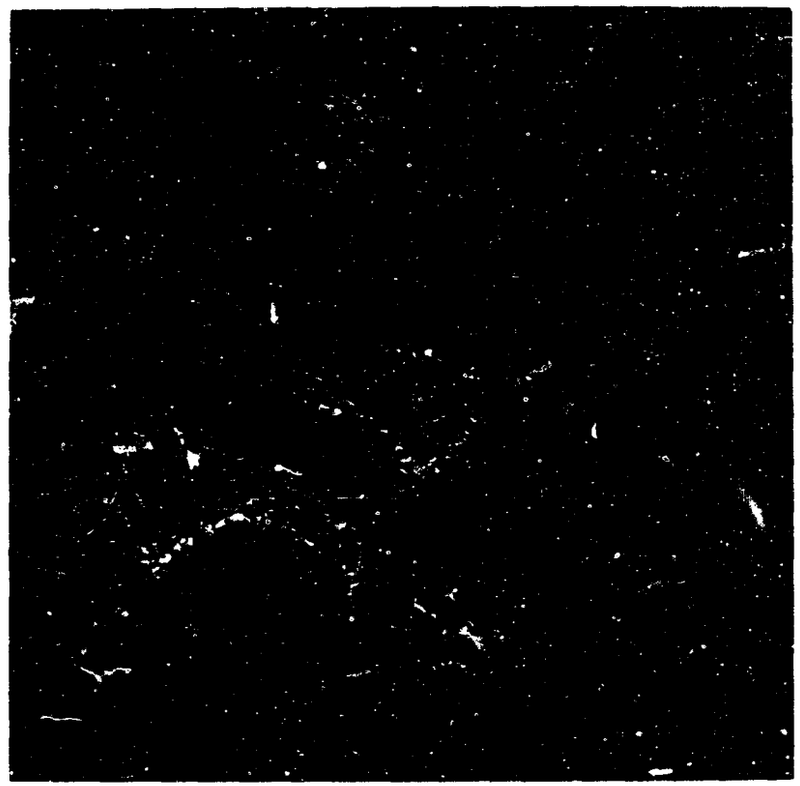

910F

(b) Rene' 100 + 0.15 A/O La + 0.68 W/O Mn Chill-Cast - Note Rare-Earth Phase Associated with γ-γ' Eutectic

Figure 66: Difference in Rare-Earth Phase Size and Distribution As a Function of Casting Technique (5000X)

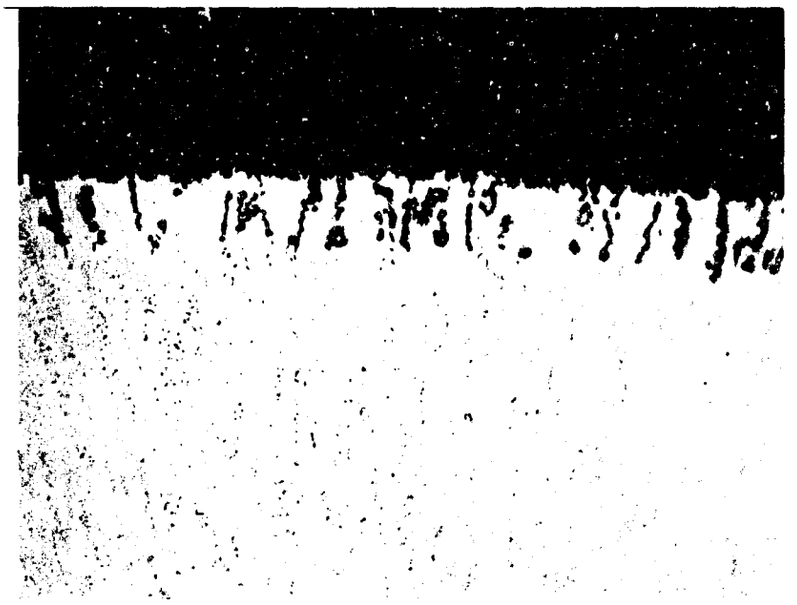

P7465 J7495

(a) Drop Cast

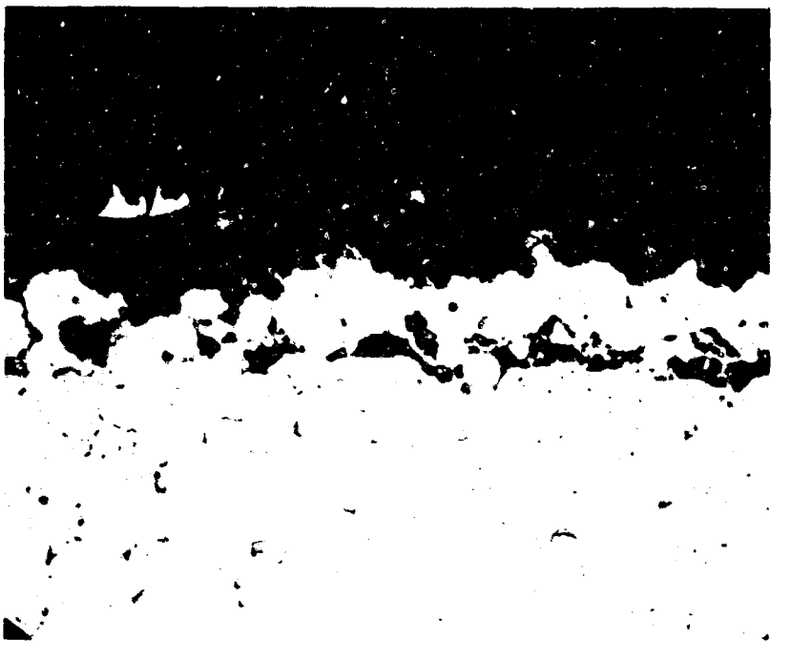

P7466 J7497

(b) Investment Cast

Figure 67:

Microstructural Appearance of 0.13 W/O Y Alloy After Hot Corrosion Testing 1725°F/50 Hrs.

(250X)

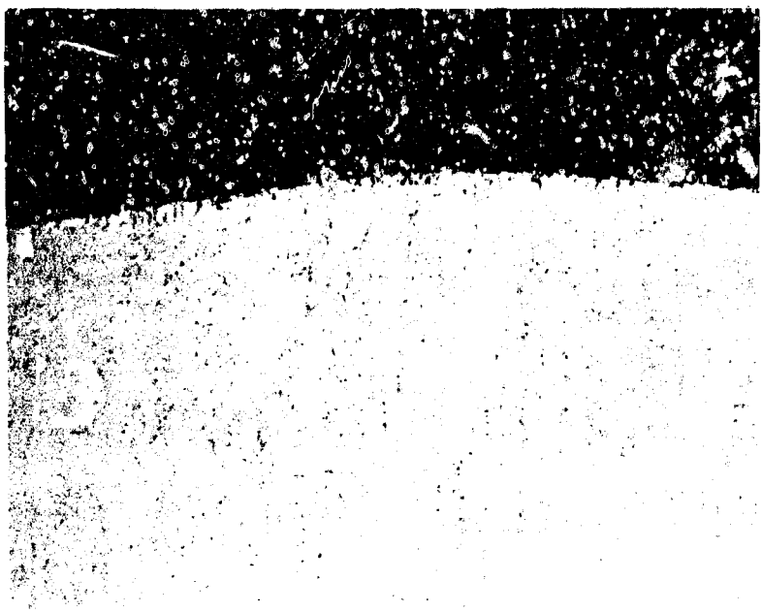

(a) Rene' 100 Base Alloy, Drop-Cast

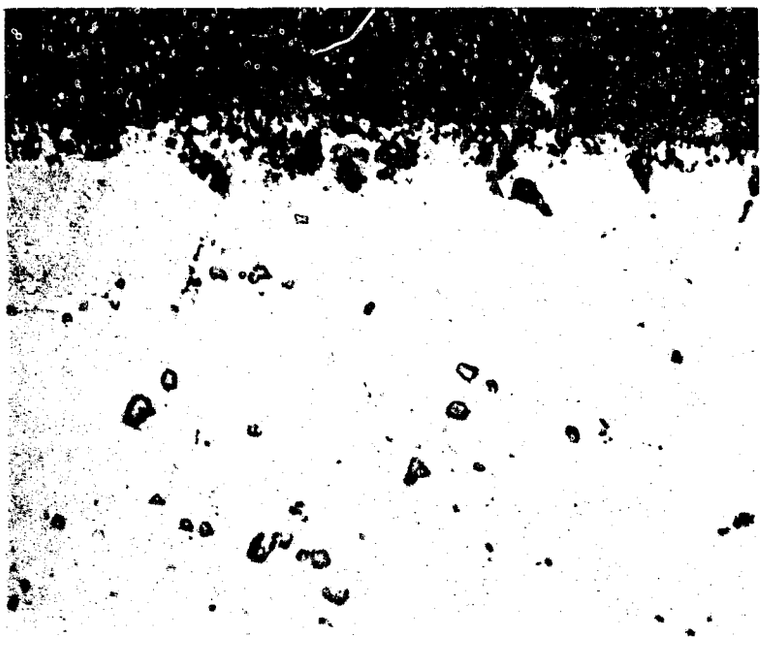

(b) 0.24 W/O Y Alloy, Investment Cast

Figure 68: Microstructural Appearance of Rene' 100 Base and 0.24 W/O Y Alloy After Hot Corrosion Tests.

(250X)

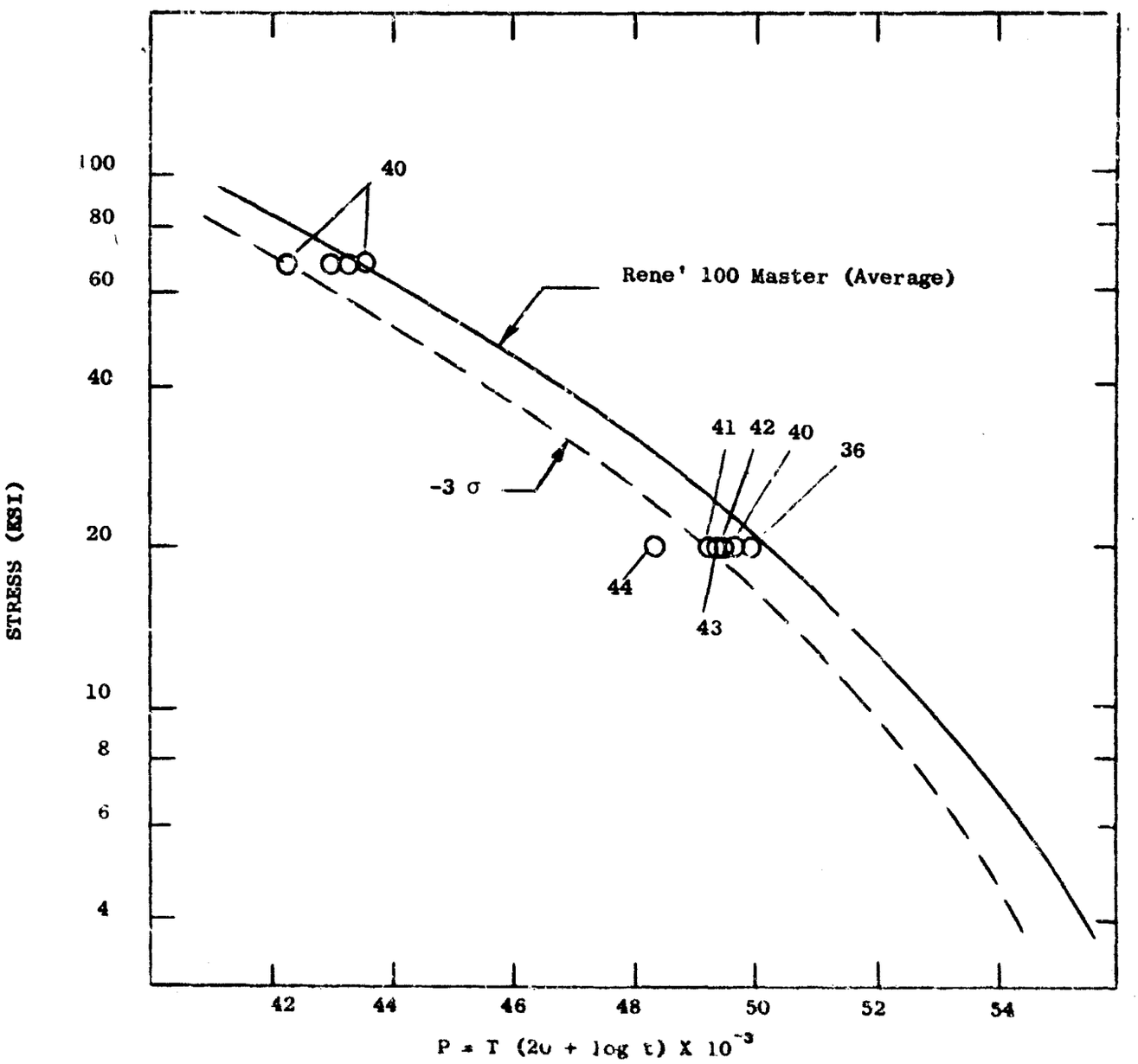

Figure 69

STRESS RUPTURE RESULTS OF PHASE II ALLOYS

Unclassified
Security Classification

DOCUMENT CONTROL DATA - R & D

(Security classification of title, body of abstract and indexing annotation must be entered when the overall report is classified)

1. ORIGINATING ACTIVITY (Corporate author)	2a. REPORT SECURITY CLASSIFICATION
General Electric Company Cincinnati, Ohio 45215	Unclassified
	2b. GROUP

3. REPORT TITLE

Nickel-Base Superalloy Oxidation

4. DESCRIPTIVE NOTES (Type of report and inclusive dates)

5. AUTHOR(S) (First name, middle initial, last name)

G. E. Wasielewski
C. S. Wukusick

6. REPORT DATE	7a. TOTAL NO. OF PAGES	7b. NO. OF REFS
February 1969	45	59

8a. CONTRACT OR GRANT NO.	9a. ORIGINATOR'S REPORT NUMBER(S)
AF 33(615)-2861	
b. PROJECT NO. 731202	
c.	9b. OTHER REPORT NO(S) (Any other numbers that may be assigned this report)
d.	

10. DISTRIBUTION STATEMENT This document is subject to special export controls and each transmittal to foreign governments or foreign nationals may be made only with prior approval of the Metals and Ceramics Division (MAM) Air Force Materials Laboratory, Wright Patterson Air Force Base, Ohio 45433

11. SUPPLEMENTARY NOTES	12. SPONSORING MILITARY ACTIVITY
	Air Force Materials Laboratory MAMP Wright-Patterson AF Base, Ohio 45433

13. ABSTRACT

A program to improve the surface stability of nickel-base turbine blade alloys is described. ~~In Phase I,~~ additions of rare-earth type elements and Mn were made singularly and in combination to cast Rene 100 and wrought Unitemp AF-2-IDA alloys. The results indicated that certain reactive metal additions are ~~markedly~~ effective in improving surface stability but tend to degrade mechanical properties. The loss in mechanical properties was attributed to segregation of reactive metal containing phases at the grain boundaries. In the wrought AF-2-IDA alloy the reactive metal additions seriously impared hot workability so that mechanical property test specimens could not be obtained. The most promising directions for future studies are suggested.

This document is subject to special export controls and each transmittal to foreign governments or foreign nationals may be made only with prior approval of the Metals and Ceramics Division (MAM) Air Force Materials Laboratory, Wright-Patterson Air Force Base, Ohio 45433

DD FORM 1 NOV 65 1473

Unclassified
Security Classification

14 KEY WORDS	LINK A		LINK B		LINK C	
	ROLE	WT	ROLE	WT	ROLE	WT
Nickel base Superalloy, Oxidation, reactive metals, surface stability, rare earths, hot corrosion, cyclic oxidation, static oxidation.						